Effect of Electric Environmental Control System Retrofit on Fuel Burn of a Medium-Range Aircraft

D.M.N. Milewski

May 16, 2019

Delft University of Technology

TU Delft Delft University of Technology

Challenge the future

Effect of Electric Environmental Control System Retrofit on Fuel Burn of a Medium-Range Aircraft

by

D.M.N. Milewski

in partial fulfillment of the requirements for the degree of

Master of Science

in Aerospace Engineering

at the Delft University of Technology,

to be defended publicly on Monday May 27, 2019 at 13:00.

Supervisor:	Dr. ir. R. Vos,	TU Delft
Thesis committee:	Prof. dr. ir. P. Colonna,	TU Delft
	Ir. P. Roling,	TU Delft
	Ir. F. Spek,	ADSE B.V.

Cover image was taken from https://www.jetphotos.com/.
An electronic version of this thesis is available at http://repository.tudelft.nl/.

TU Delft Delft University of Technology

Preface

The thesis lying before you was written in fulfilment of the graduation requirements of the Master of Aerospace Engineering at Delft University of Technology. It is the result of almost a year of hard work and dedication, through good and more difficult times. During this long process I hit the proverbial wall a few times, giving me the chance to learn more about such a process and about myself. The end result is a thesis report of which I am proud.

A word of thanks goes to my supervisor Roelof Vos for his guidance, support and optimism. His questions, discussions and evaluations during the project were interesting and ensured critical thinking and his optimism helped me to stay focused on the end goal.

I would like to thank my second supervisor Ferdinand Spek for his guidance and insights. His knowledge and experience with practical applicability have helped this project to be more than just a modelling exercise. I would also like to thank all his colleagues at ADSE B.V. They welcomed me with open arms and were always happy to answer questions.

Finally I would like to thank my parents, brother, family and friends. They helped me to stay motivated and relax. It makes me happy to know that I can always count on them.

This thesis marks the end of an almost 9-year long period as a student at the Delft University of Technology. After the Aerospace Engineering Bachelor and Master programs, a number of extracurricular activities including a year as board member at Formula Student Team Delft and an internship abroad at Lockheed Martin, I feel well prepared for what is to come and am confident about my next challenges.

D.M.N. Milewski
Delft, May 16, 2019

Summary

The environmental control system is an essential system for ventilation, pressure and temperature control on all modern aircraft. It is the largest consumer of secondary power on modern aircraft. For current systems this power comes from bleed air from the main engine compressors, increasing specific fuel consumption. The penalty of taking bleed air grows as the engine bypass ratio increases.

Environmental control system power consumption can potentially be reduced by using electric compressors that compress ambient air to feed the system, replacing engine bleed air. Energy off-takes from the engine in the form of shaft power are less efficient, but can be more precisely controlled compared to bleed air, ultimately reducing system power consumption. Such an electric environmental control system is currently operational in the twin aisle long range Boeing 787 and is said to reduce fuel consumption during cruise by 1-2%.

The Boeing 737 and Airbus A320 medium range single aisle passenger aircraft families are currently the most abundant in service aircraft at European airlines, with almost 4000 in use and over 1600 on order. Approximately 51% of these operational aircraft is less than nine years old, while the expected average fleet retirement age in Europe is 26 years. Thus, a new aircraft of this type is unlikely to be introduced in the near future, resulting in a gap between technology availability and realization of its benefits in new aircraft programs. To realize benefits of an electric environmental control system architecture before a new aircraft program is launched, a retrofit scenario is considered.

The aim of this research is to bridge the gap between current aircraft and new programs and provide a first order estimate of the potential benefits on mission fuel burn resulting from retrofit of an electric environmental control system architecture on a medium-range aircraft. The research question is “How much change in mission fuel burn requirement results from converting a conventional environmental control system on existing medium range single aisle commercial type aircraft to a bleedless electric environmental control system?”

For this purpose a steady state component model of the Airbus A320 is used, comparing mission fuel burn data between the conventional and electric environmental control system architectures. Different international standard atmosphere conditions and passenger arrangements are considered. The models are evaluated for a number of typical flight missions as based on statistics and fuel burn is compared.

The model consists of a general aircraft performance platform model to which system impact is appended. Sizing of the aircraft and performance over the mission profile is based on empirical sizing methods and general aircraft data. Engine performance is based on a sampling of actual engine performance data and linear interpolation between data points. Mission performance is calculated by dividing the flight profile segments in a number of time steps for which the steady state solution is computed, resulting in mission fuel burn. System impact on fuel burn is assessed by evaluation of a steady state component based system model for the baseline and electric environmental control system architectures. Each component in the system is modelled separately based on simple physical principles and basic relations. A basic representation of the electronics subsystem is included. The pneumatic flow rates through the system are dictated by the demand from the cabin model with several factors contributing to the heat load. The effect of the system off-takes on mission performance is added to the aircraft platform model in terms of correction factors for thrust and fuel flow.

Results show a potential for fuel burn reduction, as the energy use of the implemented electric architecture is approximately 50% less than that of a conventional architecture during cruise. A larger difference is found during take-off, climb and descent phases. This translates to a mission fuel burn reduction that is dependent on range of 1.6% at 250 nautical mile range and 0.6% at 2000 nautical mile range in the baseline case. When a 200 kilogram retrofit weight penalty is included, based on additional power electronics and associated power density, these numbers reduce to 1.4% reduction at 250 nautical mile range and almost 0.4% at 2000 nautical mile range.

It is concluded that the implemented EECS architecture has the potential for fuel burn reduction, due to

almost 50% less energy demand during cruise compared to a conventional architecture. With an estimated retrofit weight increase of 200 kg, fuel burn is reduced by 0.35% to 1.4% for the baseline case. The effect of retrofit is dependent on range, ambient conditions and fullness of the cabin, but a positive effect on fuel burn is achieved in almost all cases. Non-quantifiable benefits in terms of cabin air quality are expected as a result from implementation of an electric architecture, due to mitigation of the risk of engine fumes entering the aircraft cabin. Thus, the research question is answered.

When the results are translated to fleet level by multiplying with statistical flight frequencies, an fleet fuel burn reduction of 0.50% is found for retrofit with a 200 kilogram weight penalty. This translates to an estimated fuel cost saving of $78 million for the entire European A320 fleet based on current fuel prices and 20 years system operability. For a net economic benefit, retrofit cost should not exceed 20 thousand dollars per aircraft, which is assumed to be unachievable.

More accurate research is recommended to improve accuracy and to assess economic and environmental benefits. A transient model is required to analyse the expected sizing conditions of the environmental control system architecture. Improvements of model accuracy are expected to improve results. Research regarding a control strategy for the electric environmental control system supply pressure is recommended, as it is expected this will enable further fuel burn improvements. A more detailed analysis of sizing and implementation of the system architecture, as well as an economic analysis are required to determine viability of the retrofit.

Contents

List of Figures

List of Tables

Nomenclature

Abbreviations

0D	Zero dimensional, only generalized quantities considered
$	United States Dollar
AC	Alternating current
ACM	Air cycle machine
APU	Auxiliary power unit
ATRU	Autotransfermer rectifier unit
ATU	Autotransformer unit
CAC	Cabin air compressor
CECS	Conventional environmental control system
CFD	Computational fluid dynamics
CS	EASA Certification specifications
CSD	Constant speed drive
DC	Direct current
E/E	Electrical/electronics
EASA	European Aviation Safety Agency
ECS	Environmental control system
EECS	Electric environmental control system
FAA	Federal Aviation Administration
FAR	FAA Federal aviation regulations
HPC	High pressure compressor
HPT	High pressure turbine
IDG	Integrated drive generator
ISA	International standard atmosphere
K	Kelvin
kg	Kilogram
lbs	Pound
LHV	Lower heating value
LPC	Low pressure compressor
LPT	Low pressure turbine
m	Meter
MEA	More electric aircraft
min	Minute

MOAT	Morris one-at-a-time	
nm	Nautical miles	
NTU	Number of transfer units	
PACK	Pressurization and air conditioning kit	
s	Second	
TRU	Transformer rectifier unit	
VAC	Volt alternating current	
VDC	Volt direct current	
VFG	Variable frequency generator	
VSCF	Variable speed constant frequency	
W	Watt	
wrt	With respect to	

Symbols

A	Surface area	[m^2]
AR	Aspect ratio	[-]
C	Capacity rate ratio	[-]
c_p	Specific heat at constant pressure	[J/kg/K]
C_D	Drag coefficient	[-]
C_L	Lift coefficient	[-]
ΔC_D	System drag coefficient increment	[-]
d_i	Elementary effect	[]
D	Drag	[N]
D_g	Ground drag	[N]
e	Oswald factor	[-]
m	Gravitational acceleration	[m/s^2]
h	Convection coefficient	[$W m^{-2} K^{-1}$]
k	Thermal conductivity	[W/m/K]
L	Lift	[N]
M	Mach number	[-]
m	Mass	[kg]
$\dot{m}$	Mass flow	[kg/s]
N	Number or amount of	[-]
Nu	Nusselt number	[-]
P	Power	[W]
P	Power	[W]
p	Pressure	[kPa]
Pr	Prandtl number	[-]
Q	Heat flux	[W]

R	Thermal resistance	[K/W]
r_c	Temperature recovery coefficient of surface in flow	[-]
Re	Reynolds number	[-]
S	Surface area	[m^2]
s	Entropy	[J/K]
u	Velocity	[m/s]
f	Correction factor	[-]
T	Temperature	[K]
T	Thrust	[N]
U	Overall heat transfer coefficient	[-]
u	Velocity	[m/s]
V	Velocity	[m/s]
W	Weight	[N]
x	Characteristic length	[m]

Greek Symbols

α	Thermal diffusivity	[m^2/s]
γ	Ratio of specific heats	[-]
γ	Flight path angle	[deg]
Δ	Difference	[-]
ε	Effectiveness	[-]
ϵ_{recirc}	Recirculation fraction	[-]
η	Efficiency	[-]
μ	Friction coefficient	[-]
μ^*	Modified mean	[-]
ν	Kinematic viscosity	[m^2/s]
Π	Pressure ratio	[-]
ρ	Densiy	[kg/m^3]
σ^*	Modified standard deviation	[-]

Subscripts

∞	Conditions far away, unaffected by the system
aw	Adiabatic wall
c	Cooling
cabin	Cabin
comp	compressor
cond	Conduction
conv	Convection
ecs	Environmental control system quantity
equip	Equipment

ext	External
fuelflow	Fuel flow
gen	Generated
hx	Heat exchanger
in	Intry condition of a component
int	Internal
loss	Loss
net	Net quantity
out	Outlet condition of a component
pack	Pressurization and conditioning kit quantity
pax	Passengers
sfc	Specific fuel consumption
skin	Skin quantity
t	Total quantity
thrust	Thrust
tot	Total
turb	Turbine
wall	Wall

1 Introduction

The environmental control system (ECS) is an essential system on all modern aircraft to maintain a healthy and comfortable environment in the aircraft cabin. Its main functions are ventilation and temperature and pressure control. This is achieved with air cycle machines (ACM). The working principle of an ACM is based on a reverse Brayton cycle, powered by main engine bleed air. Since bleed air off-takes increase specific fuel consumption and this penalty grows with increasing engine bypass ratio [2], potential improvements to ECS efficiency are continuously researched.

One way of potentially reducing ECS power consumption is by using electric compressors to compress ram air to feed the ACM, thus removing the dependency on engine bleed air. Such a system is currently operational in the twin aisle long range Boeing 787 and is said to reduce fuel consumption during cruise by 1-2% [1]. As a more electric aircraft (MEA), the Boeing 787 replaces numerous systems conventionally using pneumatic or hydraulic power with electrically powered systems.

The Boeing 737 and Airbus A320 medium range single aisle passenger aircraft families are currently the most abundant in service aircraft at European airlines with almost 4000 in operation in July 2017 as taken from the 2017 world airliner census[2]. Approximately 21% of the airline fleet in the European Union (EU) is less than five years old and 51% in total is less than nine years old, as found by the European Commissions Eurostat[3]. Furthermore, European airlines have over 1600 aircraft of these aircraft families on order according to the world airliner census. With an expected average fleet retirement age in Europe of 26 years[4], this means that a new aircraft of this type is unlikely to be introduced in the near future, resulting in a gap between technology availability and realization of its benefits in new aircraft programs. To realize benefits of an electric environmental control system architecture before a new aircraft program is launched, a retrofit scenario is considered.

According to data from Eurostat, kerosene type jet fuel consumption in the EU was approximately 50 million tons in 2015[5]. While no data is readily available to estimate the fraction of jet fuel used by medium range type of aircraft, these numbers imply that a small relative reduction in fuel consumption may result in a large absolute reduction. This potentially reduces aviation environmental impact and reduces aircraft operating expense.

Other benefits of an electric ECS are also to be expected. While no data is publicly available to quantify the cost of maintenance, repair and overhaul of the pneumatic systems of commercial aircraft, it is accepted as common knowledge that these systems are maintenance intensive. More electric system architectures are expected to reduce maintenance effort. Furthermore, bleed air can contain fractions of engine shaft lubricant or its decomposition products. By changing the source of air supply to ambient air compressed with an electric compressor using foil air bearings, these impurities can no longer enter the aircraft passenger compartments. Since these topics cannot be quantified with the resources available for this research, it will not be the focus of this discussion. However, these effects can be regarded as added benefits.

[1] Andre Brasseur, Will Leppert and Alexis Pradille. Inside the 747-8 New Environmental Control System. *Aero Magazine*, pages 18-25, 2012.

[2] Flight International. World Airliner Census 2017. Technical report, FlightGlobal, 2017

[3] European Commission - Eurostat. How old is the EU's commercial aircraft fleet?. Article, 2015. http://ec.europa.eu/eurostat/en/web/products-eurostat-news/-/EDN-20171207-1

[4] Dick Forsberg. Aircraft Retirement Trends & Outlook. Avolon, 2012.

[5] European Commission. Oil and petroleum products - a statistical overview - Statistics Explained 2017. http://ec.europa.eu/eurostat/statistics-explained/index.php/Oil_and_petroleum_products_-_a_statistical_overview

The ECS demands a large amount of secondary power from the main engines in the form of bleed air, thus increasing specific fuel consumption [3]. Research has been published investigating the effect of a Boeing 787 style electric ECS on various aircraft types [4–11], but is shortcoming regarding improvement of the existing fleet.

The proposed research aims to bridge the identified gap between technology availability and realization of its benefits in new aircraft programs by investigating potential reduction of fuel burn when the bleed air driven ECS architecture is replaced with an electric ECS (EECS) architecture. The research objective is to quantify potential fuel burn reduction by converting from a conventional ECS (CECS) to a bleedless EECS with an electrically driven compressor on existing medium range single aisle commercial type aircraft. To achieve this, typical mission fuel consumption obtained from simulations with conventional and electric ECS architectures will be compared. Due to time constraints the scope is limited as follows: Detailed sizing of electric components is considered outside of the scope of the research. Integration into the airframe, including location and attachment is not considered. Only one EECS architecture will be modelled. Analysis of other ECS architectures is outside the scope of this research. The research is limited to one aircraft type. The number of evaluated mission profiles and atmospheric conditions is limited. The research question is defined as follows:

- How much change in mission fuel burn requirement results from converting a conventional environmental control system on existing medium range single aisle commercial type aircraft to a bleedless electric environmental control system?
  - What is the fuel consumption of a conventional environmental control system?
    - What is the dependency on mission distance?
    - What is the dependency on atmospheric conditions?
  - What is the fuel consumption of the electric environmental control system?
    - What is the weight differential caused by implementation of the electric environmental control system?
    - What is the power required by the electric compressor?
    - What is the dependency on mission distance?
    - What is the dependency on atmospheric conditions?
    - What are the implications for the electrical power generation and distribution system?

2

Background Information

Background information about aircraft environmental control system operation is required to appreciate the modelling approach and the system effects on aircraft fuel burn. To this end, the aircraft ECS system architecture and its components are discussed in Section 2.1. State of the art developments in aircraft environmental control systems are discussed in Section 2.2. Engine thermodynamic performance characteristics and the effect of off-takes are discussed in Section 2.3. Section 2.4 presents a discussion of the more electric aircraft (MEA) concept. Finally, Section 2.5 briefly introduces the concept of retrofit.

2.1. Aircraft ECS System Architecture

A conventional aircraft environmental control system is present on almost all commercial transport aircraft in service today. While the details of these systems might be different, the working principles are similar. Pneumatic power is extracted in the form of bleed air from the main engines. Depending on engine type, flight condition and other parameters this bleed air might need to be cooled in a pre-cooler inside the engine. A valve regulates pressure supplied to the aircraft. In other words, energy needs to be dissipated before it can be fed into the main aircraft structure, because of material limits and temperature and pressure restrictions by subsequent ducting and components. A heat exchanger and throttle valve reduce the temperature and pressure of bleed air before it enters the aircraft structure. The bleed air is distributed by a manifold over the various systems that demand pneumatic power. These systems typically include the ECS and wing anti-ice system, the major consumers of pneumatic power, and a number of pneumatic drive hydraulic pumps and secondary systems[6]. The bleed air directed to the ECS is divided over a number pressurization and conditioning kits (PACK), consisting of an ACM and some secondary components to improve performance and efficiency. A schematic of a typical aircraft ECS is shown in Figure 2.1.

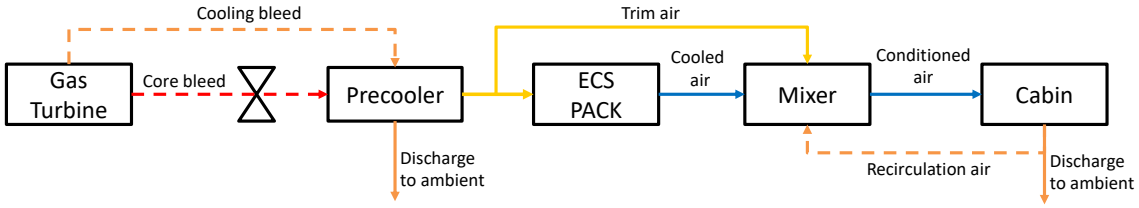

Figure 2.1: Schematic of a typical ECS architecture and associated air flows, based on Shi *et al.* [12] and Brasseur[1].

2.1.1. The air cycle machine

An ACM is a refrigeration system based on the reverse Brayton cycle and is the core of the ECS PACK. A qualitative temperature (T) - entropy (s) diagram of the reverse Brayton cycle is shown in Figure 2.2. Incoming gas is compressed in a compressor. This raises the gas temperature, creating a temperature difference with the ambient. The gas flows through a heat exchanger to dissipate heat. Finally the gas is expanded in a turbine, resulting in a decreased temperature compared to the incoming gas. These machines are at the core of aircraft environmental control.

[6]Andre Brasseur, Will Leppert and Alexis Pradille. Inside the 747-8 New Environmental Control System. *Aero Magazine*, pages 18-25, 2012.

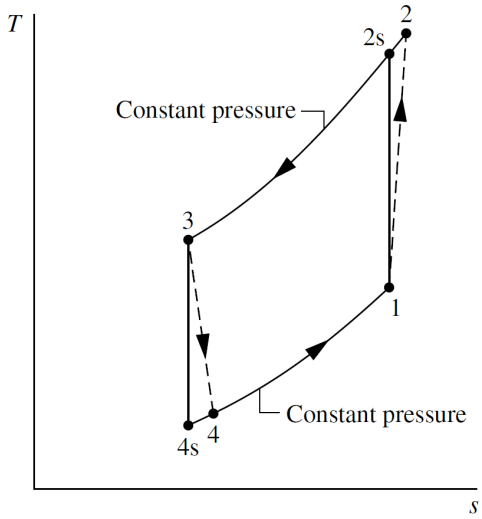

Figure 2.2: *T*-*s* diagram of an ideal and real reverse Brayton cycle, adapted from Moran and Shapiro [13]. 1 is compressor inlet, 2 is heat exchanger inlet, 3 is turbine inlet, 4 is turbine outlet.

2.1.2. The pressurization and conditioning kit

The PACK in an aircraft works according to the same principles as the general ACM described above, with some differences. The working fluid is engine bleed air. The heat sink is ram air from the ambient. This means there already exists a temperature difference before the working fluid enters the PACK. A primary heat exchanger is placed before the compressor, utilizing this temperature difference.

Water separation

The air cycle machine can cool air to below the freezing temperature of water, as evidenced by the application to liquid natural gas production [14]. In aircraft, outlet temperature of the ACM is tightly controlled by control systems to values typically close to the freezing point of water[1], but lower temperatures are reached internally. This means condensation and ice build-up can occur within the ACM, potentially damaging the system. To prevent ice build-up, the PACK contains components to reduce the humidity of the working fluid. After compression and heat exchange to the ambient, the working fluid is cooled in a condenser, using ACM turbine outlet flow as heat sink, and then flows through a high pressure water separator. This device works by adding swirl to the flow, using centrifugal force to separate the condensed water droplets from the main flow. The working fluid is then reheated in a heat exchanger and expanded in the turbine.

Temperature control

Control of the PACK outlet temperature and final ECS outlet temperature that is fed into the cabin is controlled by partially redirecting the airflow to bypass part of the ACM components or the full PACK. A fraction of cabin air, typically 50% as allowed by regulations, is filtered and reused. The three air flows consisting of PACK outlet air, PACK bypass air and cabin recirculation air are mixed such that the temperature demanded by the ECS control panel is achieved before being fed into the cabin. More about the current state of the art PACK is discussed in Section 2.2.

2.2. State of the Art Environmental Control System

The state of the art in aircraft ECS can be split in two categories. Most aircraft have a bleed air driven ECS, in the remaining of this thesis referred to as conventional environmental control system (CECS). On modern airliners, these are highly optimized machines. Due to the transition to more electric aircraft architectures, an electric environmental control system (EECS) is currently installed on one commercial aircraft, the Boeing 787. Therefore, both systems are shortly discussed in this section.

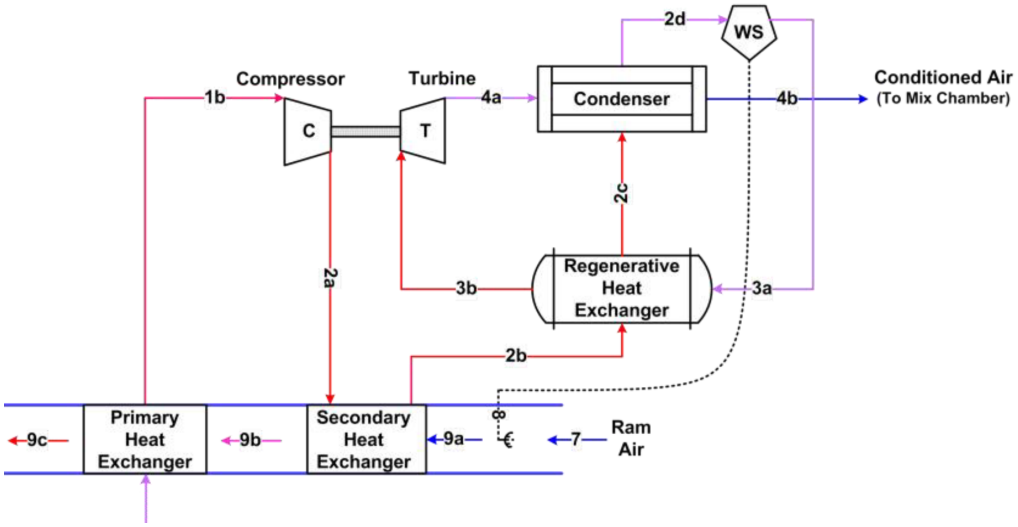

Figure 2.3: Schematic of a typical ECS PACK with two heat exchangers and water separator components, adapted from Long *et al.* [6]

2.2.1. State of the Art Bleed Air Powered Environmental Control System

Most modern commercial transport aircraft, such as the Airbus A380 and A350 still rely on the engine bleed air for the ECS as apparent from Aerospace Technology[7] and investigated by Sarlioglu and Morris [15]. These systems have a similar architecture as described in Section 2.1, the developments have been focused on reducing system weight and improving efficiency and control systems. These developments do not only affect new aircraft, but are also introduced as improvements of existing aircraft programs, such as the Boeing 747[1].

Using the Boeing 747-8 air conditioning pack system as the example for state of the art conventional systems, a few differences with the basic PACK are observed. The system employs a number of sensors and valves to regulate temperature at various intermediate stages of the PACK as well as the outlet temperature. A water separation system is implemented so that ice build-up within the PACK is prevented and freezing temperatures can be achieved at altitudes where humidity is high enough for this to be of concern. Bypass flows for compressor and turbine are present and regulated to control speed of the machine, thus controlling temperature. Generally speaking, the system has been designed in such a way that the separate components of the PACK can work optimally so total system performance is optimised. A general schematic of the state of the art conventional ECS PACK without bypass flows is shown in Figure 2.3.

While research on reducing ECS fuel consumption by changing the system architecture has been performed for more than 10 years, a deviation from the conventional ECS system is not yet widespread. Possible causes for adherence to the conventional system might be the risk involved in implementation of the electrical system, see Section 2.4. To maximize benefits, a complete redesign of the aircraft electrical system is required, resulting in large investments and development risks.

The Boeing 787 is the only commercial transport aircraft with an electric ECS at the time of writing. Such a system is discussed in Section 2.2.2. After battery and other electrical problems received attention in the news [8] [9], the reputation with the general public declined. This possibly served as additional barrier against the further electrification of aircraft, next to the greatly increased development effort for a new system architecture.

Most modern PACKs are complex machines. Bleed air from the main engine compressor is cooled by a primary heat exchanger, compressed in a compressor and cooled in a secondary heat exchanger. Both heat exchangers use ambient air flow as a heat sink. The air flows through a recuperator, condenser and water separator to remove any excess moisture that might be present in the air. In some systems, the removed

[7] Aerospace Technology. Airbus A350 XWB - Aerospace Technology, 2016, https://www.aerospace-technology.com/projects/a350wxb/

[8] NOS. Weer Dreamliner 787 in de problemen, jul 2013. News article. https://nos.nl/artikel/528999-weer-dreamliner-787-in-problemen.html

[9] The Mercury News. A list of Boeing 787 Dreamliner problems, 2013. News article. https://www.mercurynews.com/2013/01/15/a-list-of-boeing-787-dreamliner-problems/

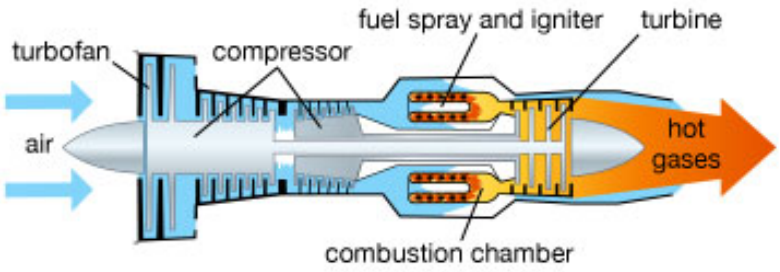

Figure 2.4: Schematic of a typical twin-spool turbofan engine, copied from Encyclopaedia Britannica [14].

water is sprayed on the heat exchangers to improve cooling capacity. After the water is removed, the air is expanded in a turbine to reach the outlet conditions of the air conditioning module. To obtain the desired pressure and temperature for the cabin, this air is often mixed with a portion of recirculating cabin air and bypass bleed air. Mixing with recirculated cabin air also decreases the bleed air demanded from the engines.

2.2.2. State of the Art Electrically Powered Environmental Control System

The Boeing 787 is the only aircraft with an EECS at the time of writing. The difference with the CECS architecture is the elimination of bleed air off-takes from the main engines. Instead, air is supplied by electric motor driven compressors that compress incoming ram air, as described by Lents *et al.* [16] [10]. The architecture of the PACKs does not need to be adapted.

The core of the ECS, the PACK, is similar to the conventional state of the art system. The electric motors in this system are the reason for the term electric ECS. Boeing also replaced the pneumatic ice protection system in the wing leading edge with an electric ice protection system[11]. Furthermore, part of the hydraulic system uses electric motor driven hydraulic pumps. The significant number of traditionally pneumatic or hydraulic systems that have been replaced with electric systems make the Boeing 787 the first commercial MEA. Major changes to the electrical system have been made for the Boeing 787 compared to conventional aircraft as a result of the large increase in electric systems. A discussion of electric systems for MEA can be found in Section 2.4. In military jets, an electric ECS has been used for a longer time. Some military aircraft carry oxygen tanks for air supply at extremely high altitudes, but in general the system does not significantly deviate.

2.3. Engine Thermodynamics and the Effect of Off-Takes

The isentropic flow relations for compressor and turbine components of a turbomachine are briefly discussed. These are also the governing equations for manual and 0D engine performance analysis, together with isentropic relations for the inlet, where ram effects are present, combustion chamber and nozzle flow. For the purpose of this thesis the full 0D analysis of an engine will not be discussed. The interested reader is referred to relevant literature, such as Farokhi [19], Visser[28], Rao[12] or the authors' literature study report[13]. In the following, first some engine performance and efficiency characterization is presented, secondly the effect of power off-takes is discussed.

Figure 2.4 shows the schematic of a typical twin-spool turbofan engine. An overview of the station numbers and their corresponding meaning is given in Table 2.1. These station numbers will be used as subscripts to variables in the following discussion and are omitted in the nomenclature for clarity. Compressor and turbine performance are shortly discussed. This serves as background knowledge to the discussion of efficiency and the effect of off-takes.

[10] The patent by Lents *et al.* [16] does not mention application to a specific aircraft. It was awarded to Hamilton Sundstrand Corp., which was later acquired by UTC Aerospace Systems [17]. UTC Aerospace Systems is the current supplier for the Boeing 787 ECS [18]. It is common knowledge that the Boeing 787 features an electric ECS, so it is concluded that the system described in the patent is in fact the Boeing 787 ECS.

[11] Mike Sinnett. 787 No-Bleed Systems: Saving Fuel and Enhancing Operational Efficiencies. *Aero Quarterly*, pages 6-11, 2007.

[12] Arvind G. Rao. AE4238 - Aero Engine Technology [Lecture notes]. 2016

[13] Literature Study - Effect of Electric Environmental Control System on Medium Range Commercial Aircraft. Milewski, D.M.N. 26-06-2018. Available at Vos, R. at TU Delft.

Table 2.1: Engine station number convention and definition as used in this document.

Station	Description
0	Ambient
1	Intake entry
13	Bypass duct
17	Bypass nozzle entry
19	Bypass nozzle exit
2	Fan entry
24	LPC entry
26	HPC entry
3	Combustor entry
4	HPT entry
45	LPT entry
7	Core nozzle entry
9	Core nozzle exit

Compressor Performance Analysis

The outlet conditions and power required for the compressor of a turbomachine P_{comp} can be determined with the following equations[28], with $p_{\text{t,out}}$ and $T_{\text{t,out}}$ the total outlet pressure and temperature, Π_{comp} the compressor compression ratio between outlet and inlet (>1), $p_{t,,\text{in}}$ and $T_{\text{t,in}}$ the total inlet pressure and temperature, η_{comp} the isentropic compressor efficiency, γ the ratio of specific heats, $\dot{m}$ the mass flow and c_p the constant pressure specific heat:

$$p_{\text{t,out}} = \Pi_{\text{comp}} \cdot p_{\text{t,in}} \tag{2.1}$$

$$T_{\text{t,out}} = T_{\text{t,in}} + \frac{T_{\text{t,in}}}{\eta_{\text{comp}}} \left[\Pi_{\text{comp}}^{\frac{\gamma-1}{\gamma}} - 1 \right] \tag{2.2}$$

$$P_{\text{comp}} = \dot{m} c_p \left(T_{\text{t,out}} - T_{\text{t,in}} \right) \tag{2.3}$$

Turbine Performance Analysis

The following equations describe the performance of a turbine[28], where P_{turb} is the turbine power, η_{turb} the turbine efficiency and Π_{turb} the turbine pressure ratio:

$$P_{\text{turb}} = \dot{m} c_p T_{\text{t,in}} \eta_{\text{turb}} \left[1 - \Pi_{\text{turb}}^{\frac{\gamma-1}{\gamma}} \right] \tag{2.4}$$

$$T_{\text{t,out}} = T_{\text{t,in}} \left[1 + \eta_{\text{turb}} \left(\Pi_{\text{turb}}^{\frac{\gamma-1}{\gamma}} - 1 \right) \right] \tag{2.5}$$

In the case of a gas generator, fixed turbine inlet temperature is usually known, since this can be well managed by adjusting fuel flow in the combustor. For the specific application to the PACK model, the outlet conditions are known. By applying a power balance between the compressor and turbine, the power required by the turbine is known, closing the system of equations.

Engine performance and efficiency

Different definitions of performance and efficiency of a gas turbine engine are used. Thermodynamic efficiency of an engine is defined as the ratio of gas generator power and combustion enthalpy increase. Gas generator power is the power that can be extracted from the flow in case of 100% isentropic efficiency after extraction of compressor and fan power from the flow. Only fan work affecting the core flow is accounted for in the gas generator power, so not all turbine work is included as a portion of turbine work is used by the fan to drive airflow through the bypass duct. Therefore the temperature and pressure are different than at station 5. To determine gas generator power P_{gg}, the difference between energy in the working fluid after the turbine

[14] Encyclopaedia Britannica, Inc. Air-breathing engines. Encyclopaedia Britannica Kids. Accessed 11-05-2019. https://kids.britannica.com/students/assembly/view/53526

and energy in the ambient in terms of turbine mass flow $\dot{m}_5$, specific heat of the gas mixture $c_{p,\text{gas}}$, total temperature at gas generator $T_{\text{t,gg}}$, total ambient and gas generator pressure $p_{\text{t},0}$ and $p_{\text{t,gg}}$, ratio of specific heats of the gas mixture γ_{gas} and ambient velocity u_0, is determined with the following equation:

$$P_{\text{gg}} = \dot{m}_5 c_{p,\text{gas}} T_{\text{t,gg}} \left(1 - \frac{p_{\text{t},0}}{p_{\text{t,gg}}}^{\frac{\gamma_{\text{gas}}-1}{\gamma_{\text{gas}}}}\right) - \frac{1}{2}\dot{m} u_0^2 \tag{2.6}$$

The thermodynamic efficiency η_{th} is then determined in terms of the gas generator power P_{gg}, mass flow through the combustion chamber $\dot{m}_3$, specific heat of the gas mixture $c_{p,\text{gas}}$ and temperature difference between combustor exit temperature $T_{\text{t},4}$ and combustor entry temperature $T_{\text{t},3}$ with the following equation:

$$\eta_{\text{th}} = \frac{P_{\text{gg}}}{\dot{m}_3 c_{p,\text{gas}} \left(T_{\text{t},4} - T_{\text{t},3}\right)} \tag{2.7}$$

Propulsive efficiency η_{prop} is the ratio of thrust power P_{thrust} generated by the engine and the power required to accelerate the working fluid, called propulsive power P_{prop}. Thermal efficiency is the efficiency η_{thm} of energy conversion in the engine. These quantities are given by the following equations, where F_{tot} is the total thrust, u_0 is the ambient velocity, $\dot{m}_9$ and $\dot{m}_{19}$ are the core and bypass nozzle mass flow, $u_{9,\text{eff}}$ and $u_{19,\text{eff}}$ are the effective core and bypass nozzle exit velocity accounting for pressure thrust of a chocked nozzle, $\dot{m}_{\text{fuel}}$ is the fuel mass flow and LHV is the lower heating value of the fuel:

$$\begin{aligned}
P_{\text{thrust}} &= F_{\text{tot}} u_0 \\
P_{\text{prop}} &= \frac{1}{2}\dot{m}_9 \left(u_{9,\text{eff}} - u_0\right)^2 + \frac{1}{2}\dot{m}_{19} \left(u_{19,\text{eff}} - u_0\right)^2 \\
\eta_{\text{prop}} &= \frac{P_{\text{thrust}}}{P_{\text{prop}}} = \frac{2}{1 + \frac{u_{9,\text{eff}}}{u_0}} \\
\eta_{\text{thm}} &= \frac{P_{\text{prop}}}{\dot{m}_{\text{fuel}} \text{LHV}}
\end{aligned} \tag{2.8}$$

In pure jet engines, ideally gas generator power and propulsion power are equal. In turbofan engines, the difference is large due to power extraction for driving the fan. To include this, jet generation efficiency η_{jet} and total efficiency of energy conversion to thrust η_{tot} are defined and computed with the following equations:

$$\begin{aligned}
\eta_{\text{jet}} &= \frac{P_{\text{prop}}}{P_{\text{gg}}} \\
\eta_{\text{tot}} &= \frac{P_{\text{thrust}}}{\dot{m}_{\text{fuel}} \text{LHV}}
\end{aligned} \tag{2.9}$$

The most practical parameter when evaluation fuel burn over a mission segment or mission profile is the specific fuel consumption (sfc) in g/kN/s. It is the ratio of fuel burned and thrust generated as given by Equation (2.10) and computed as follows:

$$\text{sfc} = \frac{\dot{m}_{\text{fuel}}}{F_{\text{tot}}} = \frac{u_0}{\eta_{\text{tot}} \text{LHV}} \tag{2.10}$$

Effect of power off-takes

The discussed 0D calculation scheme can be used to estimate the effect of power off-takes on performance as well. Depending on the required accuracy or design case, some modifications have to be made.

When bleed air is extracted from the compressor, mass flow from inlet to combustion chamber is no longer constant. Instead, at the point of bleed air extraction the mass flow is reduced. By setting up equations for LPC and HPC as a whole, only bleed air off-takes at the end of the LPC or HPC can be modelled with relative accuracy. To more accurately capture the effect of bleed air off-takes from intermediate compressor stages, the LPC and HPC equations need to be set-up for each stage.

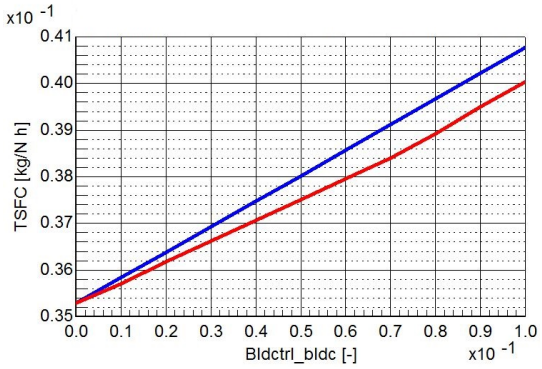

(a) Comparison of sfc at various bleed fractions for constant maximum fuel flow (blue) and constant $T_{t,4}$ limit (red), showing that increasing bleed air off-takes increase sfc.

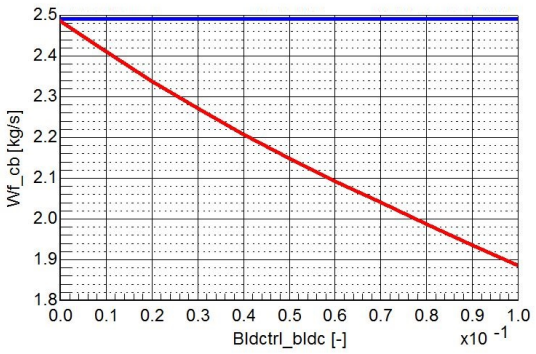

(b) Comparison of $\dot{m}_{fuel}$ at various bleed fractions for constant maximum fuel flow (blue) and $T_{t,4}$ limit (red), showing that less fuel can be added as an effect of reduced air mass flow to the system to keep turbine entry temperature constant.

Figure 2.5: Simulation results showing the notional effect of bleed air off-takes on turbofan sfc and $\dot{m}_{fuel}$ generated with GSP[15], showing that bleed air negatively impacts sfc despite reduced fuel burn. Not shown is the thrust reduction that also results from bleed air off-takes.

Bleed air off-takes reduce efficiency and increase sfc. This can be readily explained. Work is performed on the flow in the compressor. Part of the flow is then removed from the cycle, meaning no energy can be extracted from this portion of flow by the turbine downstream. Therefore there is a loss of energy, reducing efficiency. A notional trend of the effect on sfc when turbine inlet temperature is limited at its maximum value can be seen in Figure 2.5 created using simulations for a course assignment. It can be seen in Figure 2.5a that the sfc is increased for increasing bleed air off-takes and that fuel flow is decreased as the decreased air flow requires less fuel to reach the limit temperature. Despite reduced fuel burn, sfc is still increased due to a reduction in thrust that also results from bleed air off-takes, not shown in the Figure.

When shaft power is extracted from the turbine, the same equations can be used to determine pressure drop in the turbine, Equations (2.4) and (2.5). Increased shaft power off-takes will reduce the energy in the flow that can be converted to thrust, hence decreasing engine efficiency and thrust and increasing sfc.

In the MEA concept, bleed-air powered systems are replaced with electric powered systems requiring increased shaft power off-takes. According to Slingerland and Zandstra [20], bleed air off-takes incur less penalty on engine performance. However, because of the high energy of the working fluid in the compressor stages, the bleed air off-takes typically overshoot the required power. As discussed in Section 2.1, energy is removed from the bleed air immediately following extraction. Temperature is reduced by a heat exchanger and pressure is reduced by a throttling valve. On the contrary, shaft off-takes can be accurately matched to the power demand. Between the energy waste by pneumatic off-takes and less efficient shaft power off-takes lies the opportunity for more electric systems to improve overall engine efficiency compared to traditional systems.

Off-design point calculation

The discussed 0D calculation scheme can be used to estimate off-design point performance as well. The same governing equations are used, but the parameters that are known and that need to be determined are different. Typically, a power setting is selected, specifying fuel flow. An iterative procedure is then used until a consistent output is found.

When the scheme used for simple manual in series calculation, an error of less than 3% can be achieved for design point calculations. However, when used for off-design point calculations, the error is significantly greater. Furthermore, other more complex phenomena such as transient behaviour or compressor stability are not captured. It is therefore recommended to employ more sophisticated models or software packages dedicated to these types of analyses when more accuracy or transient behaviour is required.

[15] NLR Netherlands Aerospace Center. Gas Turbine Simulation Program. Accessed 22-07-2018. https://www.gspteam.com/

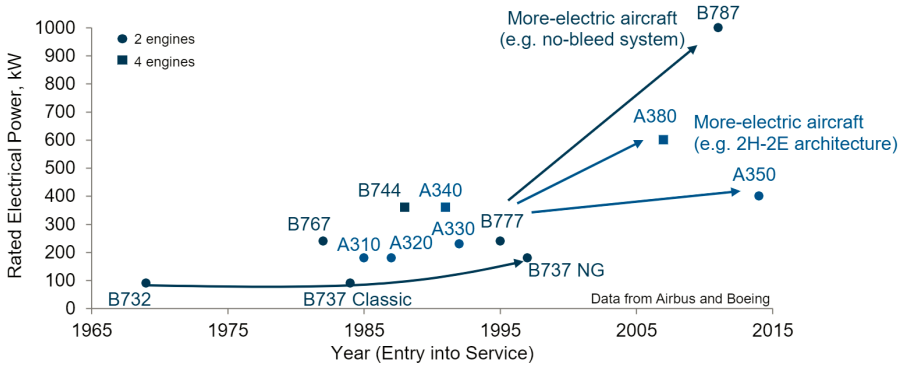

Figure 2.6: Trend in electrical power of commercial aircraft showing a clear increase for MEA concepts, copied from Lampl *et al.* [26]

2.4. The more electric aircraft

The more electric aircraft (MEA) concept has been known since the 1940s, according to Madonna *et al.* [21]. It has received increasing interest since the early 1990s, when Weimer [22] published a paper "to review and update the Air Force's on-going and planned programs to develop the electrical power technologies for the near and far term MEA". His focus was on military aviation, the interest in the MEA concept for commercial transport aviation followed later. Besides research on specific power electronic components or replacement of specific pneumatic or hydraulic systems by electric systems, a number of publications discuss the electric power generation, conversion and distribution. These latter topics are shortly discussed in this Chapter as they relate to this research. Several publications discuss the required performance of power electronics or suggest new power electronics system design. These topics are not discussed in this report as these topics are considered outside the scope of this thesis.

2.4.1. Electric power generation and conversion

Modern conventional aircraft already use electric power for a number of systems, such as fans for cabin air circulation, avionics, cabin lighting and entertainment systems and galleys [23]. The power consumed by these systems is relatively low, in the order of 50-150 kW as can be seen by the installed electric power generation of a number of aircraft in Figure 2.6. Installed electric power generation is more than the system power requirements, due to generator redundancy.

During flight, electric power is generated by the main engines as shaft power off-takes through an accessory gearbox that feeds a generator. The shaft speed of the generator varies during flight operations as engine speed varies, typically between ±50% shaft speed at idle and 100% shaft speed at full take-off power [24]. Conventionally, an integrated drive generator (IDG) is used, which provides constant voltage constant frequency alternating current (AC) power by mechanically converting the varying speed of the engine to a constant speed, resulting in constant frequency power generation. The constant voltage is then controlled using an exciter and a control loop [25].

As hydraulic and pneumatic systems on the aircraft are replaced with electric systems, the electric power consumption increases, thus the generated power also increases. This is evident from Figure 2.6, where the rated power of the A350 is significantly increased compared to the similar sized B777. The A350 features partly electric flight control actuation[16], but still uses hydraulic brakes [17] and pneumatic ECS, wing ice protection system (IPS) and main engine start [18]. The A380 has comparable electrical systems as the A350, the higher rated power a consequence of the much larger size of the aircraft. The Boeing 787 has a much higher rated power. It features electric engine start system, electric ECS and wing IPS, partly electric flight controls and electric brakes[11]. As a consequence, the rated electrical power is more than doubled compared to the similar size A350.

[16] Olivier Criou. Composites in Airbus [Presentation], 2007
[17] Eric Drouin. Airbus A350XWB brake - Safran Landing Systems, 2018.
[18] Airbus Customer Services. A350-900 Flight Deck and Systems Briefing for Pilots, 2006

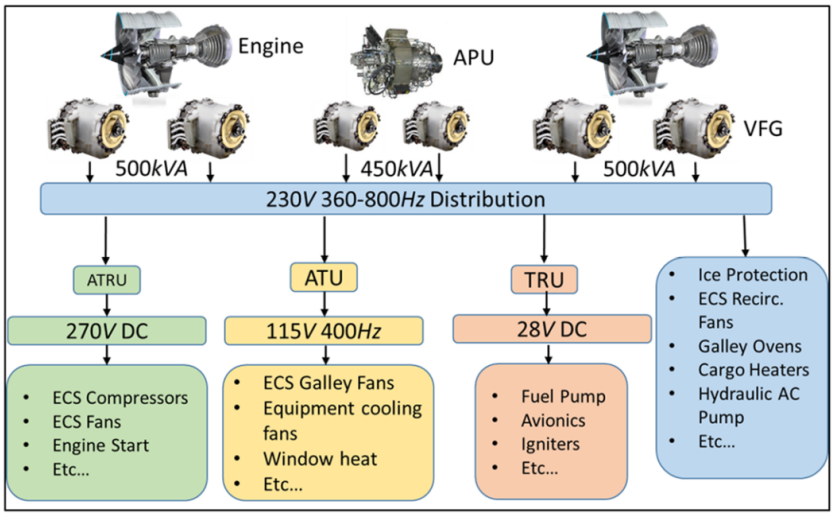

Figure 2.7: Boeing 787 power generation and conversion system showing the different voltage and currents used and the systems supplied by each bus, copied from Madonna *et al.* [21]. ATRU: autotransfermer rectifier unit, ATU: autotransformer unit, TRU: transformer rectifier unit.

Constant frequency power generation

The constant speed drive (CSD) part of the IDG is an expensive and complex system [24]. Numbers on the frequency and cost of IDG maintenance are not publicly available, but it is generally known in the airline industry that it is a component that requires frequent maintenance or repair[19] [15]. Increasing loads on the IDG will likely increase cost of the system and its maintenance.

An alternative system to the IDG is a variable speed constant frequency (VSCF) system where the CSD is omitted. The variable frequency electricity can be distributed to the loads via a DC link and then converted back to AC using rectifiers and inverters. Such a system is used for the back-up generators on the Boeing 777. Another option is to use AC/AC converters, implemented on some military aircraft. These two types of VSCF system is not widespread, because the power electronics converter represents a single point of failure, resulting in high power rating and reliability requirements [21].

A typical commercial transport aircraft is equipped with an IDG in each engine, coupled through the accessory gearbox. During ground operations or in case of emergency the auxiliary power unit (APU), batteries or ground facilities can provide power. The power is generated as 115 V alternating current (VAC) at 400 Hertz (Hz). The generated power is routed to the electronics bay containing transformers and safety systems. Some low power systems on the aircraft require DC power at 28 V, such as the avionics. Other high power systems require 270 V direct current (VDC) or 115 VAC [21].

Variable frequency power generation

The Airbus A350 and A380 and the Boeing 787 feature a variable frequency electrical system. The variable frequency generator (VFG) is directly coupled to the engine shaft through the accessory gearbox, making the frequency of the generated power dependent on engine speed with typical values between 350 and 800 Hertz [21]. A benefit of this system is the removal of the expensive and unreliable IDG. However, the complexity of the electric system is increased, especially on the Boeing 787 as shown in Figure 2.7.

On a conventional aircraft the power generated by the IDGs can be directly fed to the consumers from the distribution and safety systems in the E/E bay and power conversion is only required for systems such as the avionics and cabin entertainment. On the Boeing 787, multiple power standards have been adopted. Some systems are still supplied by the conventional 115 VAC 400 Hz constant frequency supply. Some of the newly electrified systems, such as the ECS compressor and engine starter require 270 VDC power. Operation of some systems is not dependent on supplied frequency, such as the cabin recirculation fans, galley ovens or the newly electrified wing IPS. These systems are supplied with variable frequency power and do not require conversion. Finally, the avionics and other low voltage systems still require the same low voltage system.

[19] J.A. Rosero, J.A. Ortega, E. Aldabas and L. Romeral. Moving towards a more electric aircraft. *IEEE Aerospace and Electronic Systems Magazine*, 22(3):3-9, mar 2007. ISSN 0885-8985. doi: 10.1109/MAES.2007.340500

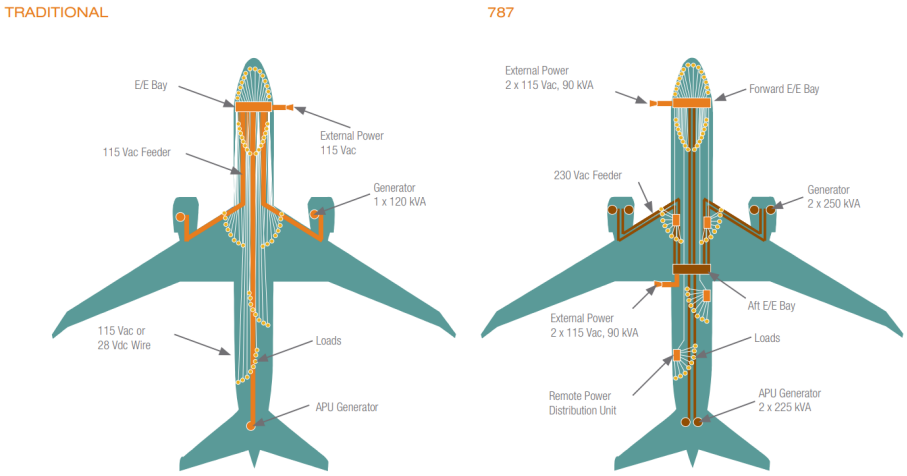

Figure 2.8: Schematic of conventional electric power distribution with all transformation equipment at one location compared to distributed electric power conversion, copied from Sinnett[11].

To conclude, a greater number of power electronic converters is required as a consequence of the variable frequency power generation system in combination with the increased number of electric systems.

It should be clear from this discussion that moving towards the MEA concept and replacing hydraulic and pneumatic systems with electronic systems increases the complexity of the electric power generation and conversion system. Still, the benefits seem to outweigh this increased complexity. Boeing reports reduced system weight and fuel consumption, in part due to the more electric architecture[11].

2.4.2. Electric power distribution

Typical values for power distribution are 115 VAC at 400 Hz as discussed in Section 2.4.1, which is mainly used by the cabin air circulation fans [15]. A 28 VDC bus is also present to power flight critical systems such as the avionics. In the Airbus A350 and A380 and in the Boeing 787 the constant voltage constant frequency bus is replaced by a constant voltage variable frequency bus. The generators are directly coupled to the engines and the CSD is removed, making the frequency dependent on engine speed through a gearbox. This results in the need for power conversion units for many systems. Furthermore, the voltage levels are increased to 230 or 400 VAC at 360 to 800 Hertz [20]. The increased voltage helps limit power wiring weight despite the increased power demand.

To better deal with the increased electric loads and the different power required by different systems, Boeing has redesigned the electric system architecture. Traditional aircraft have a single electrical/electronics (E/E) bay housing distribution and safety systems for distribution of electrical power to the aircraft systems. The B787 has a distributed system with two E/E bays and multiple remote power distribution units[11], see Figure 2.8. By distributing power at a higher voltage and converting power at the user, the system becomes more dynamic and weight is limited. The downside of requiring multiple power electronic converters has been used as an advantage for redesign of the distribution system. In comparison, the A350 has 28 VDC and a 115 VAC and 230 VAC system and a conventional lay-out for the conversion and distribution system[18].

2.5. The Retrofit Scenario

The lifespan of the average airliner is well over 20 years [4]. Typically, significant technological advancements are made in such a time period. It is not uncommon for operators to replace systems on ageing aircraft with updated systems in order to increase operating performance. These modifications need to certified and must be compatible with the existing aircraft configuration.

In the case of replacement of an electric component or system, the new part should fit into the existing electronics system of the aircraft. For components with low power consumption this rarely poses a problem. However, when replacing components with large power demand, this can prove more complex. In case of

[20] Xavier Roboam, Bruno Sareni and Andre Andrade. More Electricity in the Air: Toward Optimized Electrical Networks Embedded in More-Electrical Aircraft. *IEEE Industrial Electronics Magazine*, 6(4):6-17, dec 2012. doi: 10.1109/MIE.2012.2221355

replacing a pneumatic component with an electric component, such as the case discussed in this thesis, significant changes to the electronic power generation and distribution system are to be expected. The extend of these changes should be kept to a minimum in order to minimize time and cost investment of the aircraft operator.

3

Methodology

The aim of this research is to provide a first order estimate of the potential benefits on mission fuel requirements resulting from retrofit of an electric environmental control system architecture on a single aisle commercial aircraft. For this purpose a generic aircraft model is used, based on the Airbus A320. Sizing of the aircraft and performance over the mission profile is based on empirical sizing methods and general aircraft data. Engine performance is based on a sampling of actual engine performance data and linear interpolation between data points. Mission performance is calculated by dividing the flight profile segments in a number of time steps for which the steady state solution is computed. This aircraft model serves as a platform to which the system impact is appended.

To assess system impact on aircraft performance, a steady state component based system model is appended to the aircraft model. One system model represents the baseline CECS architecture, a second model represents the EECS architecture. Each component in the system is modelled separately based on simple physical principles and basic relations. The focus of the system modelling is at the ECS subsystem and its components, as this is the topic of this study. A basic representation of the electronics subsystem is included in the model to allow for honest comparison in the difference in shaft power off-takes between the two system architectures. To represent the retrofit scenario, the only difference between the CECS and EECS model exists in the additional components required for the EECS architecture.

The pneumatic flow rates through the system are dictated by the demand from the cabin component. Several factors contributing to the heat load of the cabin are considered, as discussed in Section 3.1.1. A supply temperature and flow rate requirement results from the cabin heat balance. This requirement serves as input to the components that supply regulated air and ultimately to off-takes from the engines. The same principle applies to the much simpler representation of the electric subsystem architecture, where generic electric load components demand power that ultimately is related to off-takes from the engines.

The effect of the system off-takes on mission performance is added to the aircraft platform model in terms of correction factors. The engine data table provides thrust and fuel flow correction factors for a given combination of shaft power and bleed air off-takes. These are added to the aircraft platform performance. This is an iterative process. When engine thrust is changed by the correction factor, a higher engine rating is necessary to provide the required thrust, increasing fuel flow and changing the correction factors.

Both the CECS and EECS model will be evaluated for a number of typical missions, based on an analysis from Husemann *et al.* [27]. This research has looked at the most frequently flown missions with A320 aircraft and plotted this in the payload-range diagram, see Figure 3.1a. The points in the payload-range spectrum that were analysed can be seen in Figure 3.1b. These points are grouped in a 'study', a set of different missions for which outputs are monitored. The outputs generated include take-off weight (TOW), landing weight, trip fuel weight and trip time. Here, the trip is defined from start of take-off until full stop at landing.

The defined study is executed for a number of cases to include relevant operating conditions. A baseline case is defined with a payload of 12000 kg, range of 1000 nm, ISA standard conditions and 160 passengers, based on a full 2-class arrangement [21]. ISA hot day and cold day are considered, Figure 3.2, as it is expected this will change the thermal requirements for the ECS due to a difference in solar intensity and a difference in heat loss or gain through conduction to the ambient. For ISA cold day the solar radiation during non-cruise phases is also reduced as will be discussed in Section 3.1.1. A different number of passengers is considered, namely full single class arrangement (196 passengers) and half-empty plane (80 passengers). This changes both the

[21] Airbus. A320 Family Aircraft. Web page. Accessed 13-03-2019. https://www.airbus.com/aircraft/passenger-aircraft/a320-family/a320neo.html

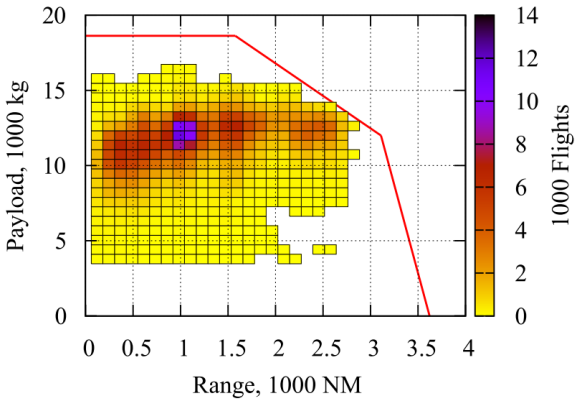

(a) Payload-range diagram of A320 with frequently flown missions, copied from Husemann *et al.* [27]

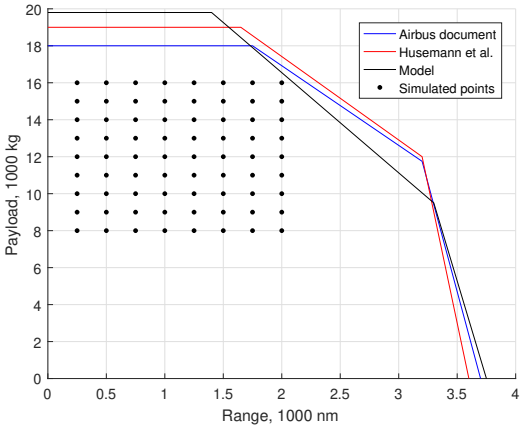

(b) Points in the payload-range spectrum that were used for analysis.

Figure 3.1: Payload-range diagrams of the Airbus A320 showing frequently flown missions and the points used for analysis to capture the most frequent missions.

Table 3.1: Overview of the different simulated cases in terms of ISA conditions, number of passengers and solar radiation value compared to nominal during cruise and non-cruise phases.

Case	**ISA Conditions**	$N_{\mathbf{pax}}$	**Cruise Radiation wrt Base, %**	**Non-Cruise Radiation wrt Base, %**
Baseline	Standard	160	100 %	100 %
Half pax	Standard	80	100 %	100 %
Max pax	Standard	196	100 %	100 %
Cold day	ISA cold	160	100 %	50 %
Hot day	ISA hot	160	100 %	100 %
Worst cold	ISA cold	80	0 %	0 %
Worst hot	ISA hot	196	150 %	150 %

thermal load on the ECS as well as the required ventilation rate, due to regulations requiring a fresh air mass flow per passenger [28]. This then directly affects the amount of bleed air required, impacting fuel consumption. A "worst case" hot day is simulated with ISA hot day conditions, less reflectivity of solar radiation and a full single class cabin and similarly a cold day with half-empty cabin with zero solar radiation, representing a night-time flight. This set of cases should represent conditions that are typically encountered as well as cases at the end of the spectrum for sizing purposes. An overview is presented in Table 3.1, where solar radiation values are given as percentage of the baseline case. A discussion of the values follows in Section 3.1.

In the remaining of this Chapter, firstly relevant thermodynamics and modelling regarding operation of the PACKs, the heat load in the cabin and the performance of electric motors and generators are discussed. This is presented in Section 3.1. Secondly, the implementation into the model is discussed in Section 3.2. Finally, Section 3.3 presents a discussion of the data generation and analysis methods.

3.1. Thermodynamic Modelling of Components

Three separate systems where the thermodynamic balance is considered can be identified. As discussed, the cabin thermodynamic balance drives the power demand of the ECS architecture. This balance is discussed in Section 3.1.1, where the relevant effects are described. The cabin thermodynamic balance results in a demand in supply temperature and flow rate for the ECS. Discussion of the mixer, which mixes the PACK outlet air with a fraction of recirculation air to reduce the bleed air demand, is also included in Section 3.1.1. This leads to a demand for PACK supply, of which the thermodynamics are discussed in Section 3.1.2. The PACK balance results in a supply air demand for the engines or CACs, depending on the ECS architecture. Thermodynamics of the CAC and electric generator is discussed in Section 3.1.3 to complete the discussion of the relevant thermodynamic systems.

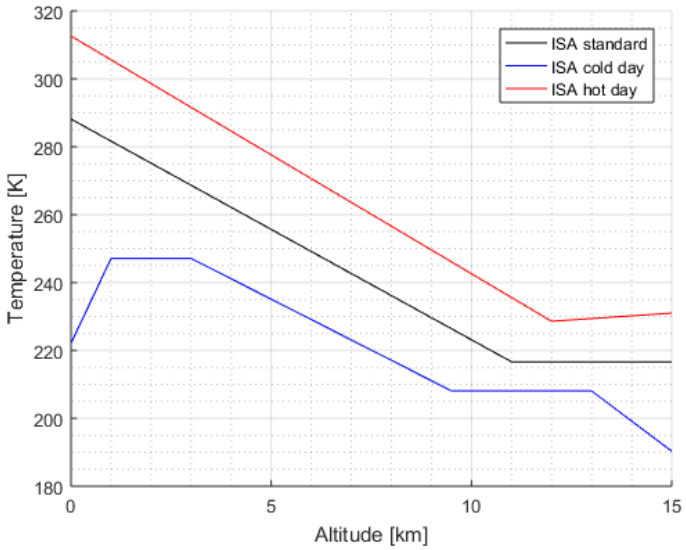

Figure 3.2: Temperature profiles for different ISA conditions as implemented in the model.

3.1.1. Cabin Thermodynamic Balance Model

To assess ECS behaviour, an adequate model of the cabin thermodynamics is required. The output of the ECS is determined by the cabin internal thermodynamic balance. When this balance is not modelled to the right order of magnitude, an overshoot or undershoot in required ECS performance can result from the model, ultimately affecting impact on fuel consumption. Therefore, careful consideration should be taken on the thermodynamic effects considered for the cabin. For this first order analysis, the heat loads in the cabin are averaged over the entire flight profile.

Other research has been performed requiring a thermodynamic model of an aircraft cabin. Yin *et al.* [29] used a 3D CFD model with passengers as surfaces with an elevated temperature and also included air inlets and outlets. The purpose was to look at the cabin thermal environment and temperature distribution as an effect of ECS operations. Frank *et al.* [30] used 2D CDF to model several cross sections of the aircraft cabin. The purpose was to evaluate different aircraft concept and characterize cabin airflow. When airflow patterns inside the cabin are not of interest, a parametric thermodynamic model of the cabin is sufficient. Such a model has been used for example by Shi *et al.* [12] and Chakraborty *et al.* [31]. While this type of model lacks detail as properties are averaged over the cabin, this level of detail is sufficient for this first order study of EECS potential. Therefore, such a model is adopted and discussed. The cabin is divided in two compartments, each with a volume equal to half of the effective A320 cabin volume, and a flight deck compartment to represent the cockpit [32].

Occupant and Equipment Heat Generation

Heat is generated by the passengers and crew in the cabin. Power consuming electronic devices in the cabin such as in flight entertainment and galleys also generate heat. This can be modelled by a steady state heat input into the system. Avionics equipment is typically cooled by air ventilation, resulting in additional heat load that can be added to the cabin for modelling purposes. For this research, in flight entertainment systems are excluded from the heat load, as these systems are typically not present on the short missions considered.

Based on EngineeringToolbox[22], a heat load of 100 Watt (W) per passenger, and 130 W per crew member is used for persons in rest and persons performing office or walking work. The heat load of galleys can also be estimated proportionally to the number of passengers, as a higher number of passengers typically corresponds to a larger number of galleys or more intensive use. Chakraborty *et al.* [31] uses 73 W per passenger and does not specify galley and electronic equipment heat load, while Shi *et al.* [12] uses a heat load of 75 W per passenger and additionally 320 W per passenger to represent the galley heat load. However, this is for a larger aircraft with in-flight entertainment systems for each passenger, typically not present on A320 aircraft.

Lampl *et al.* [26] presents a parametric overview of electric power requirements of miscellaneous systems

Table 3.2: A320 parametric electric loads contributing to ECS thermal load.

Parameter	Electric Load	Reference	A320 Parameter	A320 Power	Flight Phase
cabin lighting	40 $^{W}/_{m}$	cabin length	25 m	1 kW	all
galleys	250 $^{W}/_{pax}$	No. of passengers	196 (max)	49 kW	cruise
fuel system	0.136 $^{W}/_{kg}$	MTOW	73500 kg	10 kW	all
other lighting	-	-	-	2 kW	all
avionics	-	-	-	8 kW	all

including cabin lighting and galleys, listed in Table 3.2. Other users of electric power are also listed such as avionics and the fuel system, but these are not cooled by the ECS. To translate the electric loads into heat loads that contribute to the thermal balance, an efficiency of 85% is used, a somewhat lower number to compensate by the partly on purpose heat generation of the galleys. As indicated in Table 3.2, not all loads are active over the entire flight.

Evaluation of the aircraft platform model for the baseline mission yields results for the duration of each flight phase. The cruise phase has a duration t_{cruise} of 112.6 minutes, all remaining phases have a duration t_{other} of 51.1 minutes for a total mission time of 163.7 minutes. This is used to determine the average heat load of electric equipment Q_{equip} over the mission as shown in the following equation:

$$Q_{\text{equip}} = \frac{t_{\text{cruise}}\left(Q_{\text{galley}} + Q_{\text{lighting}}\right) + t_{\text{other}} Q_{\text{lighting}}}{t_{\text{cruise}} + t_{\text{other}}} \tag{3.1}$$

Filling in the numbers from Table 3.2, this results in a flight averaged equipment heat load of 5.5 kW. This number is assumed not to vary with number of passengers, as the installed power of the equipment does not change.

Based on this data, a heat load of 100 W per passenger, 130 W per crew member and 5.5 kW for electronic equipment is used. The total generated heat rate Q_{gen} generated by passengers, Q_{pax}, and equipment, Q_{equip}, is given by the following equation, where N_{pax} is the number of passengers:

$$Q_{\text{gen}} = N_{\text{pax}}\left(Q_{\text{pax}} + Q_{\text{equip}}\right) \tag{3.2}$$

Heat Loss to the Ambient

The fuselage skin is in contact with both the ambient conditions outside and the conditions inside the cabin. In general, a temperature difference will be present across the fuselage wall. Depending on the weather conditions and flight phase the temperature difference can cause a positive or negative heat flux, where heat addition to the cabin interior is taken as positive. Heat generated due to skin friction should also be taken into account as this has an effect on the skin temperature and heat exchange.

Heat loss to the ambient Q_{loss} in W can be represented with Equation (3.3) where T_{aw} is the adiabatic wall temperature and R_{tot} is the total thermal resistance of the cabin wall. The total thermal resistance of the cabin wall can be modelled as three thermal resistances in series [33], such that R_{tot} in K/W is given in terms of $R_{\text{conv,int}}$ and $R_{\text{conv,ext}}$ the internal and external convection resistance and R_{wall} the conductive resistance of the fuselage wall, by the following equations:

$$Q_{\text{loss}} = \frac{T_{\text{cabin}} - T_{\text{aw}}}{R_{\text{tot}}} \tag{3.3}$$

$$R_{\text{tot}} = \left(R_{\text{conv,int}} + R_{\text{wall}} + R_{\text{conv,ext}}\right) \tag{3.4}$$

[22] Engineering Toolbox. Metabolic Heat Gain from Persons. Accessed 18-07-2018. URL https://www.engineeringtoolbox.com/metabolic-heat-persons-d_706.html

Adiabatic Wall Temperature During flight the fuselage skin is heated by friction with the air. For an accurate model, this heat transfer should be taken into account. In a compressible airflow with temperature T_∞ in K and flow Mach number M the adiabatic wall temperature T_{aw} is given by the following equation, where r_c is the recovery coefficient:

$$T_{\text{aw}} = T_\infty \left(1 + r_c \frac{\gamma - 1}{2} M^2\right) \tag{3.5}$$

The recovery coefficient is a variable that depends on flow regime, thermal properties of the medium and flow type on the surface [23]. For simple calculations it can be estimated using the Prandtl number, a dimensionless number approximating the ratio of kinematic viscosity ν and thermal diffusivity α as given by the following equation:

$$\text{Pr} = \frac{\nu}{\alpha} \tag{3.6}$$

For laminar flow, the recovery factor can be estimated by the square root of the Prandlt number. For turbulent flow, the recovery factor can be estimated by the cubic root of the Prandtl number. Alternatively, Chakraborty *et al.* [31] uses the following equation:

$$r_c = 1 - 0.99\left(1 - \sqrt{\text{Pr}}\right) \tag{3.7}$$

For this research, the more widely used cubic root of Prandtl number for turbulent flows will be used. It is assumed most of the flow over the fuselage skin is be turbulent.

Cabin Wall Thermal Resistance The cabin wall thermal resistance, as presented in Equation (3.4), consists of three components. The internal convection resistance $R_{\text{conv,int}}$ can be expressed in terms of the convective heat transfer coefficient. Estimates of its value are readily available. Chakraborty [33] uses a value of 5 W/m^2/K for free air convection. However, it may be argued that convection inside the cabin is not free. Circulation of air in the cabin is continuously forced by circulation fans, so forced circulation is present at least at part of the boundary. Different sources [24] [25] state a value of 10 W/m^2/K for low speed flow over a surface. Because flow inside the aircraft cabin is not uniform, is blocked by various objects and can be complex, the value of Chakraborty [33] is used, as it is applied to a similar model.

The conductive resistance on the wall needs to be composed of the conductive resistances of the materials used, most importantly the aluminium skin and the insulation. It is more convenient to express this value in terms of the thermal conductivity since these numbers are more readily available for estimation. Based on general values[26] for the thermal conductivity of these materials and an assumption of their respective thickness, a thermal conductivity of the wall of 2.5 W/m^2/K is found [27]. Chakraborty [33] uses a value of 5 W/m^2/K which again is different, but no reasoning for the number is given.

The external convective heat transfer coefficient is heavily dependent on the ambient flow making it more complicated to determine. Furthermore, the outside flow varies greatly over the flight cycle from ground operations to cruise and back to ground. Chakraborty *et al.* [31] uses an estimation based on the non-dimensional Reynolds number (Re) and Prandtl number (Pr) as in the following equation, where Nu is the Nusselt number, x the characteristic length and k_∞ the thermal conductivity of the ambient:

$$\begin{aligned} h_{\text{ext}} &= \frac{\text{Nu} k_\infty}{x} \\ \text{Nu} &= 0.0296 \text{Re}^{4/5} \text{Pr}^{1/3} \end{aligned} \tag{3.8}$$

Total Cabin Wall Thermal Resistance Combining the different components as described above, the total cabin wall thermal resistance can be constructed. It is a function of ambient conditions, flow regime, Mach number, cabin wall materials, cabin internal convection and cabin wall area. Omitting the detailed terms, the total cabin wall thermal resistance R_{tot} in KW^{-1} expressed in terms of the determined convection and

[23] Adiabatic Wall Temperature, *Kurganov, V.A.* accessed 18-07-2018 [http://www.thermopedia.com/content/291/]

[24] Engineers Edge. Convective Heat Transfer Coefficients Table Chart. accessed 19-07-2018. URL https://www.engineersedge.com/heat_transfer/convective_heat_transfer_coefficients__13378.htm

[25] Thermopedia. Convective Heat Transfer. accessed 19-07-2018. URL http://thermopedia.com/content/660/

[26] Engineering Toolbox. Thermal Conductivity of Common Materials and Gases. Accessed 19-07-2018. URL https://www.engineeringtoolbox.com/thermal-conductivity-d_429.html

[27] Aluminium skin 1 mm thickness at 200 W/m^2/K, generic insulation 10 cm thickness at 0.03 W/m^2/K

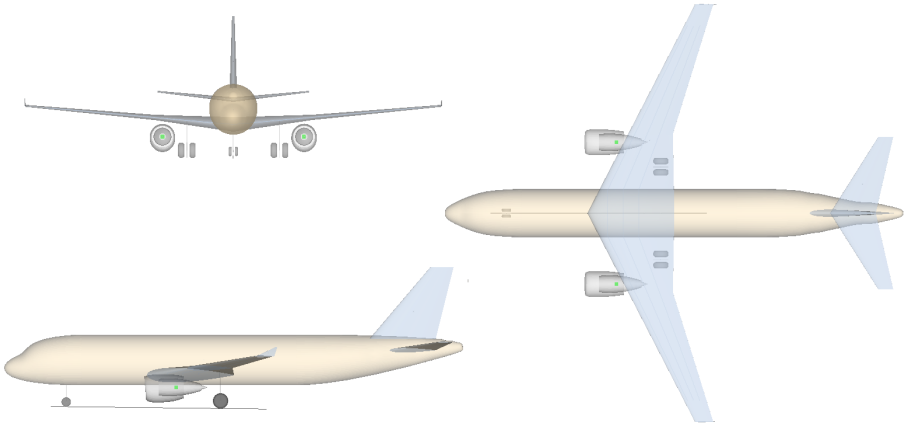

Figure 3.3: Overview of the A320 geometric model from the Pacelab library

conduction coefficients is given by the following equation, where A_{cabin} is the cabin surface area in m^2, h_{int} is the convection coefficient between the inner wall surface and the cabin air in $\text{W m}^{-2}\,\text{K}^{-1}$, k_{wall} is the wall thermal conductivity and h_{ext} is the convection coefficient between the outer wall surface and the ambient:

$$R_{\text{tot}} = \frac{1}{A_{\text{cabin}}}\left(\frac{1}{h_{\text{int}}} + \frac{1}{k_{\text{wall}}} + \frac{1}{h_{\text{ext}}}\right) \tag{3.9}$$

It should be noted that the value of R_{tot} is entirely based on assumptions, some of which are softly supported. It is therefore suggested that the model is tested for sensitivity to the value of R_{tot}. If the model appears to be sensitive to its value, a more accurate estimate can be attempted by not generalizing the cabin wall area. Instead, the internal and external area can be used for the respective transfer coefficients. If results after this are still not adequate, more accurate data needs to be acquired to better estimate its value.

Solar Radiation Heat Load

The intensity of solar radiation is affected by the atmosphere. Logically, the radiation intensity is increased at higher altitudes, because there is less attenuation by the atmosphere. Ahlers [34] suggest a method developed by Marggraf *et al.* [35] to calculate the increase in solar radiation with respect to altitude. However, this method is too elaborate for the scope of this research. Furthermore, there is continuous high speed airflow along the fuselage skin during flight, leading to a large convective heat transfer term, as discussed in Section 3.1.1. Therefore, according to Ahlers [34] the skin temperature increase due to solar radiation can be neglected, as the convective term will be dominant.

At sea level the solar radiation is approximately 1000 W/m^2 and 500 W/m^2 on a cloudy day. At cruise altitude this can be as high as 1350 W/m^2. To determine solar heat load, the projected area of the fuselage is considered. The cabin outer diameter of the A320 is 3.95 m and the fuselage length is 37.57 m [21]. However, the fuselage is not a perfect cylinder, so the surface area needs to be corrected. The cabin length is approximately 10 meters shorter than the overall length. As an estimation, the area of a cylinder of 30 m length is used where 25% of the non-cylindrical sections is added to the cabin length. This results in a projected area of 120 m^2, corresponding closely to the geometric model that was used for the A320, see Figure 3.3, where a top view projected area of 127 m^2 for the fuselage is found.

Not all energy is absorbed by the fuselage, a portion is also reflected. This reflection factor depends on paint colour and dirt on the skin amongst others and is estimated at 0.2 for white paint by Committee [36], which present official calculations and guidelines for aircraft system design. Using these methods and the following equation:

$$\dot{Q}_{\text{solar}} = A_{\text{p}}\,\alpha\,Q_{\text{sun}} \tag{3.10}$$

This results in a heat load of 32.4 kW at cruise altitude and 24 kW at sea level on a sunny day. On a cloudy day, solar intensity is approximately halved, resulting in a load of 12 kW at sea level.

Solar heat load is averaged over the mission based on duration of each segment. For the baseline mission, this means 112.6 minutes at cruise and 51.1 minutes in other flight stages as also discussed in Section 3.1.1.

The solar heat load is then averaged to 29.8 kW for ISA standard conditions. For a cold cloudy day, this is 26 kW. For worst case hot conditions a skin reflectivity factor of 0.3 is assumed, representing a more dirty aircraft with darker paint, resulting in a solar heat load of 44.7 kW. For worst case cold conditions, night time is assumed so the solar heat load is 0 kW in this case.

Calculation of ECS Supply Air Temperature

To complete the energy balance of the aircraft cabin, the heat input of the ECS needs to be included. When thermal equilibrium inside the cabin is assumed, the required ECS heat load can be determined and finally the ECS outlet temperature. In equilibrium, the ECS heat load (negative when cooling, positive when heating) is given by the following equation, where $\dot{m}_{\text{ecs}}$ is the air mass flow supplied by the ECS, T_{ecs} is the temperature of air supplied by the ECS and c_p is the specific heat of air:

$$\begin{aligned} Q_{\text{ecs}} &= Q_{\text{loss}} - Q_{\text{gen}} \\ Q_{\text{ecs}} &= \dot{m}_{\text{ecs}} c_p \left(T_{\text{ecs}} - T_{\text{cabin}}\right) \\ \Rightarrow T_{\text{ecs}} &= T_{\text{cabin}} + \frac{Q_{\text{ecs}}}{\dot{m} c_p} \end{aligned} \tag{3.11}$$

On modern commercial transport aircraft, part of the cabin air is recirculated and mixed with the PACK outlet air before being fed into the cabin. Defining ϵ_{recirc} as the fraction of recirculation air, the combined PACK supply air mass flow is given by the following equation:

$$\dot{m}_{\text{pack}} = \dot{m}_{\text{ecs}} \left(1 - \epsilon_{\text{recirc}}\right) \tag{3.12}$$

The required PACK supply air temperature T_{pack} can then be determined by evaluating the enthalpy balance between the ECS supply air, PACK supply air and cabin recirculation air as presented in the following equation:

$$\begin{aligned} \dot{m}_{\text{ecs}} c_p T_{\text{ecs}} &= \epsilon_{\text{recirc}} \dot{m}_{\text{ecs}} c_p T_{\text{cabin}} + \left(1 - \epsilon_{\text{recirc}}\right) \dot{m}_{\text{ecs}} c_p T_{\text{cabin}} \\ \Rightarrow T_{\text{pack}} &= \frac{T_{\text{ecs}} - \epsilon_{\text{recirc}} T_{\text{cabin}}}{1 - \epsilon_{\text{recirc}}} \end{aligned} \tag{3.13}$$

In some cases, the required temperature to be supplied by the ECS to achieve thermodynamic balance at the desired cabin temperature is below a practical limit. This limit is a result of passenger comfort and to prevent condensation inside the pneumatic ducts. When this is the case, Equation (3.13) is rewritten to solve for the required ECS and PACK mass flows at the fixed ECS outlet temperature.

3.1.2. PACK Thermodynamic Performance Calculations

Thermodynamic analysis of the reverse Brayton cycle is similar to analysis of the Brayton power cycle [13] [19], making use of isentropic component efficiencies and isentropic relations. Thermodynamic analysis of heat exchangers also uses the standard relations of the number of transfer units (NTU) method, based on heat capacity of the hot and cold flow and the heat exchanger effectiveness. The use of standard equations simplifies the thermodynamic analysis of the PACK.

Different calculation schemes can be used. Moran and Shapiro [13] assumes known compressor inlet temperature, pressure and volumetric flow rate, compressor and turbine compression ratios and turbine inlet temperature. These inputs are used to determine power required by the compressor, power delivered by the turbine, refrigeration capacity and coefficient of performance. do Porto Neves Júnior *et al.* [37] takes a more inclusive approach, analysing the complete cycle including aircraft main engine compressor. Cabin pressure is used as outlet pressure for the final turbine and it is assumed the turbine powers the ACM.

In the component based model for this thesis, the engine compressor is already included in the engine component model, so only the PACK must be considered. As discussed in Section 2.2.1, the PACK consists of a number of additional components to enhance the ACM performance. These components are omitted in this first order study, as the vapour content of the gas is not considered and these components only have a minor effect on pressure loss which can be captured by the radiator pressure loss. Two heat exchangers, a compressor and a turbine are included in the model. The formulas used for analysis are the general isentropic relations with isentropic efficiency factor used for turbomachinery applications, for example by Van Buijtenen and Visser [28]. Compressor and turbine performance has already been discussed in Section 2.3.

[28] Jos P. van Buijtenen and Wilfried P.J. Visser. *Gas Turbines, WB4420/4421* [Lecture notes]. Fourth edition, 2009.

The following will be a discussion of general equations for each component of the ACM. When applied to the model, these are combined and rearranged to solve for the unknown parameters. The PACK will be modelled as a single component in the system. The final PACK outlet temperature, pressure and flow rate are known, as they follow from the analysis of cabin thermal load presented in Section 3.1.1. Ambient conditions are also known and through ram air inlets give the coolant temperature and pressure. PACK entry pressure and temperature result from the engine model in the CECS architecture or from the CAC model in the EECS architecture. The PACK supply mass flow follows from the cabin demand. The coolant mass flow follows from the balance of the radiator components. Pressure ratio of the compressor and turbine are linked through the power balance. When all equations are combined, this system can be iteratively solved to reach a steady state solution that fits the desired output and given input conditions.

Heat Exchanger Performance Analysis

Energy extracted by the heat exchanger is dependent on heat exchanger design, represented by effectiveness, and temperature differential. The outlet temperature after the heat exchanger can be determined with the standard isentropic heat exchanger equation using heat exchanger effectiveness as given by the following equation, where T_{out} and $T_{,in}$ are outlet and inlet temperature, ε_{hx} is the heat exchanger effectiveness and ΔT is the temperature difference between the working fluid and the heat sink:

$$T_{out} = T_{in} - \varepsilon_{hx} \Delta T \tag{3.14}$$

When inlet and outlet conditions of the heat exchanger are not specified, as is the case when the entire PACK is modelled as a single component, the heat exchanged can be computed by the number of transfer units (NTU) method [29]. It is based on the maximum possible heat exchange between two fluids and the effectiveness of the heat exchanger, which is based on the fluids' heat capacity ratio.

First, the heat capacity rate is defined as the mass flow multiplied with specific heat. The capacity rate ratio $C$of the heat exchanger is then given by the following equation, where $C_{gas,min}$ and $C_{gas,max}$ are the heat capacity rate of the fluid with the lowest and highest capacity rate respectively:

$$\begin{aligned} C_{gas} &= \dot{m}_{gas} c_p \\ C &= \frac{C_{gas,min}}{C_{gas,max}} \end{aligned} \tag{3.15}$$

The number of transfer units can then be computed with the following equation, where U and A are the radiator overall heat transfer coefficient and heat transfer area:

$$N = NTU = \frac{UA}{C_{min}} \tag{3.16}$$

The heat transferred now depends on the radiator effectiveness and the maximum achievable heat transfer, which are determined with the following equations, where Q and Q_{max} are the actual and maximum achievable heat transfer, $T_{hot,in}$ and $T_{cold,in}$ are the cold and hot flow inlet temperature and ε is the heat exchanger effectiveness:

$$\begin{aligned} \varepsilon &= \frac{Q}{Q_{max}} \\ Q_{max} &= C_{gas,min} \left(T_{hot,in} - T_{cold,in} \right) \\ \Rightarrow Q &= \varepsilon Q_{max} \end{aligned} \tag{3.17}$$

Finally the heat exchanger effectiveness must be computed to close the system of equations and obtain a result for the heat transfer. The heat transferred in a heat exchanger depends on the layout of the flows, leading to different effectiveness values for parallel flow or counter flow arrangement for example. The NTU method is able to capture this effect, by providing different equations for effectiveness, depending on flow type. As no data is publicly available about PACK radiator design, three typical arrangements are implemented and

[29] S.B.A. Invent. Effectiveness - NTU Method. Accessed 21-12-2018. https://sbainvent.com/heat-transfer/heat-exchangers/effectiveness-ntu-method/

importance of the assumption is checked in the sensitivity study described in Chapter 4. The following equations give the heat exchanger effectiveness for parallel flow, counter flow and cross flow heat exchangers respectively:

$$\varepsilon = \frac{1 - e^{N(1+C)}}{1+C} \tag{3.18}$$

$$\varepsilon = \frac{1 - e^{-N(1-C)}}{1 - Ce^{-N(1-C)}} \tag{3.19}$$

$$\begin{aligned} n &= N^{-0.22} \\ \varepsilon &= 1 - e^{\left[\frac{e^{nNC}-1}{nC}\right]} \end{aligned} \tag{3.20}$$

Ram Inlet Performance Analysis

Ambient air to supply the cold side of the PACK heat exchangers and to supply the CACs of the EECS architecture is drawn in by ram inlet components. These inlet components are modelled with standard isentropic relations with an efficiency factor [38]. In practice, the inlet area is controlled during the flight to supply the optimal airflow for cooling of the bleed air in the PACK radiators. This level of detail is outside the scope of this first order analysis. Therefore, the inlet area is fixed at a value that always allows sufficient cold flow supply as demanded by the PACK. The analysis of the inlet and its contribution to drag due to deceleration of the flow, represented by ΔD, are described by the following equations:

$$\begin{aligned} p_{t,out} &= p_{t,in}\left(1 + \eta_{inlet}\frac{\gamma-1}{2}M^2\right)^{\frac{\gamma}{\gamma-1}} \\ T_{t,out} &= T_{t,in}\left(1 + \frac{\gamma-1}{2}M^2\right) \\ \dot{m} &= \rho A_{inlet} V \\ \Delta D &= \dot{m} V \end{aligned} \tag{3.21}$$

Ram Outlet Performance Analysis

Outflow of the PACK heat exchanger cold side flow is modeled by ram air outlet components. A portion of cabin recirculation air is also dumped, in order to maintain constant pressure, by a ram air outlet. Analysis of the outlet components is similar to the inlet, it is also modelled with isentropic relations. In the case of the outlet, the outlet pressure is the ambient, so it is a known quantity. Instead, the velocity must be calculated. This is described by the following equation:

$$\begin{aligned} T_{t,out} &= T_{t,in}\left[1 - \eta_{outlet}\left(1 - \Pi^{\frac{\gamma-1}{\gamma}}\right)\right] \\ V &= \frac{\dot{m}}{\rho A_{outlet}}\Delta D \qquad\qquad = \dot{m} V \end{aligned} \tag{3.22}$$

The outlet area is chosen such that the flow is never chocked, while in reality the outlet area is controlled for optimum performance. This way of modelling results in an error in the model. However, the ΔD are very small and the inlet and outlet area have negligible impact on the system results, as shown in Section 4.2.

3.1.3. Cabin Air Compressor and Electric Generator Modelling

Analysis of the compressor performance itself uses the same methods as described in Section 3.1.2, but is less complex. The inlet conditions follow from intake of the ambient conditions and the flow rate follows from the supply demand of the cabin. Outlet pressure is prescribed at a fixed overpressure ratio of the cabin pressure. The two compressor equations as follows can now be solved for the two unknowns, the outlet temperature $T_{t,out}$ and compression power P_{comp}:

$$T_{t,out} = T_{t,in} + \frac{T_{t,in}}{\eta_{comp}}\left[\Pi_{comp}^{\frac{\gamma-1}{\gamma}} - 1\right] \tag{3.23}$$

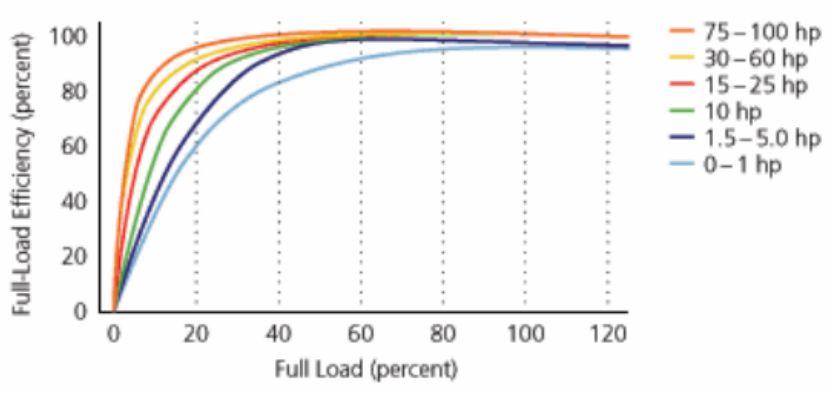

Figure 3.4: Typical electric motor efficiency curves as function of load, copied from Burt *et al.* [1]

$$P_{\text{comp}} = \dot{m} c_p \left(T_{\text{t,out}} - T_{\text{t,in}} \right) \tag{3.24}$$

The overpressure ratio defined for the CAC is required to supply the PACK with energy, which it takes from air flowing through the system, and to compensate for pressure losses. When this ratio is increased, more work is required by the CAC to compress the ambient air to the pressure target. This extra work directly translates to more power off-takes on the engine, through the generator and gearbox. Through analysis of the PACK entry temperature for a similar aircraft by ADSE B.V.[30], this ratio was estimated to 10% overpressure compared to cabin conditions. In reality, this number would vary over the flight envelope, but for this first order study it is kept constant.

The CAC is powered by an electric motor. Through a shaft power efficiency factor the required shaft power to be delivered by the motor is obtained. The electric motor itself also has a certain efficiency, dependent on the load factor [39]. Electric motor behaviour is complex to analyse in detail, but is more or less constant over a wide range of power ratings. Therefore, a constant efficiency of 90% is used for this first order study. This then results in a power demand to be supplied by the electric generators.

Many types of electric generators exist. On aircraft, typically an IDG in installed, which is a generator coupled with a gearbox. This unit generates constant frequency, constant voltage power independent of engine shaft speed. Power efficiency is dependent amongst other on the load factor, the ratio of output power to nominal power, and drops especially fast when power demand is higher than nominal power [40]. Since IDG behaviour is complex to model, a simplified generic generator model is used. Efficiency with respect to load factor is given by Figure 3.5 [31]. The load factor γ on the x-axis is given by the following equation, where P_{nom} is the nominal power and P_{out} is the output power:

$$\gamma = \frac{P_{\text{nom}} - P_{\text{out}}}{P_{\text{nom}}} \tag{3.25}$$

As indicated in the Figure, when output power is 25% more than nominal power, efficiency is reduced to 50%. On the other hand, when output power is 50% of nominal power, efficiency is 95%.

3.2. Model Implementation and System Model Impact on Mission Performance Analysis

The following is a description of the implementation into the model of the methods that were discussed. As was discussed in the introduction to this chapter, a generic aircraft model of the Airbus A320 is used as platform. Two models representing the CECS and EECS system architecture are then added to this platform and results are compared. Pacelab SysArc is used as the modelling tool for this research. It is a commer-

[31] Taken from Pacelab Sysarc Knowledge Database. Modelled to represent generic generator behaviour, as was discussed with Pacelab support department.

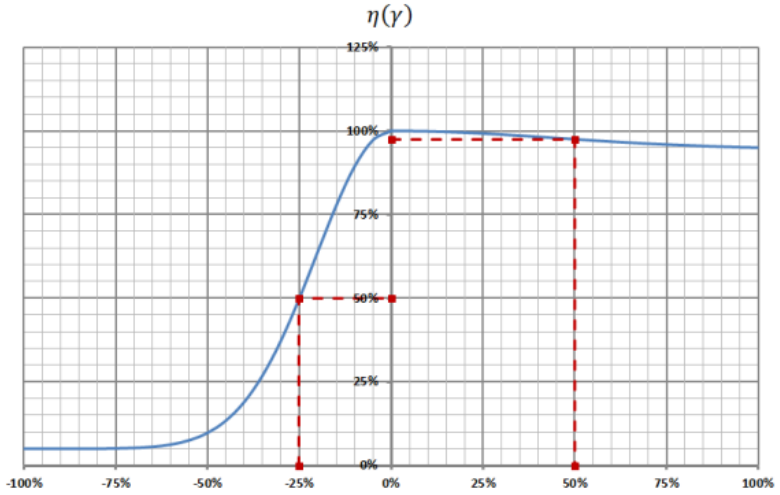

Figure 3.5: Generator efficiency with respect to load factor, copied from Pacelab Sysarc Knowledge Database[31]

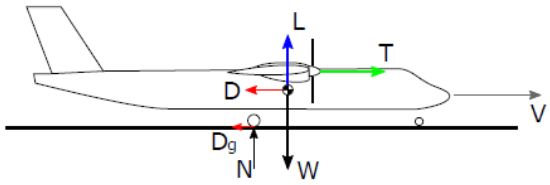

(a) Generic free body diagram of an aircraft moving with velocity V on the ground, showing lift L, weight W, thrust T, drag D, ground drag D_g and normal force N, copied from Zamboni [41].

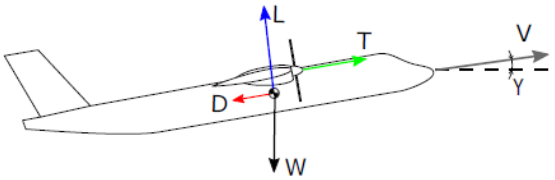

(b) Generic free body diagram of an aircraft moving with velocity V in the air, showing lift L, weight W, thrust T, drag D and flight path angle γ copied from Zamboni [41].

Figure 3.6: Generic free body diagrams for an aircraft on the ground and in the air.

cially available knowledge-based software package that is designed for aircraft preliminary sizing and system architecture impact analysis at aircraft level[32]. The A320 model platform is provided by Pacelab [32].

The model is mostly based on a geometric model of the A320 and quasi-empirical sizing methods such as Toorenbeek and Raymer, calibrated in such a way that they represent the A320 within an acceptable margin. This results in estimations for aircraft weight definitions, such as operational empty weight (OEW), and in a number of aerodynamic coefficients, wing and power loading, field length requirements and more. To compute mission performance, a flight profile is defined and each segment is divided in a number of time steps. A point performance analysis is performed at each time step, resulting in a thrust requirement at each point. The point performance analysis is presented in Section 3.2.1.

The system diagrams for the CECS and EECS architecture are discussed in Section 3.2.2, including a discussion of the components that were not discussed in Section 3.1.2. Furthermore, the way that off-takes are determined and imposed on the system results is treated.

3.2.1. Point Performance Analysis

With the aircraft thrust loading and aerodynamic performance sorted and the MTOW of the A320 known, the point performance analysis can be used to calculate thrust required at each time step. The point performance uses the simple equations of motion for an aircraft. Two sets of equations are defined. The first set applies to ground operations of the aircraft, the second set applies to flight segments. Equations for the lift and drag coefficient are defined, as they vary depending on flight segment (due to flap or landing gear deployment), flight conditions and aircraft attitude. To close the set of equations additional equations or assumptions are required, which are listed for each segment.

The free body diagram of a generic aircraft on the ground is presented in Figure 3.6a and is used to derive

[32] TXT e-solutions. Aerospace & Aviation. Accessed 23-07-2018. https://www.txtgroup.com/markets/aerospace-aviation/

the equations of motion applicable during taxi and take-off. Using thrust T, aerodynamic drag D, ground resistance D_g, air density ρ, speed V, wing reference area S, aerodynamic drag coefficient C_D, ground friction coefficient μ, aircraft weight W, aircraft lift L and drag increment caused by deployment of flaps or landing gear ΔC_D, the aircraft mass m, the gravitational acceleration g and air density ρ, the equations of motion are as follows:

$$\begin{aligned} F = m \cdot a &= T - D - D_g \\ D &= \frac{1}{2}\rho V^2 S C_D \\ D_g = \mu (W - L) &= \mu \left(m \cdot g - \frac{1}{2}\rho V^2 S C_L \right) \end{aligned} \tag{3.26}$$

The free body diagram of a generic aircraft during flight is presented in Figure 3.6b. The main difference with the aircraft on the ground is the removal of ground resistance and the addition of the flight path angle γ, which has an influence on the equations of motion and the aerodynamic coefficients. The set of equations describing the motion of an aircraft in flight is given by the following equations, where AR is the wing aspect ratio and e is the wings' Oswald factor:

$$\begin{aligned} F_{\text{net}} = m \cdot a &= T - D - m \cdot g \cdot \cos(\gamma) \\ D &= \frac{1}{2}\rho V^2 S C_D \\ L = \frac{1}{2}\rho V^2 S C_D &= m \cdot g \cdot \sin(\gamma) \\ C_D &= C_{D,0} + \frac{C_L^2}{\pi A R e} + \Delta C_D \end{aligned} \tag{3.27}$$

To close the set of equations of motion for an aircraft during flight, two additional equations or constraints are required as described below. This leads to a solvable set of equations that can be solved for each time step. The results of a particular time step serve as input conditions to the next time step. This way, a required thrust for each time step can be determined. Through the engine model this leads to a fuel flow for each time step, which can be integrated to obtain the total mission fuel requirement.

Take-off A constand flight path angle γ and constant engine power rating are assumed. The latter allows for the engine model to provide a thrust value.

Climb During climb also a fixed engine power rating is selected. The acceleration of the aircraft is determined by assuming a constant calibrated air speed (CAS), leading to a division of thrust to climb and acceleration. When the cruise Mach number is reached, this Mach number is kept constant until the top of climb at 31000 feet.

Cruise Steady state motion is assumed, so the acceleration is zero and the flight path angle is zero.

Descent A constant rate of descent is assumed together with the same CAS procedure as during climb.

Landing During the first part of the landing segment until touchdown a constant approach speed and angle are assumed.

3.2.2. System Model and Performance Impact

In order to model the effect of aircraft systems, the general aircraft platform model as discussed in Section 3.2.1 needs to be augmented with models for the systems under consideration. This is done by logically connecting the separate component model blocks according to the system diagram. When these are connected they represent a system of equations that can be iteratively solved.

To evaluate system impact on the mission performance, the bleed-air and shaft power requirements are evaluated for an array of points covering the A320 flight envelope, as determined by the quasi-empirical sizing of the aircraft model platform. These off-takes can be translated by the engine model to a penalty factor for the thrust and fuel flow. When the mission is evaluated, these factors are then included in the point performance calculations, resulting in modified mission performance results compared to the aircraft model platform.

In the following discussion, first the ECS system diagram is presented. This architecture will remain unchanged for the CECS and EECS system, only the air supply will be changed. Secondly, the system diagram

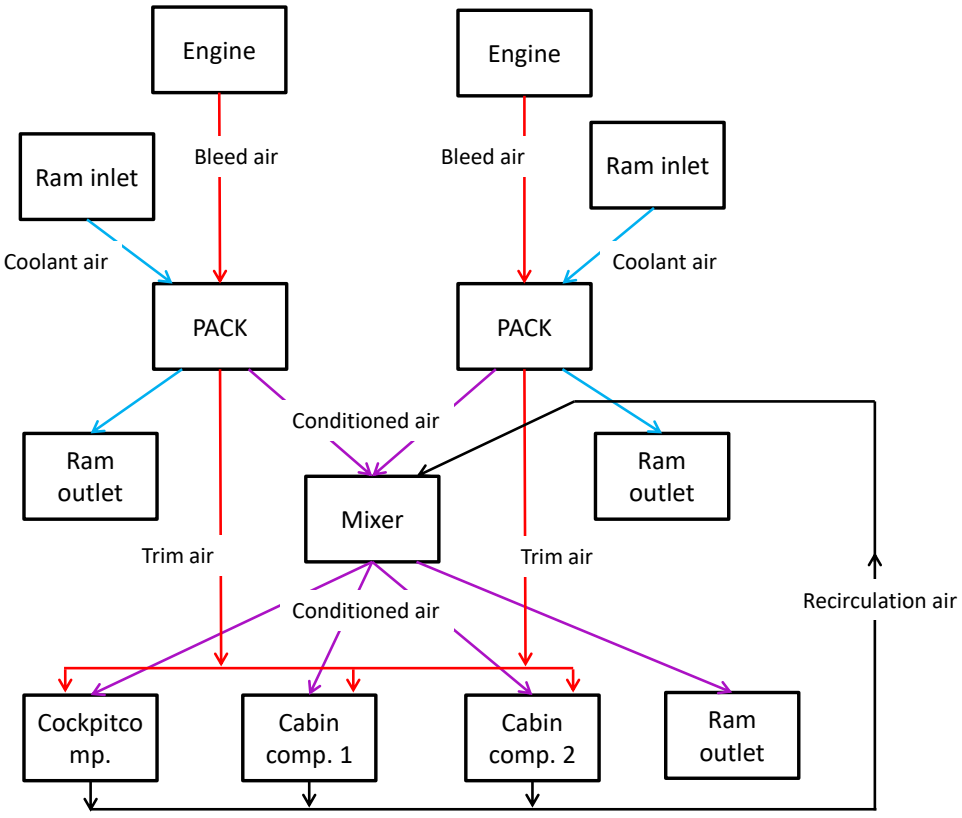

Figure 3.7: System diagram of the CECS architecture as implemented in the model, including indication of different air flows.

of the electric subsystem that represents the loads of avionics and miscellaneous systems are presented, followed by the discussion of modifications made to these systems to arrive at the EECS architecture.

CECS System Diagram

The ECS is modelled such as to represent the system architecture of the A320 [33]. The ECS part of the system diagram can bee seen in Figure 3.7 and represents the process described in Chapter 2. Following the actual aircraft, three compartments where flow is regulated are modelled, the cockpit and two cabin compartments representing cabin zones of the A320 [33]. This allows the model to be used for exploration of different cabin environments within the same aircraft, which is outside the scope of this thesis. Modelling of these compartments, as well as modelling of the PACKs, mixer and engines is already discussed in Sections 2.3, 3.1.1 and 3.1.2.

Electric Loads System Diagram

The electric loads of the aircraft, partly discussed in Section 3.1.1, are modelled as simply as possible. Two 115 VAC electric load components each represent half of the electric power usage of the aircraft. The efficiency of these components or the losses associated with the electrical wires are not taken into account. Accurate modelling of the electronics system is outside the scope of this research. These loads are represented to allow for comparison of the EECS power requirement compared to the baseline A320 power requirements.

The avionics loads are on a separate system. Power is first transformed from 115 VAC to 28 VDC by a transformer and then fed to the avionics load. For these components, also the efficiency is not taken into account. Converting the voltage to the correct level has an effect on the current required. While this has no effect on the current model, it enables the extension of this model to include for example energy losses in the wiring.

EECS System Diagram

The PACK portion of the CECS system architecture remains unchanged for the EECS system. This way the retrofit scenario is represented. By leaving the PACK components unchanged, only the effect of a different

[33] Airbus. A320 Flight Crew Operating Manual. *Instruction Manual*

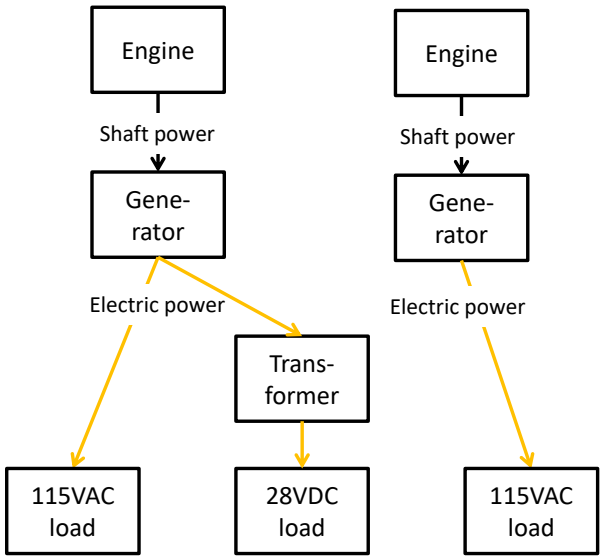

Figure 3.8: System diagram of the electronics system architecture as implemented in the model.

supply source is evaluated. In the EECS case, no bleed air is extracted from the engines. Instead, the PACK is supplied by ambient air compressed by electric CACs, which are powered by the generators. The system diagram is shown in Figure 3.9.

3.2.3. Engine Model Implementation

Correct implementation of the engine performance in the model is required for accurate results. Furthermore, the model should be quickly evaluated to prevent long simulation times. Therefore, engine performance is simulated only once and the results are tabulated. This way, for any combination of flight conditions, power rating and off-takes, the required data can be easily extracted from the table, which essentially represents a response surface. Through linear interpolation, any combination of inputs yields a response from the model. Verification of the engine model is discussed in Chapter 4.

3.2.4. Practical Modelling Limitations

As with any project, some practical limitations must be considered. First of all, the timespan of this research project is limited to 30 weeks. This means the scope of this research is limited to only one aircraft and one electric ECS architecture. In reality, multiple architectures fitting a retrofit scenario can be identified. These should be the focus for other research projects.

A second limitation lies in the availability of reliable data. General dimensions and parameters of A320 aircraft design are readily available, even some data is published by Airbus itself [21]. Some more specific data, such as installed generator power or PACK schematic, are found through online research and can be used if the same values are mentioned on multiple non-scientific sources. Detailed data however, such as PACK sizing parameters, ram inlet and outlet performance and reference values for ECS or IPS bleed flow are not available. This data is often proprietary and therefore not available for this research. This means some values need to be estimated based on engineering best practise. Automatically this results in a model error that is not readily measured or verified. A sensitivity study of these input parameters is performed to check influence on the model and importance of using correct values.

A further limitation is the fact that Pacelab is restricted to static calculations, transient calculations are not possible. In general, this is not a big limitation for the purpose of this research. However, as mentioned before in Section 3.1.1, the expected sizing condition for an ECS system is a transient case. To cope with this limitation and approach the sizing criterion, worst case hot and cold conditions are used for system sizing.

I final limitation worth mentioning is inherent in the way system impact on the mission performance and fuel burn is determined. Based on a set of user-defined flight conditions specifying flight conditions for flight segments, the system architecture is evaluated on a predefined number of points in the flight envelope. This results in a matrix storing shaft power and bleed air requirement information over the flight envelope. When

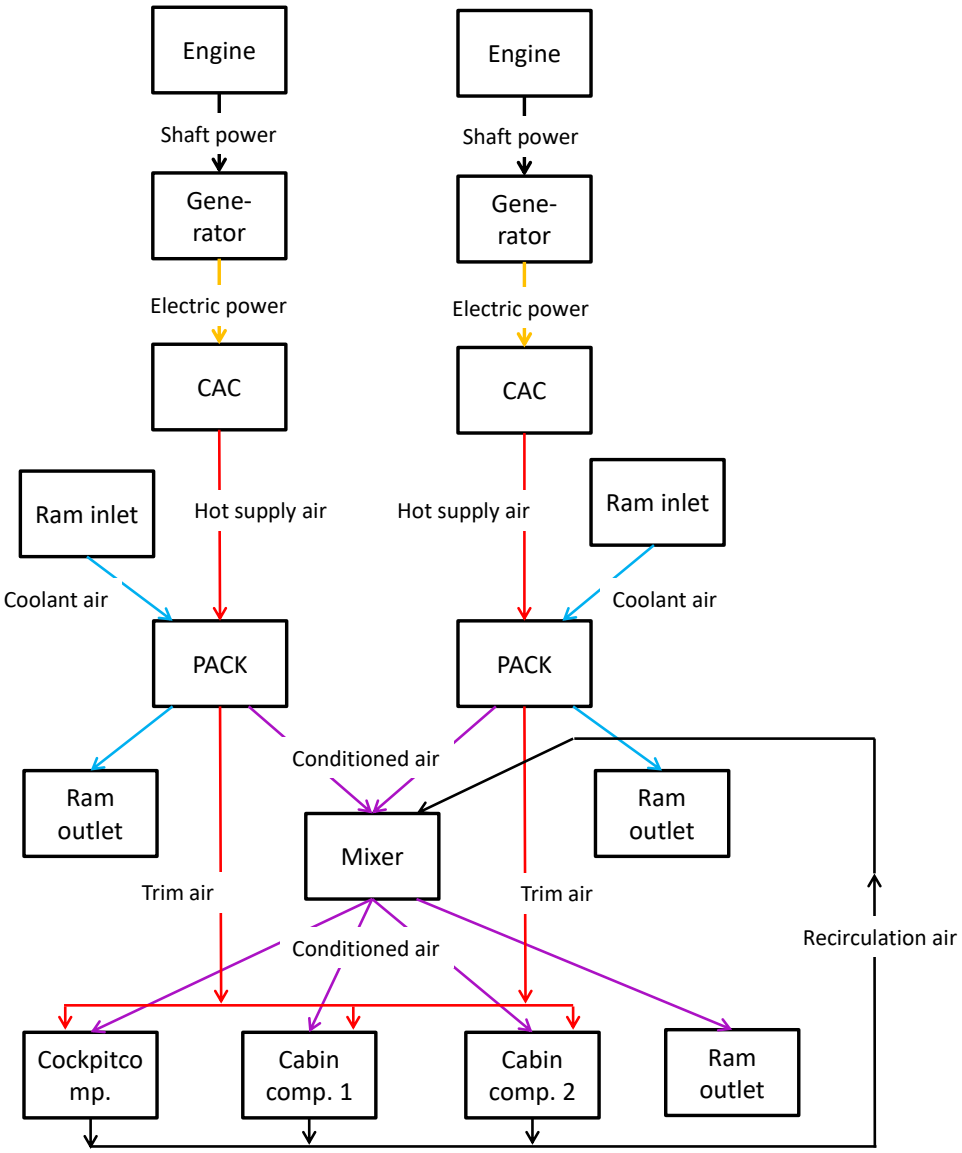

Figure 3.9: System diagram of the EECS architecture as implemented in the model, including indication of different air flows.

performing a study to determine mission performance for a number of different missions, this matrix is not evaluated at runtime, but simply consulted at each time-step to determine the system impact on the thrust and fuel consumption, which is then corrected. Interpolation between the points is performed when necessary. This way of evaluating system impact results in a rather static set-up. Connecting the payload to the number of passengers, for example, becomes a rather time intensive process as the number of passengers affects the system power and bleed air demand. Therefore, the payload is considered as an independent variable, resulting in some combinations of payload and number of passengers that are impractical.

3.3. Data Generation and Analysis

Two types of data are generated with the models. Mainly, for the simulated points in the payload-range diagram presented in Figure 3.1b, total mission quantities were generated, most importantly trip and block fuel. This means for each of the simulated points, the total amount of fuel required to fly that mission was output, but no intermediate data points were exported. Other monitored parameters include take-off weight and landing weight, but these are not included in this analysis for conciseness. These data points do not require any filtering and can be used directly to generate graphs and tables used to draw conclusions.

The second type of data consist of detailed data for a particular flight mission. The baseline mission, defined

at 1000 M range with 12000 kg payload is chosen to inspect this data. This mission is most frequently flown, as can be seen from Figure 3.1a [27]. The detailed data is generated for every timestep for which the equation system is solved, resulting in a complete flight history. The data extracted this way includes fuel consumed up to the particular time step, current mass of the aircraft and for each engine momentary thrust, fuel flow, bleed air and shaft power off-takes. This data is also ready to use, except for some formatting to allow easy processing.

4

Verification and Validation

Verification and validation are crucial steps whenever a model is used to generate results. Without these steps, no confidence can be placed on the generated data. Verification is the process of checking if the components used and the model itself are correct. This is discussed in Section 4.1. Another factor to consider is the sensitivity of the model to input parameters. In order to close the system of equations making up the model, a number of parameters need to be assumed. By performing a sensitivity study of these parameters, the importance of correct estimation of these parameters becomes clear. When sensitivity to a parameter is low, the accuracy with which it is set is less critical than for a parameter to which the system response shows a large sensitivity. The sensitivity study is discussed in Section 4.2. Validation is the process of checking that the model delivers the desired outputs and is discussed in Section 4.3.

4.1. Verification

Verification is the process of confirming that the model components are performing correctly. Since the models used for this thesis consist for a large part of physics-based components, a large portion of this process consists of verifying that the physical equations are correctly implemented. This is done by physically checking the equations used against theory and by isolating the components and checking the response to a change in input. Correct behaviour of each component was verified during the modelling process and implementation of the physical behaviour, as discussed in Chapter 3. For conciseness, these basic components are not discussed in detail in this work. Only verification of the engine is discussed, since it is more complex and requires additional analysis to verify the model.

4.1.1. Verification of Engine Response to Off-Takes

As discussed in Chapter 3, thrust and fuel flow for the engine at each point in the mission simulation is determined by consulting a large table. This table contains data points for a number of combinations of altitude, temperature, power rating, bleed air off-takes and shaft power off-takes combinations and provides not only thrust and fuel flow, but also bleed air temperature and pressure. The effect of off-takes on the nominal thrust and fuel flow values is determined with correction factors.

The most important thing of engine model verification for this research is to confirm the response in performance to a variation in off-takes follows the correct trend. The absolute response is of less interest. A comparison in mission fuel burn is made between two models with the same engine behaviour, so any absolute error is present in both results and has no impact on the answer to the research question. The best way to analyse the trend in performance response to off-takes is to analyse the indicative sfc correction factor, which is computed by dividing the fuel flow correction factor by the thrust correction factor as presented in the following equation, where f_{sfc} is the indicative sfc correction factor, f_{fuelflow} is the fuel flow correction factor and f_{thrust} is the thrust correction factor:

$$f_{\text{sfc}} = \frac{f_{\text{fuelflow}}}{f_{\text{thrust}}} \tag{4.1}$$

To verify the engine in the model, a verified engine performance card deck for a comparable turbofan engine as installed on the A320 was loaded into the Pacelab model. This was done to ensure model response of both engine datasets is similar. The indicative sfc for both engines was computed and plotted in order to compare the effects. Since the two datasets are not for the same engine, a step difference is to be expected. However, as the purpose of this study is to compare data from two similar models and as explained previously,

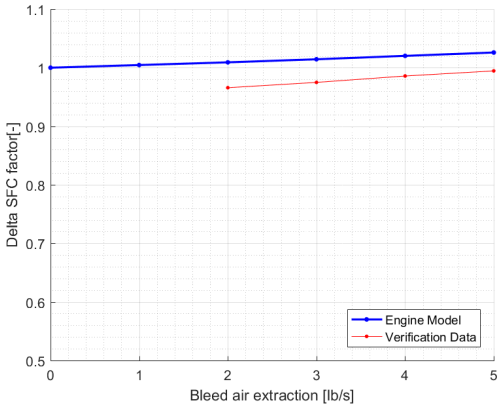

(a) Comparison of indicative specific fuel consumption correction factor for variation in bleed air off-takes, showing similar trend in response for both engine data sets.

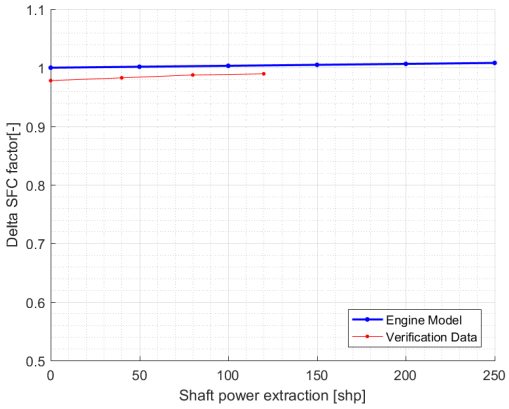

(b) Comparison of indicative specific fuel consumption correction factor for variation in shaft power off-takes, showing similar trend in response for both engine data sets.

Figure 4.1: Comparison of indicative specific fuel consumption correction factor for variation in off-takes for verification of the engine model response. A step difference and small slope difference are acceptable and expected, due to difference in engines for which data is used.

a step difference has no net effect on the results. Rather, the trends in performance by variation of certain parameters and conditions observed for the implemented engine model should be similar to those observed for the verification dataset to consider the model verified.

Figure 4.1a shows a comparison of the effect of increasing bleed air off-takes on the indicative sfc correction factor for the engine model and the verified engine data. It is clear that for both datasets the increase in bleed air extraction results in an increase in sfc, as would be expected. As discussed in Section 3.2.3, work is performed on the bleed air before the bleed air port, which can not be extracted by the turbine. As a result, sfc rises. Even though the trends of the two engine datasets do not have exactly same slope, the difference is small enough that the model is accepted for this first order study.

Figure 4.1b shows a comparison of the effect of increasing shaft power off-takes on the indicative sfc correction factor for the engine model and the verified engine data. Again, both datasets show an increase in sfc with increasing shaft power off-takes. A slight kink is visible in the verification data, showing a larger slope for low shaft power off-take values. For increasing shaft power off-takes, the slopes of the two datasets are close to identical, meaning that the same trend is found for the off-take values that are expected. Therefore, the engine model is accepted.

A comparison in engine behaviour for variation of other parameters was also made. The effect of off-takes on bleed air pressure and temperature and shaft speed was investigated, as well as the effect of varying temperature, altitude and mach number. These results proved more difficult to interpret, as the verification engine data showed non-linear behaviour with spikes in the solution. It appears this behaviour was the result of inadequate filtering and the data processing performed by Pacelab. Since the accuracy on the main effects of interest has been accepted and more data points are available for engine model compared to the verification dataset, the implemented engine model is accepted.

4.2. Sensitivity Study of System Response to Input Parameters

A sensitivity study is performed in order to assess the response of the system solution to a change in input parameters. The parameters that are included in this sensitivity study include all the user defined inputs required by the model. The Morris One-at-a-Time (MOAT) method, as discussed by Van Haver and Vos [42], is then used to evaluate the sensitivity of the system to a change in these input parameters. The output monitored to assess the sensitivity is the trip fuel (TF). As two models are used, the sensitivity study is performed twice, once for each model.

In the MOAT method a nominal value, upper- and lower bound are assigned to each parameter. A number of p levels is selected, in this case five, and the resulting interval is divided in $p-1$ partitions. This is done for all parameters. Then one parameter at a time is changed and the change in system result, called elementary

effect, is recorded. The elementary effect d_i as a function of, y the system giving the result, x the input vector, Δ the interval and e_i the parameter in the input vector being changed, is given by the following equation:

$$d_i = \frac{y(x + \Delta e_i) - y(x)}{\Delta} \tag{4.2}$$

When this process is complete for all parameters, the modified mean μ^* and modified standard deviation σ^* can be determined using the following equations:

$$\begin{aligned} \mu^* &= \sum \frac{|d_i|}{p} \\ \sigma^* &= \sqrt{\sum \frac{(d_i - \mu^*)^2}{p}} \end{aligned} \tag{4.3}$$

The results are then plotted with the modified mean on the x-axis and the modified standard deviation on the y-axis. Parameters for which a high mean and low standard deviation is found have a linear impact on the system results. Parameters for which a low mean and high standard deviation is found have a non-linear but small impact on the system results. Parameters of most interest have a high mean and high standard deviation, as these parameters have a large, non-linear impact on system results.

4.2.1. Sensitivity Study of the Conventional Environmental Control System Model

When all input parameters are considered separately, the study set becomes too large and the sensitivity study too time intensive. With over 60 separate parameters to be evaluated for five values and a run time of approximately 5 minutes, ways to reduce this number are exploited. Firstly, for components with multiple instances in the system, the same parameters are grouped and changed simultaneously. This reduces the number of parameters to 40, a significant time improvement. To further reduce the number of parameters, a smart grouping of additive parameters is suggested. As an example, multiple thermal loads need to be defined for the aircraft cabin components, such as occupant heat load, solar heat load and miscellaneous equipment heat load. However, all of these parameters directly effect the total ECS thermal load by simple addition and subtraction. By temporarily modifying the systems' input and output definitions, study of these parameters can be replaced by only studying the effect of total ECS thermal load. This way, the number of parameters for the study is reduced to 32, a manageable number. These parameters are shown in Table 4.1, including the range for which they are varied. The results of the study are presented in Figures 4.2a and 4.2b for the CECS model.

From Figure 4.2a it is immediately clear that the system is very sensitive to the cabin compartment air cycle time, the time required to completely refresh the compartment air volume. In reality this is not a design parameter but a consequence, as the required airflow is specified by the regulations as a fixed mass flow or volume flow per passenger. The air cycle time is used as a substitute parameter for all input parameters of the cabin compartment component directly affecting the required supply air flow. The large impact of this parameter is then to be expected, as a small change in air cycle time has a significant effect on supply air flow rate, directly increasing bleed air requirements. The parameters influencing air cycle time are directly taken from data, so enough confidence can be placed on their values.

Looking closer to the collection of points in the bottom left corner and omitting points 8 and 16, the latter of which has increased values due to rounding and significant digits, Figure 4.2b is obtained. Six more parameters of interest can be identified. Parameter 6 on the top right is the mixing manifold recirculation ratio. This parameter also directly affects the PACK airflow, thus changing the engine bleed air flow. It directly impacts required amount of bleed air flow, directly affecting fuel consumption. A higher recirculation ratio means more recirculated cabin air is used. To supply the cabin with the same amount of air, less bleed air must be mixed. The effect is similar to that of the air cycle time, but the effect on bleed air is smaller for the standard delta.

Parameter 15, the compartment minimal allowable supply air temperature, can be readily understood. When the the thermal loads of the cabin can be balanced by the ECS with minimum required airflow and a temperature that falls within the limit, this parameter does not affect the system. When this limit increases to a

Table 4.1: List of parameters considered for the sensitivity analysis of the CECS model.

Index	Name	Unit	Lower Bound	Upper Bound
	RamAirInlet			
1	Efficiency	%	80	100
2	EntryCrossSectionArea	dm^2	1	5
	RamAirOutlet			
3	Efficiency	%	80	100
4	PressureRatio	-	0.80	1.0
5	ExitCrossSectionArea	dm^2	1	5
	MixingManifold			
6	RecirculationRatio	%	37	57
7	RelPressureDrop	%	0	4
	RegulatedAirflowCompartment			
8	AirCycleTime	min	1.48	2.2
9	TargetTemperature	°C	18	24
10	TotalECSThermalLoad	kW	14	26
11	InternalConvectionCoeff	W/m^2K	3	7
12	WallThermalConductance	W/m^2K	1.5	3.5
13	TotalVolume	m^3	120	160
14	MaxSupplyAirTemperature	°C	30	60
15	MinSupplyAirTemperature	°C	0	8
	GearBox			
16	GearRatio	-	0.8	1.2
17	NominalPower	kW	80	100
	Generator115VAC			
18	NominalPower	kW	80	100
19	UtilityFrequency	Hz	380	420
	PowerConverter115VAC28VDC			
20	NominalPower	kW	10	20
	Bus28VDC			
21	NominalPower	kW	10	20
	Bus115VAC			
22	NominalPower	kW	40	60
	ElectricLoad28VDC			
23	NominalPower	kW	5	25
24	PowerEfficiency	%	80	100
	ElectricLoad115VAC			
25	NominalPower	kW	40	60
26	PowerEfficiency	%	80	100
	ECSPackDHXAirCycleMachine			
27	HXCoolantRelPressureDrop	%	2	10
28	HXPackRelPressureDrop	%	8	24
29	HeatTransferCoefficient	W/K	50	250
30	CompressorEfficiency	%	66	90
31	TurbineEfficiency	%	75	95
32	HXFlowType	-	Parallel, Cross, Counter	

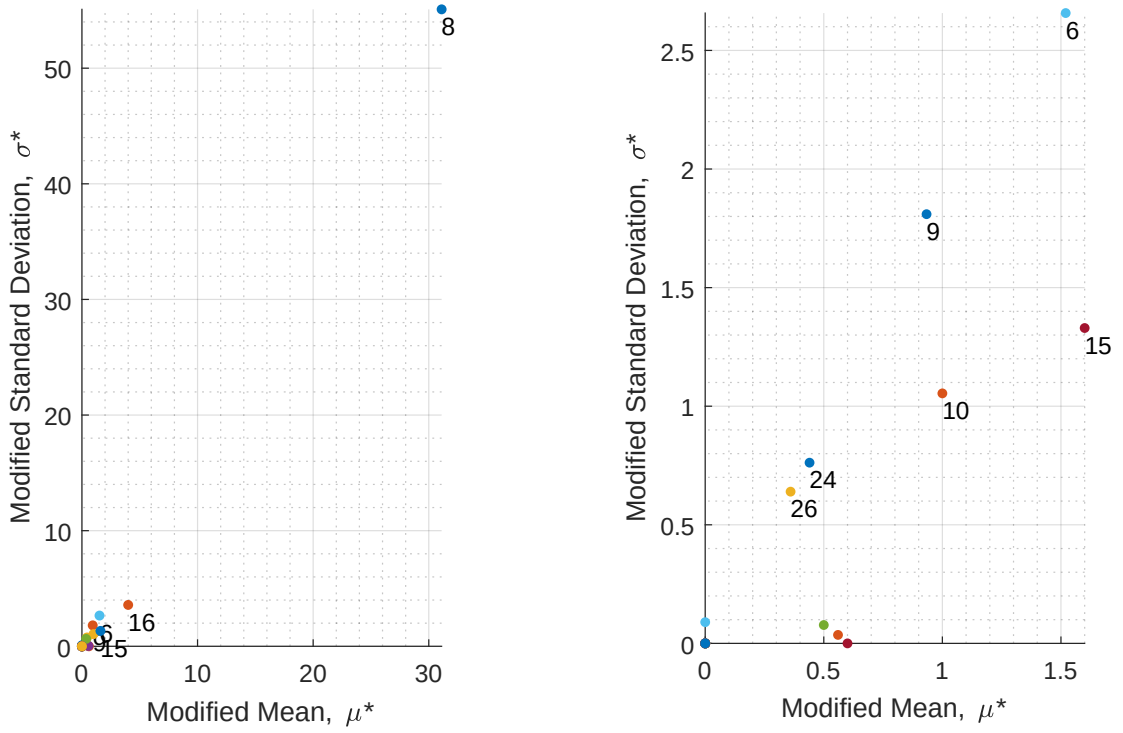

(a) Sensitivity of CECS baseline mission fuel burn to input parameters as given by modified standard deviation against modified mean.

(b) Zoomed view of sensitivity of CECS baseline mission fuel to input parameters as given by modified standard deviation against modified mean.

Figure 4.2: Sensitivity of CECS baseline mission fuel as given by modified standard deviation against modified mean.

higher temperature than that required for the ECS to comply with minimum airflow, the ECS supply temperature is set on the limit and airflow must be increased to cope with the thermal load. As discussed previously, increased ECS airflow increases engine bleed air, therefore affecting fuel consumption.

It is easily accepted that parameters 9 and 10, the compartment target temperature and total ECS thermal load respectively, have an effect on the fuel consumption. Both parameters have an effect on the work required by the PACKs, the cabin temperature through changing the equilibrium conditions of the cabin. Varying work required by the PACK results in slightly increased bleed air requirements, but also increased cooling air requirements and increased compressor and turbine work which increases component losses.

The final parameters, 24 and 26 which represent the efficiency of the electric loads, affect the electric power required by the system. A higher electric power demand directly translates to more shaft power off-takes from the engine, impacting fuel burn. Despite the fact that shaft power off-takes are less efficient than bleed air off-takes [20], the impact of these parameters on CECS architecture system output is smaller than of those parameters affecting bleed air. This is due to the relatively small amount of shaft power off-takes and high amount of bleed air off-takes in this scenario. A relative change in bleed air thus has a bigger impact than the same relative change in shaft-power off-takes.

From this sensitivity study it can be concluded that a good approximation of the parameters discussed above is important to help ensure quality of the model results. Luckily, this is viable. The recirculation rate (6) for nominal conditions can be extracted from airbus documentation[34]. The thermal loads of the cabin (10) have already been discussed in Chapter 3 and can be based on multiple sources and calculations. The air cycle time (8) translates into parameters determining the cabin minimum airflow rate, consisting of number of passengers and airflow per passenger requirement specified in the regulations [28, 43] and can also be based on data. The electric power demand by aircraft systems can be based on data [12, 26, 31]. The component efficiency, minimum supply air temperature limit and cabin temperature are obtained through discussion with peers and public online discussions.

[34] Property of ADSE B.V.

Table 4.2: List of parameters considered for the sensitivity analysis of the EECS model.

Index	Name	Unit	Lower Bound	Upper Bound
	ElectricCompressor115VAC			
1	IsentropicEfficiency	%	80	100
2	MechanicalEfficiency	%	80	100
3	MotorDriveEfficiency	%	80	100
4	OverpressureRatio	-	1.1	1.5
	RegulatedAirflowCompartment			
5	AirCycleTime	min	1.48	2.2
6	TargetTemperature	°C	18	24
7	TotalECSThermalLoad	kW	14	26
8	MinSupplyAirTemperature	°C	0	8
	MixingManifold			
9	RecirculationRatio	%	37	57

4.2.2. Sensitivity Study of the Electric Environmental Control System Model

A sensitivity analysis is also performed on the model of the EECS configuration. To reduce the calculation time, only parameters unique for the EECS model are considered as well as the parameters identified in Section 4.2.1. The same procedure is followed to generate the results presented in Figures 4.3a and 4.3b. A list of parameters is shown in Table 4.2. Note that the numbering does not correspond to Table 4.1.

Looking at Figure 4.3a, it can be seen that the system is sensitive to parameter 4, the CAC overpressure ratio. This parameter describes the ratio of the output pressure of the CAC compared to the target cabin pressure. As discussed in Section 3.1.3, this parameter can be directly related to shaft power off-takes on the engine. When this ratio is increased, more work is required by the CAC to compress the ambient air to the pressure target. Through analysis of the PACK entry temperature for a similar aircraft by ADSE B.V.[35], this ratio was estimated to 10% overpressure compared to cabin conditions.

Figure 4.3b is a zoomed version of Figure 4.3b. It shows notable sensitivity to all the parameters considered, including the same points discussed as in Section 4.2.1. The additional parameters each represent efficiency of a different process of the CAC. Isentropic efficiency of the compressor applies to the thermodynamic efficiency of compression. This value can be well estimated from typical compressor efficiency values. The motordrive efficiency, as discussed in Section 3.1.3 is kept constant at a value supported by typical performance data, as well as the mechanical efficiency. This completes the sensitivity study, allowing the research to move forward, as all parameters that have a large impact on the results can be relatively well approximated.

4.3. Validation of the Aircraft Model and Mission Performance Analysis

Validation of the aircraft model and the mission performance analysis should also be considered. The best way to do this is to compare the payload-range diagram generated by the model with payload-range diagrams found in literature, it serves as a summary of the aircraft performance methods. Verified payload-range data is not readily available, but notional diagrams can be found. Two such diagrams are used, from Husemann *et al.* [27] and Airbus [44], and compared with the diagram constructed with the model, Figure 4.4.

Inspecting Figure 4.4 it is found that the three diagrams are similar, but show some differences that should be discussed. The maximum payload for each diagram, found by reading the constant section at low range, shows a difference of almost 10% between the highest and lowest value. The lowest value is given by the aircraft characteristics document [44], while the highest value is given by the model. Different types of A320 models are available with various configurations and updates, but the document only shows data for three, each differing in payload-range performance. This makes it difficult to compare the proper data.

Another difference to address is the point of the first kink in the diagrams. This kink location is the point where the MTOW is reached and range can only be increased by reducing payload and take more fuel. Again, all diagrams show a different location of this point, with the largest difference between the model and Airbus data. Data from Husemann *et al.* [27] shows more similarity to the model.

The slope of the second diagram segment shows a difference between the model and the other datasets,

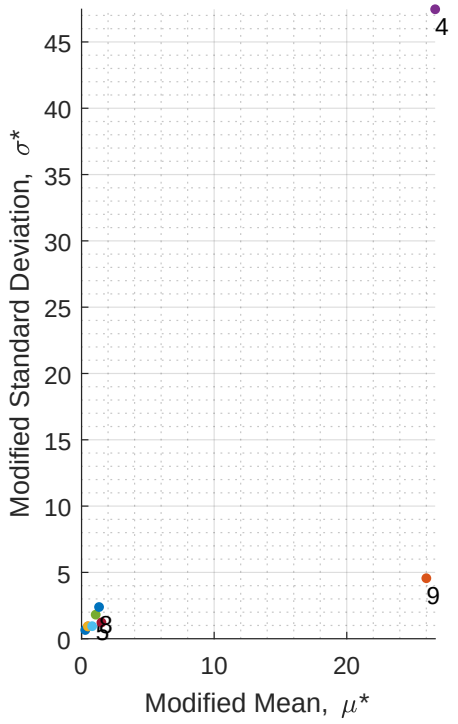

(a) Sensitivity of EECS baseline mission fuel burn as given by modified standard deviation against modified mean.

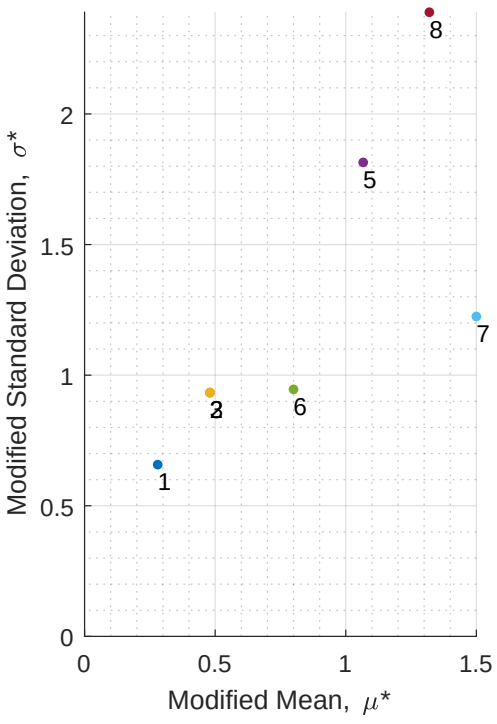

(b) Zoomed view of sensitivity of EECS baseline mission fuel burn as given by modified standard deviation against modified mean.

Figure 4.3: Sensitivity of CECS baseline mission fuel as given by modified standard deviation against modified mean.

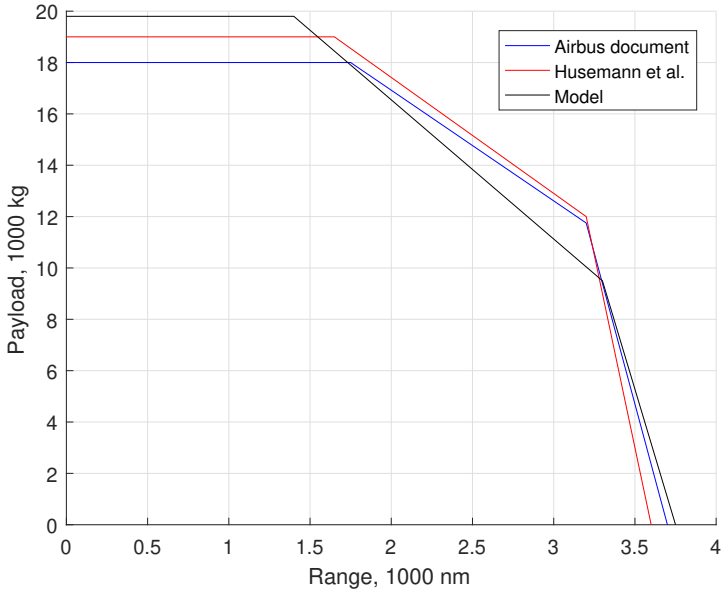

Figure 4.4: Comparison of payload-range diagrams from Husemann *et al.* [27], Airbus [44] and the model.

where the slope of the model data is steeper. This means that more payload must be exchanged for fuel to achieve a range increase, translating to poorer fuel efficiency performance of the model aircraft compared to the other datasets. The poorer performance can be caused by reduced engine performance, reduced aerodynamic performance or less accuracy in performance evaluation methods.

The final kink location is the point where the fuel capacity limit is reached. To increase range beyond this point, weight has to be reduced, so rapid decrease of payload and fuel is needed. Interestingly, the range for all three datasets is similar, but the model has a significantly lower payload compared to the other data. The difference can be explained by the discrepancy in accuracy of the methods, as the model only uses a simplistic geometric approximation.

Overall, a number of differences in the payload-range diagram between the aircraft model and comparison data are observed. The general shape of the payload-range diagrams is comparable. It should be noted, that the goal of this research is a first order analysis, where some inaccuracies are acceptable. Furthermore, the simulated points of payload-range combinations lie within the bounds of all datasets, as was shown in Figure 3.1b. Therefore, it is concluded the differences are small enough that there is sufficient confidence in the model.

5
Results

In the following, the results of this research are discussed. Results are divided in four Sections. Section 5.1 presents a comparison of results for the different ISA condition cases and different number of passenger cases that were investigated. This includes the worst case hot and cold conditions, which vary in both ISA and passenger conditions. Section 5.2 presents more detailed results for a single flight mission using data for each time step of a particular mission simulation. Section 5.3 uses the results from Section 5.2 to determine retrofit weight penalty on aircraft OEW. A discussion of the effect of the increased OEW on mission performance is included. Finally, Section 5.4 aims to translate the results found for a single mission to the implications on airline fleet level. Total mission results for all simulated points and cases can be found in Appendices A to C.

5.1. Mission Total Results Without Retrofit Weight Penalty

Figure 5.1 shows the absolute trip fuel required for missions with 12000 kg payload and range between 250 and 2000 nm. The first thing that should be noted is that the different cases appear to have a minor effect on the fuel requirement for the CECS, displayed on the left. The same is true for the EECS architecture, displayed on the right. Since the differences cannot be appreciated in absolute sense, these will be analysed in relative sense.

Figure 5.2 shows the relative difference in trip fuel required compared to the baseline mission with 12000 kg payload and range between 250 and 2000 nm. The first thing that should be noted is that the different cases have a definite effect on the fuel requirement for the CECS, displayed on the left. The relative difference in fuel consumption compared to the baseline mission for the CECS is -0.5% to +0.5% for most cases, but over +1% for the worst hot case and -2% for the worst cold case. The effect on fuel burn of a half-full two-class or completely full single-class cabin is almost equal to ISA cold or hot conditions respectively, leading to the appearance that the total load for the ECS changes by a comparable amount in these cases.

The EECS graph on the right in Figure 5.2 shows the relative fuel burn of the aircraft with EECS architecture compared to the same case of the CECS architecture. A number of observations are made. It is interesting to note that the effects of the worst cold case on fuel consumption seem much smaller for the EECS architecture compared to the CECS architecture. The curve represents the relative mission fuel burn compared to the CECS architecture in the same case. While the curve is higher than the baseline case, it still indicates a fuel reduction compared to the conventional architecture. As the required CAC work reduces, the efficiency of the generator is also reduced, but this is not enough to explain the difference. Instead, it is reasoned that ECS demand is no longer dictated by the thermodynamic requirements, but by the required cabin ventilation rate, explaining why such a small difference is found.

The results for all EECS cases show a large fuel burn reduction for low range and a rise in relative fuel burn until an asymptote is reached. This behaviour can be readily explained, it is a consequence of one of the major differences between bleed air and shaft power off-takes. During take-off and climb the engine is set to a high thrust setting, resulting in high bleed air temperature and pressure. A lot of work is already performed on the extracted amount of bleed air during these phases, resulting in a large energy waste. On the other hand, the EECS architecture only takes the exact amount of shaft power required to power the system. During descent the engines are in a low thrust setting and mass flow through the engine core is low. The fraction of bleed air off-takes in this case is much larger compared to nominal engine rating, resulting in a larger penalty on engine sfc. This effect is much less significant in case of shaft power off-takes. This phenomenon will be visually demonstrated in Section 5.2.

For short range missions, the relative duration of the climb and descent phases is much larger than for long

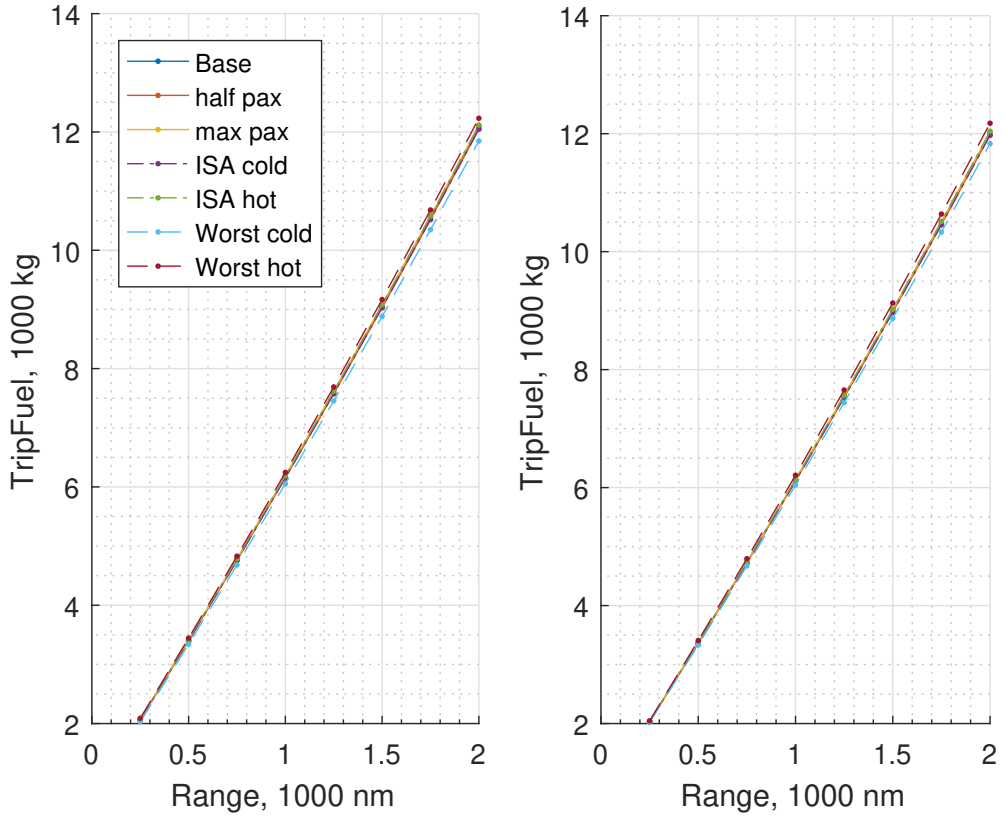

Figure 5.1: Comparison of absolute trip fuel for missions with 12000 kg payload for CECS on the left and EECS on the right for all cases.

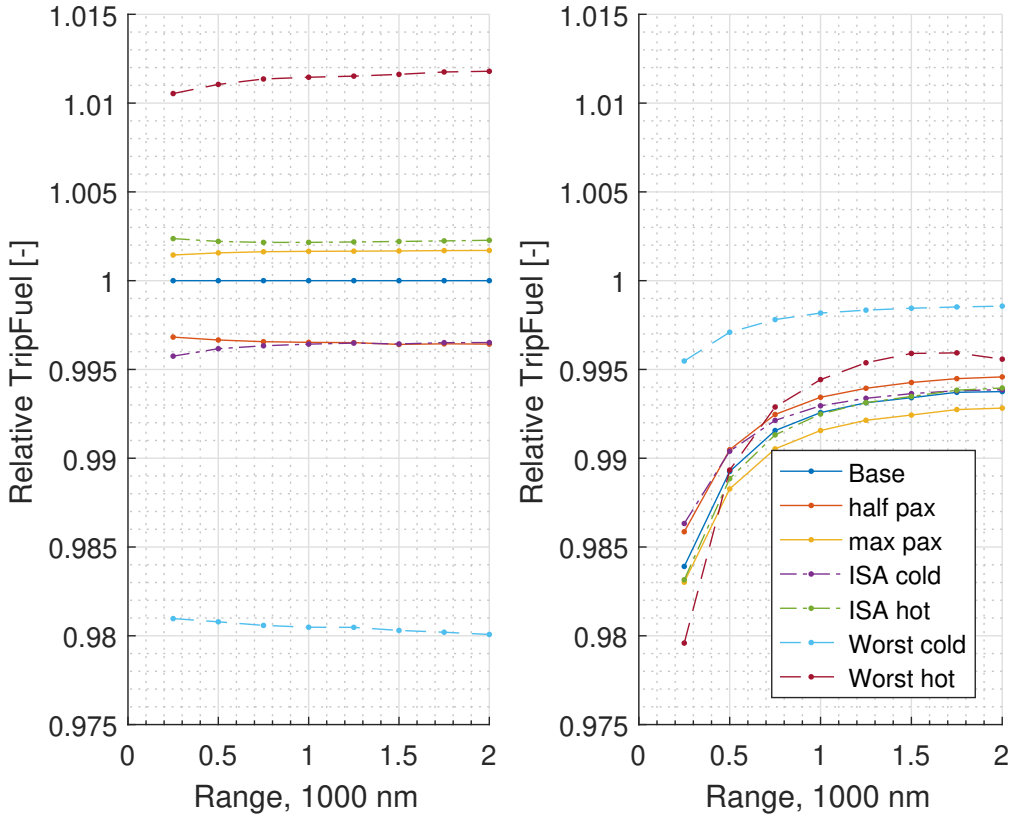

Figure 5.2: Relative comparison of trip fuel for missions with 12000 kg payload for CECS on the left with respect to baseline and EECS on the right with respect to the same case CECS fuel burn for all cases.

range mission, resulting in a dominance of this effect. As range is increased, the fuel consumption during cruise becomes the dominant effect and results tend towards this value.

It can be seen from Figure 5.2 that the EECS consumes slightly less fuel than the CECS for all cases and this difference decreases with increasing range, as explained above. The baseline case requires approximately 1.6% less fuel for a range of 250 nm and 0.6% less fuel for a range of 2000 nm. When the number of passengers is increased this difference increases, while colder conditions or less passengers reduce the fuel burn savings.

The above described effect can be attributed to the generator modelling and sizing. Optimal efficiency of the generator is only achieved at one power output, the nominal power. The generator is sized such that this nominal power output is close to the required maximum power, which is found in worst hot conditions. For all other cases, generator efficiency drops and reaches its lowest values for lowest ECS thermal loads. Despite this effect, the EECS is still more efficient in terms of fuel burn.

However, it should be noted that the presented results have not been compensated for the increased OEW for the aircraft with EECS retrofit. Installing the CACs with corresponding pneumatic ducting and electrical wiring, as well as installing ram air scoops for CAC supply and adding extra generators to the engines or upgrading the existing generators will come with a significant weight penalty. This will be discussed in Section 5.3, after the detailed mission results have been analysed and an estimate of retrofit weight penalty is made in Section 5.2.

5.2. Analysis of Detailed Mission Results

In this Section the baseline mission is analysed in more detail. As discussed in Chapter 3, mission performance is calculated by dividing each phase in a number of steps. The data for each step is extracted in the form of tabular data, which is done for the baseline mission of 1000 nm range with 12000 kg payload for both ECS architectures. These results are presented here.

Figure 5.3 shows the amount of bleed air used during the mission. The first thing to notice is that the bleed air requirement is not constant during the mission, in contrast to the minimum airflow requirement of 0.55 lbs/min used by the FAA [28], also shown in the Figure. This implies that the required amount of bleed air is dictated by the thermodynamic requirements in the cabin rather than the ventilation requirements. A decrease in bleed air requirement at the start of the mission, as the aircraft is gaining altitude, indicates that the cooling of the cabin is dominant. As altitude increases, ambient temperature drops and heat loss to the ambient is increased, reducing cooling load. This is the case for the steady state model with averaged heat loads over the entire mission, but could be different when direct values are used. As a check, the bleed air for the EECS system is also plotted, which is correctly zero during the entire mission.

It should be noted that the amount of bleed air extraction during cruise, as indicated in Figure 5.3, is approximately a factor two higher than would be expected [45]. This is attributed to incorrect modelling of the ECS thermodynamic balance, despite the care that was taken in the modelling and verification steps that were executed. During verification, correct implementation of each component and the system interactions was confirmed. However, correct sizing of the parameters proved difficult, as accurate data was not available. Indeed, increase of PACK performance or reduction of thermal loads lowers the bleed air value. The overestimation of ECS thermal load is also present for evaluation of the EECS architecture. While the effect on both architectures is expected to slightly differ due to the difference in effect of off-takes, it is not seen as a reason to disregard results.

Figure 5.4 shows the shaft power off-takes during the mission. The CECS results show a constant shaft power throughout the cruise phase. This is the consequence of the averaging of the electric power requirements over the mission, as discussed in Chapter 3 in terms of auxiliary cabin thermal loads. These are caused by lighting, circulation fans and galleys, which are all powered electrically. In addition, avionics power supply is also considered. As expected, the shaft power off-takes with the EECS configuration are much higher, as the CACs are now also powered electrically. During cruise of the baseline mission, approximately 250 kW of power is used for all systems, of which about 190 kW is used by the EECS itself.

The power demand of the EECS increases with increasing altitude. This is a result of the simple implementation of the system in the model. The CACs regulate to supply air with a pressure 10% higher than the cabin pressure. At low altitude, this results in a very minor compression, requiring a small amount of work. As altitude increases, the pressure difference between the cabin and the ambient increases also, resulting in a larger

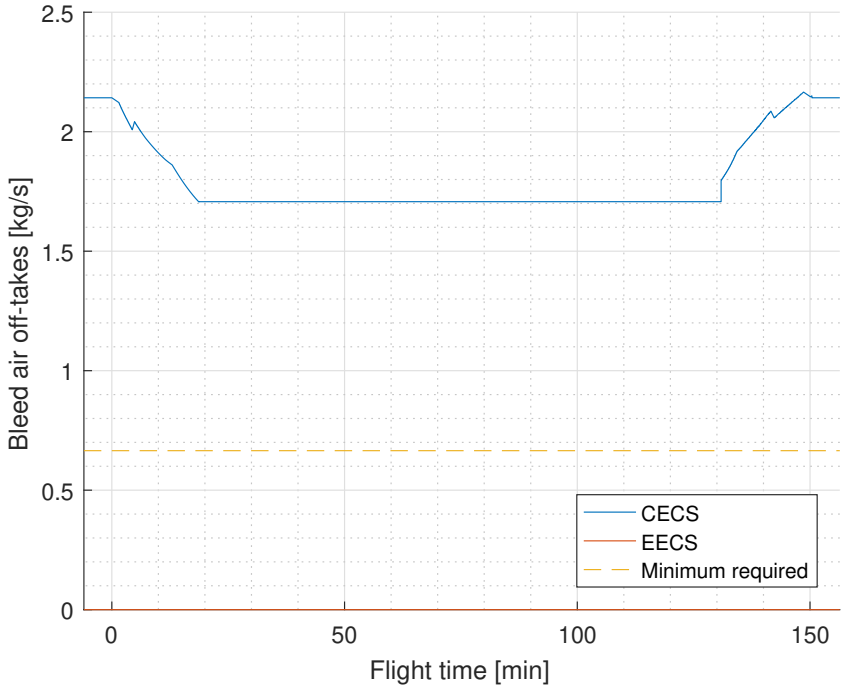

Figure 5.3: Bleed air off-takes history of baseline mission and indication of minimum ventilation requirement posed by the FAA [28].

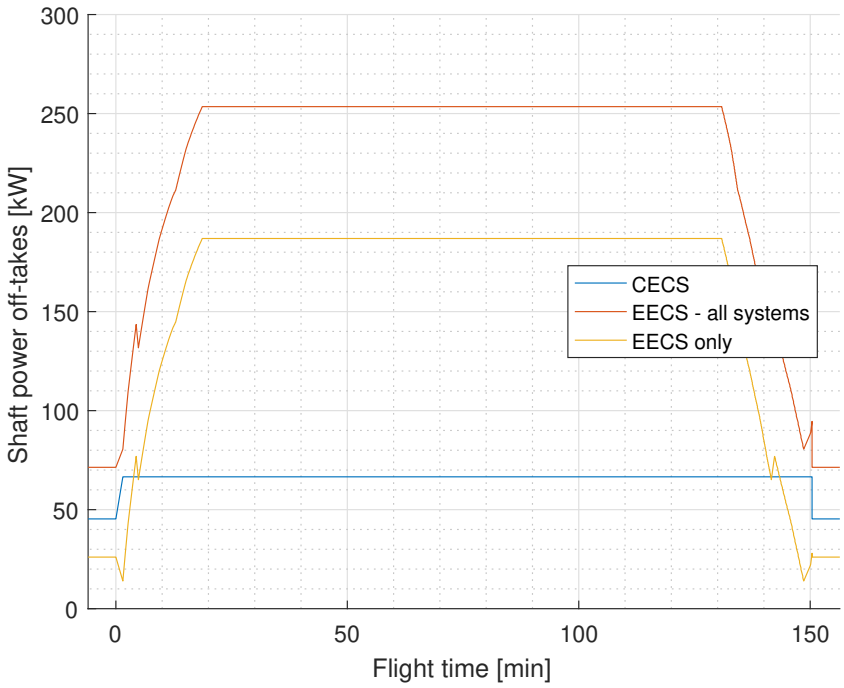

Figure 5.4: Shaft power off-takes history of baseline mission for CECS and EECS.

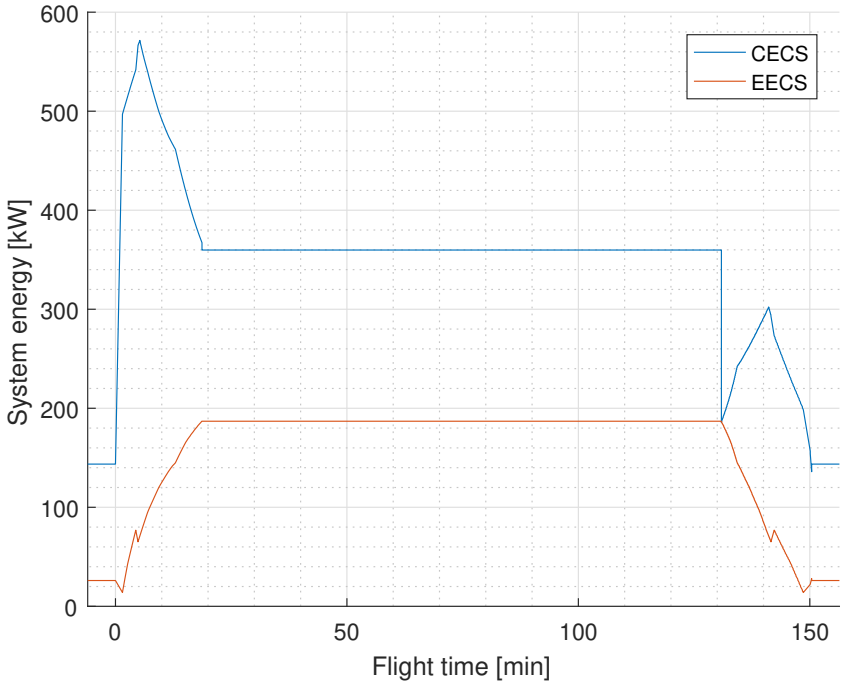

Figure 5.5: Detailed history comparison of CECS and EECS system energy input during baseline mission.

required compression ratio hence more work required.

Figure 5.5 shows the energy input to the CECS and EECS system, where the energy input to CECS is determined using the following equation:

$$Q = \dot{m} c_p \left(T_{\text{bleed}} - T_{\text{amb}}\right) \tag{5.1}$$

These results perfectly illustrate the potential for fuel burn reduction of electrification of the ECS. The energy off-takes from the engine in the form of bleed air are restricted to available pressure and temperature, which often are higher than required. It should be noted that the bleed air temperature used is taken at the engine interface to the aircraft, after regulation has already taken place and a large portion of energy was already dissipated. Still the energy input the the EECS is approximately half of the CECS energy input during cruise.

Another important observation is the spike in energy input to the CECS during climb and landing phase as predicted in Section 5.1. This is caused by the restrictions in bleed air availability. During the high thrust setting of the engine during take-off and climb, bleed air temperature and pressure are also high, resulting in more energy input into the system that needs to be dissipated.

Despite the large difference in energy input between the CECS and EECS, the difference in fuel flow correction factor is small, approximately 0.5% during cruise as can be seen in Figure 5.6. The difference is largest during low power setting of the engine as seen in the taxi, descent and landing phases. In these situations, the relative amount of bleed air off-takes is much higher due to lower mass flow through the engine. Therefore, the impact on engine performance is more severe.

5.3. Mission Total Results With Retrofit Weight Penalty

As can be seen from Figure 5.4, approximately 200 kW of extra power is required for implementation of an EECS. Using a power density of 1.5 kW/kg [21] for the constant speed drive generator and CAC, this amounts to 267 kg. Wire weight to connect the CACs to the electric system is estimated by the model at 120 kg. This high number is the result of extremely high currents needed to supply the approximately 100 kW of power to each CAC at only 115 Volt. Assuming an installation penalty for the system of 5% to account for fastening elements and the ram air scoops required to supply sufficient amount of air, the retrofit mass is estimated as 400 kg. This weight is now added to the aircraft and the same analysis is performed.

The retrofit weight penalty estimate of 400 kg is based on the current installed technology in the A320. Since

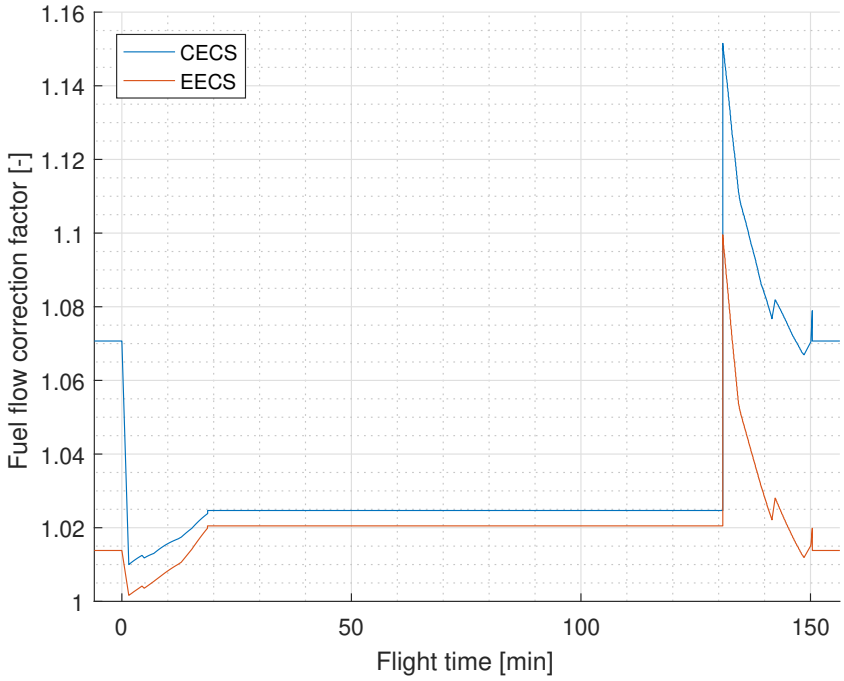

Figure 5.6: Detailed history comparison of CECS and EECS fuel flow correction factor during baseline mission.

the introduction of this aircraft, advances have been made in technology. Electronic component power densities of 3kW/kg to 8kW/kg are achieved or expected in the near future [21]. The existing more electric aircraft, such as the Boeing 787, have a high voltage variable frequency electric system of 270 Volt, Section 2.4. Such a system allows for more efficient power electronics and reduced wire weight as an effect of lower currents. Therefore, a retrofit weight penalty of 200 kg is arguably more realistic at present and is therefore also considered.

5.3.1. Effect of 400 kg Retrofit Weight Penalty

Figure 5.7 shows a comparison of trip fuel consumption for the CECS and EECS including 400 kg weight penalty. It can be seen in the EECS graph, that all lines have shifted upwards due to the effect of extra weight, as expected. While the extra weight has no effect on the efficiency of the EECS, the aircraft must take extra fuel and provide extra thrust to transport the extra mass, resulting in increased fuel consumption. The extra fuel that must be taken incurs an additional penalty on fuel consumption. As a result, fuel burn reduction by the EECS is dependent on the case and mission range.

Only the baseline case and full cabin case maintain a positive effect on fuel burn by a small margin of 0.1%. The other cases have a positive effect at shorter range and negative effect at longer range missions, with the turning point between approximately 1000 nm and 1500 nm. The worst cold case has a negative effect on fuel consumption for all ranges.

5.3.2. Effect of 200 kg Retrofit Weight Penalty

Figure 5.8 shows a comparison of trip fuel consumption for the CECS and EECS including 200 kg weight penalty. In comparison to the results without a weight penalty as presented in Section 5.1, all lines for the EECS architecture are shifted upwards, but a clear improvement is made over the system with 400 kg weight penalty presented in Section 5.3.1. With a 200 kg retrofit weight penalty, a fuel burn reduction is realised for all simulated ranges in the baseline case. These results tend to a reduction of almost 0.4% when range is increased. In the half-full two-class cabin case and ISA cold case, similar results are obtained. For the worst cold case a fuel burn reduction is only realised for missions with a range up to 500 nm.

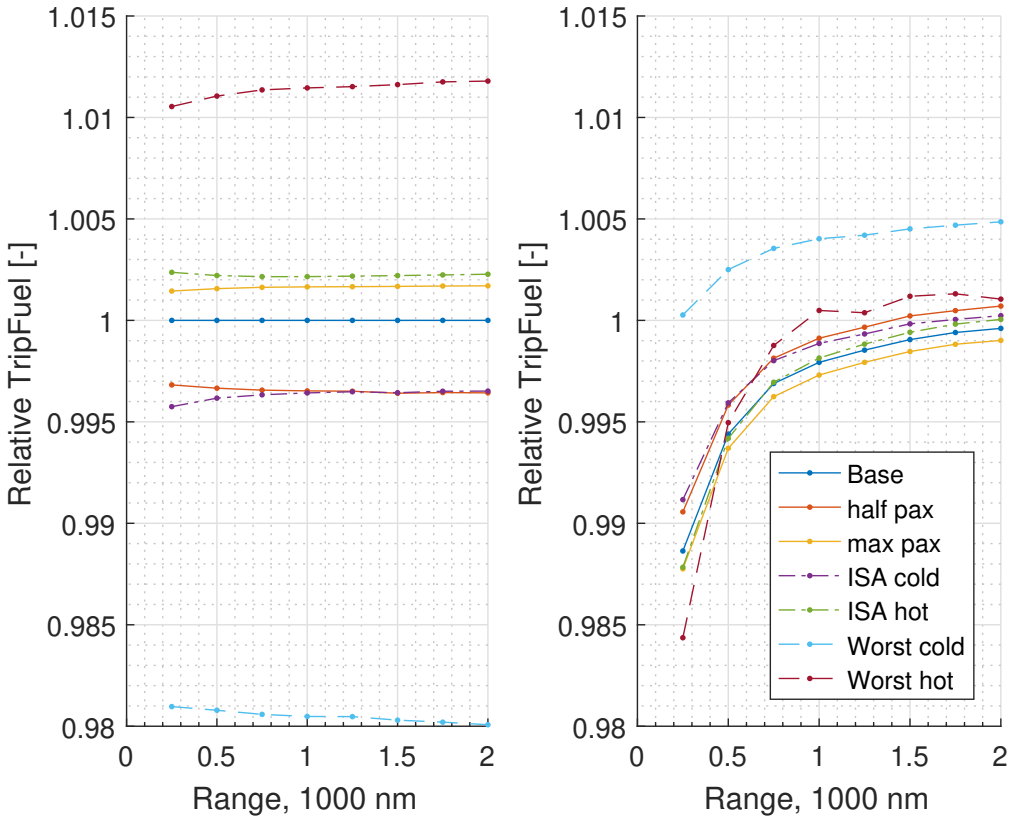

Figure 5.7: Relative comparison of trip fuel for missions with 12000 kg payload for CECS on the left with respect to baseline and EECS on the right with respect to the same case CECS fuel burn for all cases, including 400 kg retrofit weight penalty.

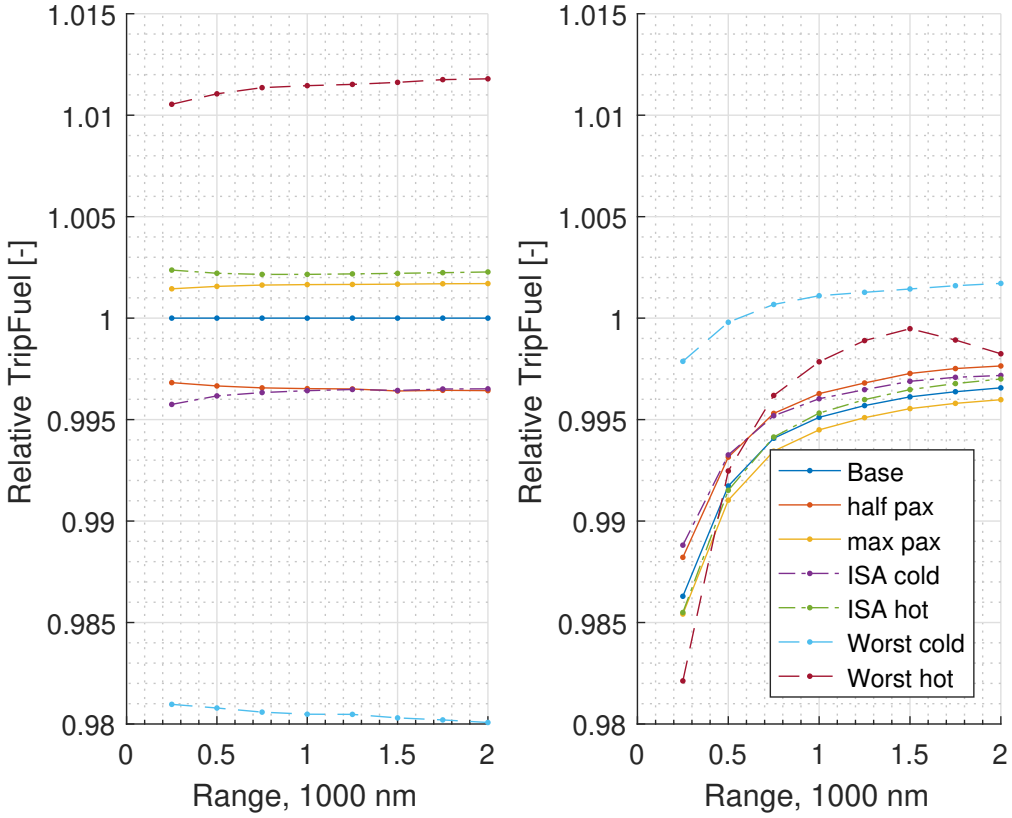

Figure 5.8: Relative comparison of trip fuel for missions with 12000 kg payload for CECS on the left with respect to baseline and EECS on the right with respect to the same case CECS fuel burn for all cases, including 200 kg retrofit weight penalty.

Table 5.1: Number of flights for each payload-range combination as taken from Figure 3.1a for computation of total yearly fuel burn reduction.

Range [nm]	Payload [kg]								
	8000	**9000**	**10000**	**11000**	**12000**	**13000**	**14000**	**15000**	**16000**
250	1000	1000	4000	4000	4000	3000	1000	1000	0
500	1000	2000	5000	5000	4000	2000	1000	1000	0
750	1000	2000	4000	6000	5000	4000	2000	1000	1000
1000	1000	2000	4000	8000	11000	10000	2000	1000	1000
1250	1000	1000	2000	4000	5000	4000	2000	1000	0
1500	1000	1000	2000	4000	6000	7000	3000	2000	0
1750	1000	1000	2000	2000	4000	2000	1000	1000	0
2000	1000	1000	1000	1000	2000	3000	2000	2000	0

Table 5.2: Annual absolute and relative fuel burn reduction on aircraft fleet level for EECS with and without retrofit weight penalty.

Architecture	Fuel Burn, kg	Absolute Reduction, kg	Relative Reduction, %
CECS	1.17×10^9	-	-
EECS	1.16×10^9	8.8×10^6	0.75 %
EECS + 200 kg	1.16×10^9	5.8×10^6	0.50 %
EECS + 400 kg	1.17×10^9	2.5×10^6	0.21 %

5.4. Implication of Results on Aircraft Fleet Level

The results discussed so far all apply to fuel burn reduction on aircraft level. For airlines to decide for a retrofit, the results must be translated to a fleet level. To this end, the flight frequencies of the A320 in the United States of America as found by [27] and presented in Figure 3.1a have been tabulated and are presented in Table 5.1.

This analysis is not very accurate, but serves purely as an indication to the effect on aircraft fleet level. The numbers presented in Table 5.1 have been estimated based on the supplied colour scale and are manual interpretations. Only the baseline case is considered. Furthermore, data on the number of aircraft used to generate the statistics is not available. Nevertheless, the relative fleet fuel burn reduction is not expected to deviate much as the fleet size changes, as the distribution of flights over the spectrum is not expected to significantly deviate.

Table 5.2 shows the results when all separate mission results are multiplied with the flight frequencies as recorded in Table 5.1. From this evaluation it is found that the fleet with CECS installed has a yearly fuel burn of 1.17 million tons, which is not likely to apply to a single airline, but rather to the entire A320 fleet in the USA or Europe. On this scale, implementation of the electric architecture considered in this research would save over 8.8×10^6 kg of fuel, or 0.75%, if no weight penalty was added. The most realistic retrofit case with a retrofit weight penalty of 200 kg would result in a fuel burn reduction of 5.8×10^6 kg, or 0.50%. A retrofit weight penalty of 400 kg results in fuel burn reduction of just over 0.2%.

While the relative fuel savings on fleet level seem small, the economic impact should not be underestimated. According to IATA [46], global airline fuel cost is estimated at $180 billion in 2018 and makes up approximately 23.5% of total operating expense. A fuel reduction of 0.5% thus translates to $890 million, or around 0.12% of the entire operating expense. It should be noted however, that the global fuel cost is given for all aircraft of all types, so this number is not realistic.

Making the gross assumption that the A320 fleet in the United States of America is similar to the EU as presented in Chapter 1 of 4000 aircraft and using the average 2018 jet fuel price of $670 per metric tonne[36], the annual savings caused by a retrofit can be estimated. Based on the 200 kg retrofit weight penalty and the assumptions mentioned, a total of $3.9 million is saved yearly for the entire EU A320 fleet. Assuming now that these aicraft on average will remain in operation for 15 to 20 more years, this amounts to $58 million to $78 million over this period. To break even, the retrofit cost should be no more than $20 thousand per aircraft, which appears to be a too small number to realize such a retrofit.

[36] Jet Fuel Price Monitor. International Air Transport Association. Accessed 13-05-2019. https://www.iata.org/publications/economics/fuel-monitor/pages/index.aspx

6

Conclusions

The goal of this thesis is to answer the research question "How much change in mission fuel requirement results from converting a conventional environmental control system on existing medium range single aisle commercial type aircraft to a bleedless electric environmental control system?" To answer this question, a number of representative flight missions for the A320 with the CECS and EECS architecture were simulated using Pacelab. A baseline case and six deviating cases for different number of passengers and ISA conditions were defined. The required power of the EECS was determined and used to estimate the weight penalty for retrofit of such a system. New simulations were then performed including the weight penalty for the EECS architecture to obtain the final results.

It can be concluded that the implemented EECS architecture has the potential for fuel reduction. Energy off-takes from the engine in the form of shaft power are less efficient, but can be more precisely controlled compared to bleed air, ultimately reducing system power consumption. This is evidenced by the 50% reduction in ECS energy demand during cruise for the electric architecture compared to the conventional bleed air powered architecture. The EECS peak power demand is approximately 200 kW during cruise, compared to 360 kw for CECS during cruise and up to 600 kW during climb. This translates to approximately 0.5% difference in the effect of off-takes on fuel consumption during cruise between the CECS and EECS architectures. During high power or idle engine operations the difference is larger, due to the higher bleed air temperature and lower engine mass flow respectively. As a consequence, relative fuel burn reductions increase for shorter range missions.

The effect of ISA hot conditions is similar to the effect of an increased number of passengers in the cabin. Thermal loads in the cabin are increased in these cases, leading to an increase in fuel burn. The opposite effect is found for the electric architecture. Due to the model implementation of the electric system, higher thermal loads lead to a higher power demand for the electric generators, which are modelled with optimal efficiency at peak load. Fuel burn for the electric architecture is still lower than for the conventional architecture.

Looking at pure system performance, without the retrofit weight penalty, the EECS outperforms the CECS by 0.1% to 2% in all cases. The largest fuel burn decrease is achieved for low range missions, due to inherent inefficiency of bleed air off-takes in take-off, climb and descent phases, which make out a larger portion of the flight when range is short.

The number of passengers directly influences the ventilation requirements for the aircraft cabin. This has a minor effect on fuel consumption, which is similar for both CECS and EECS architecture. It was seen that the thermal load in the cabin is the dominant factor for the supply air mass flow. The amount of air flow deviates from A320 service information data, making this observation less valuable as it is likely caused by incorrect estimation of thermal loads in the cabin.

The power demand of the EECS far exceeds the limits of the installed electrical system on the A320. Additional power generation and distribution elements need to be installed to accommodate the system. This can be a parallel system, minimizing retrofit effort and impact on the existing electric architecture.

When the retrofit weight penalty is added, the above mentioned benefits change. The weight penalty of an EECS retrofit on the A320 was estimated at 400 kg in worst case and 200 kg in a realistic case. With a 400 kg weight penalty included, fuel burn savings are reduced. In the baseline case a fuel burn reduction is still found at all ranges, but for the half-filled cabin, ISA hot and cold and the worst case conditions, the benefits decrease with increasing range and eventually perform worse than the CECS architecture. The turning point

is found at approximately 900 nm for the worst hot conditions and at around 1500 nm for other cases. It is therefore concluded that with the configuration considered in this research, retrofit of an EECS with 400 kg weight penalty is only beneficial for short range missions.

When a retrofit weight penalty of 200 kg is considered, positive results are found for all ranges in all cases except worst cold conditions. However, it is concluded that the negative results in this case are largely an effect of generator model implementation. At a 2000 nm range, fuel burn is reduced by 0.2% to 0.4% in all remaining cases and this number can increase to 1.8% when range is reduced.

When these results are translated to aircraft fleet level by multiplying with statistical flight frequencies, a fleet fuel burn reduction of 0.50% is found for retrofit with a 200 kilogram weight penalty. When retrofit weight penalty is reduced, this number can increase to a maximum of 0.75% for the current system implementation. It is concluded that a fuel burn reduction on fleet level can be achieved by retrofit of the considered EECS architecture.

For the European A320 fleet, a total economic fuel burn saving of $3.9 million annually is estimated, resulting in a $78 million dollar saving over a 20 year lifespan, making a retrofit financially viable is the cost is below $20 thousand per aircraft. This is a low value and seems unachievable, but no conclusion on viability can be drawn with the data available for this research.

A non-quantifiable benefit of an EECS architecture is the mitigation of risk of engine lubrication fumes and combustion products contaminating cabin air. While no conclusive data is available, there is increasing concern of the effect of these products on the health of passengers, as discussed by Committee on Air Quality in Passenger Cabins of Commercial Aircraft [47]. By removing the dependency on bleed air and instead supplying air to the cabin from the ambient, this risk is mitigated.

To conclude, the research question “How much change in mission fuel burn requirement results from converting a conventional environmental control system on existing medium range single aisle commercial type aircraft to a bleedless electric environmental control system?” has been answered. The answer is dependent on ambient conditions, number of passengers, mission range and retrofit weight penalty. On a single aircraft, a fuel burn reduction of 0.6% to 1.8% can be achieved in the baseline case without retrofit weight penalty based on range, with lower range showing the largest relative reduction. When a 200 kg retrofit weight penalty is included, these numbers change to 0.4% to 1.4%. On aircraft fleet level, a fuel burn reduction of 0.75% is estimated with zero retrofit weight penalty, a reduction of 0.50% with 200 kg retrofit weight penalty and a reduction of 0.21% with 400 kg retrofit weight penalty.

7

Recommendations

Based on this thesis, a number of recommendations are made for improvement of the current work or additional research opportunities. These recommendations are aimed at improving model accuracy, improved results in favour of EECS retrofit by improvement on the architecture and implementation and possible future research directions.

To better integrate with the existing electric system of the A320, the CACs were implemented at the existing A320 electrical system voltage level of 115 VAC. Due to the power consumption of the CACs of approximately 100 kW per unit, this leads to very high currents in the order of 1000 Ampere. This requires large cables, resulting in a large weight penalty. It is suggested to investigate implementation of a higher voltage system of 230 VAC or even 270 VDC as used on current more electric aircraft. It is expected this will reduce retrofit weight penalty by half of the cable weight, or 60 kg. This also allows for higher power density of electric motors and generators, further reducing weight penalty.

It was observed that the baseline ECS performance deviates from expected results. The amount of required airflow is far greater than the minimum ventilation requirement and one data point from an Airbus service letter. It was concluded that an inaccuracy exists in the thermodynamic modelling of the cabin or the PACKs. It is therefore recommended to obtain additional data about PACK performance parameters and cabin thermodynamics parameters in order to improve model accuracy and results. Generally, it is expected that better data availability for validation purposes can potentially increase model accuracy.

Another potential improvement of the model can be made by improving the engine model used. The current engine model uses a relatively small number of data points and linear interpolation to determine engine performance parameters at any given condition. Sensitivity of the engine model was verified to follow the same trends as a verified engine model, but it remains a generic dataset. A more sophisticated engine model with coupling to Pacelab or improved implementation should improve model accuracy.

Furthermore, a transient model is required to allow for accurate sizing of the system, since the expected limit cases are transient conditions which are not modelled in this steady state approach. Improved sizing of the system and its component allows for a more detailed study of the implementation in the aircraft and its effects on performance. A more accurate sizing should also serve as the starting point of an economic study, to estimate the cost of retrofit and assess economic viability.

One of the benefits of EECS is the ability to directly control pressure supplied to the PACKs. In this research, a fixed ratio of cabin pressure was used as supply pressure, as optimization is considered outside of the scope. It is expected that an improvement in fuel consumption can be achieved by optimization of the CAC pressure schedule. This might be the topic for a follow-up research.

By introducing a source of pneumatic energy to the aircraft, it should be investigated if other pneumatically powered systems on the aircraft can also be decoupled from the engine and fed by electric compressors. The most significant system is the aircraft wing ice protection system. Since this system is not operative during the entire flight, conversion of this system might not lead to fuel burn benefits, as a large weight increase is expected for relatively minor fuel burn reductions. However, the engine pneumatic system is maintenance intensive, although exact numbers on maintenance cost and effort are not readily available. Decoupling of all pneumatic systems from the engine bleed system could potentially save cost of maintenance and repair. It also slightly reduces retrofit weight penalty, as a number of pneumatic parts and ducts can be removed from the engine.

Other research can be initiated based on this thesis. Sizing and installation of the CACs, generators and other

components falls outside the scope of this research. A more detailed analysis and sizing of these components will lead to more accurate weight estimations. Implementation of a higher voltage system is expected to improve viability of an EECS retrofit scenario and should be investigated. As mentioned previously, more accurate modelling of the PACK performance and cabin thermodynamics is expected to improve results. Finally, optimization of the CAC control strategy is also expected to improve fuel efficiency of the EECS and should be investigated.

Bibliography

[1] C. M. Burt, X. Piao, F. Gaudi, B. Busch, and N. F. Taufik, *Irrigation Training and Research Center Report*, Tech. Rep. (California Polytechnic State University, San Luis Obispo, 2006).

[2] Rolls Royce plc, *Rolls Royce - The Jet Engine*, fifth edition ed. (Rolls Royce plc, Derby, England, 1996) p. 278.

[3] I. Moir and A. Seabridge, *Aircraft Pneumatic Subsystems,* in *Encyclopedia of Aerospace Engineering* (John Wiley & Sons, Ltd, Chichester, UK, 2013) pp. 1–18.

[4] W. J. Christoff, *Aircraft environmental control system with auxiliary power output,* (1983).

[5] H. M. Claeys, K. J. Clarke, and D. S. Matulich, *Integrated power and cooling environmental control system,* (1994).

[6] C. Long, Z. Xingjuan, and Y. Chunxin, *A New Concept Environmental Control System with Energy Recovery Considerations for Commercial Aircraft,* (44th International Conference on Environmental Systems, Tuscon, Arizona, USA, 2014).

[7] H. Yang, X. Zhang, C. Wang, and C. Yang, *Design Analysis of Power Recovery Systems for Cabin Exhaust Air,* Procedia Engineering **121**, 248 (2015).

[8] Y. Han, Z. Xingjuan, W. Chao, and Y. Chunxin, *Experimental and theoretical study on a novel energy-saving ECS for commercial airliners,* Applied Thermal Engineering **127**, 1372 (2017).

[9] T. Ensign and J. Gallman, *Energy Optimized Equipment Systems for General Aviation Jets,* in *44th AIAA Aerospace Sciences Meeting and Exhibit* (American Institute of Aeronautics and Astronautics, Reston, Virigina, 2006).

[10] I. Chakraborty, D. N. Mavris, M. Emeneth, and A. Schneegans, *A methodology for vehicle and mission level comparison of More Electric Aircraft subsystem solutions: Application to the flight control actuation system,* Proceedings of the Institution of Mechanical Engineers, Part G: Journal of Aerospace Engineering **229**, 1088 (2015).

[11] M. Shi, I. Chakraborty, Y. Cai, J. C. Tai, and D. N. Mavris, *Mission-Level Study of Integrated Gas Turbine and Environmental Control System Architectures,* in *2018 AIAA Aerospace Sciences Meeting* (American Institute of Aeronautics and Astronautics, Kissimmee, Florida, 2018).

[12] M. Shi, I. Chakraborty, J. Tai, and D. N. Mavris, *Integrated Gas Turbine and Environmental Control System Pack Sizing and Analysis,* in *2018 AIAA Aerospace Sciences Meeting* (AIAA, Kissimmee, 2018).

[13] M. J. Moran and H. N. Shapiro, *Refrigeration and Heat Pump Systems,* in *Fundamentals of Engineering Thermodynamics* (Wiley, 2006) Chap. 10, pp. 454–486.

[14] Y. Hou, H. Zhao, C. Chen, and L. Xiong, *Developments in reverse Brayton cycle cryocooler in China,* Cryogenics **46**, 403 (2006).

[15] B. Sarlioglu and C. T. Morris, *More Electric Aircraft: Review, Challenges, and Opportunities for Commercial Transport Aircraft,* IEEE Transactions on Transportation Electrification **1**, 54 (2015).

[16] C. E. Lents, S. E. Squier, and W. A. Thresher, *Electrically driven aircraft cabin ventilation and environmental control system,* (2002).

[17] Defense-aerospace.com, *United Technologies Corp. Agrees to Acquire Sundstrand Corp. Hamilton Sundstrand Positioned as Aerospace and Industrial Leader,* (2012).

[18] UTC Aerospace Systems, *UTC Aerospace Systems delivers 100th CACTCS pack shipset for Boeing 787 Dreamliner,* (2012).

[19] S. Farokhi, *Aircraft propulsion*, second edi ed. (Wiley, 2014) p. 399.

[20] R. Slingerland and S. Zandstra, *Bleed air versus electric power off-takes from a turbofan gas turbine over the flight cycle,* (2007) pp. 1516–1527.

[21] V. Madonna, P. Giangrande, and M. Galea, *Electrical Power Generation in Aircraft: review, challenges and opportunities,* IEEE Transactions on Transportation Electrification (2018), 10.1109/TTE.2018.2834142.

[22] J. Weimer, *Electrical power technology for the more electric aircraft,* in *AIAA/IEEE Digital Avionics Systems Conference* (IEEE, Fort Worth, Texas, 1993) pp. 445–450.

[23] P. Wheeler, *Technology for the more and all electric aircraft of the future,* in *2016 IEEE International Conference on Automatica (ICA-ACCA)* (IEEE, Curico, Chile, 2016) pp. 1–5.

[24] I. Moir and A. Seabridge, *Design and Development of Aircraft Systems*, 2nd ed., Vol. 12 (John Wiley & Sons, Ltd, Chichester, UK, 2013) p. 331.

[25] P. Wheeler and S. Bozhko, *The More Electric Aircraft: Technology and challenges.* IEEE Electrification Magazine **2**, 6 (2014).

[26] T. Lampl, S. Muschkorgel, and M. Hornung, *Parameterized flight mission for secondary power requirement estimations of commercial transport aircraft,* (American Institute of Aeronautics and Astronautics Inc, AIAA, 2017).

[27] M. Husemann, K. Schäfer, and E. Stumpf, *Flexibility within flight operations as an evaluation criterion for preliminary aircraft design,* Journal of Air Transport Management **71**, 201 (2018).

[28] Federal Aviation Administration, *eCFR — Code of Federal Regulations,* (2019).

[29] H. Yin, X. Shen, Y. Huang, Z. Feng, Z. Long, R. Duan, C. H. Lin, D. Wei, B. Sasanapuri, and Q. Chen, *Modeling dynamic responses of aircraft environmental control systems by coupling with cabin thermal environment simulations,* Building Simulation (2016), 10.1007/s12273-016-0278-3.

[30] C. P. Frank, W. A. Levy, J.-G. D. Durand, E. Garcia, and D. N. Mavris, *An Integrated and Parametric Environment for Generation, Selection and Evaluation of New Architectures at a Conceptual Level: Application to the Environmental Control System,* in *52nd Aerospace Sciences Meeting* (AIAA, National Harbor, Maryland, 2014) p. 18.

[31] I. Chakraborty, M. F. Ozcan, and D. N. Mavris, *Effect of Major Subsystem Power Off-takes on Aircraft Performance in More Electric Aircraft Architectures,* in *15th AIAA Aviation Technology, Integration, and Operations Conference* (Dallas, Texas, 2015) p. 14.

[32] Airbus Corporation, *Aircraft Cabin Air Quality - Service Information Letter 21-050,* (2010).

[33] I. Chakraborty, *Subsystem architecture sizing and analysis for aircraft conceptual design*, Ph.D. thesis, Geargia Tech (2015).

[34] M. F. Ahlers, *Aircraft Thermal Management,* in *Encyclopedia of Aerospace Engineering* (John Wiley & Sons, Ltd, Chichester, UK, 2011).

[35] W. A. Marggraf, M. Griggs, W. A. Marggraf, and M. Griggs, *Aircraft Measurements and Calculations of the Total Downward Flux of Solar Radiation as a Function of Altitude,* Journal of the Atmospheric Sciences **26**, 469 (1969).

[36] A.-. A. E. S. Committee, *AIR1168/3 Aerothermodynamic Systems Engineering and Design* (2011).

[37] J. B. do Porto Neves Júnior, C. R. de Andrade, and E. L. Zaparoli, *Numerical Analysis of Tipical Aircraft Air-Conditioning Air Cycle Machines,* in *20th International Congress of Mechanical Engineering* (ABCM, Gramado, Brazil, 2009).

[38] J. P. van Buijtenen and W. P. Visser, *Gas Turbines, WB4420 / 4421*, 4th ed. (2009) p. 180.

[39] US Department of Energy, *Determining Electric Motor Load Ranges,* (1997), 10.1109/WAINA.2011.89.

[40] F. Andersson, *Integrated generator for use in aircraft engines*, Pre-study, Lunds Universitet (2018).

[41] J. Zamboni, *Correction: A Method for the Conceptual Design of Hybrid Electric Aircraft*, Master of science thesis, Delft University of Technology (2018).

[42] S. Van Haver and R. Vos, *A Practical Method for Uncertainty Analysis in the Aircraft Conceptual Design Phase,* in *53rd AIAA Aerospace Sciences Meeting* (American Institute of Aeronautics and Astronautics, Reston, Virginia, 2015).

[43] European Aviation Safety Agency, *CS-25 / Amendment 21: Large Aeroplanes,* (2018).

[44] Airbus, *Airbus A320 Aircraft Characteristics - Airport and Maintenance Planning*, Tech. Rep. (Airbus S.A.S., Blagnac, 2018).

[45] Airbus, *Service Information Letter,* (2010).

[46] IATA, *Fuel Fact Sheet,* Iata , 1 (2018).

[47] Committee on Air Quality in Passenger Cabins of Commercial Aircraft, *The Airliner Cabin Environment and the Health of Passengers and Crew* (National Academy Press, Washington, D.C., 2002) p. 344.

A

Total Mission Results Without Retrofit Weight Penalty

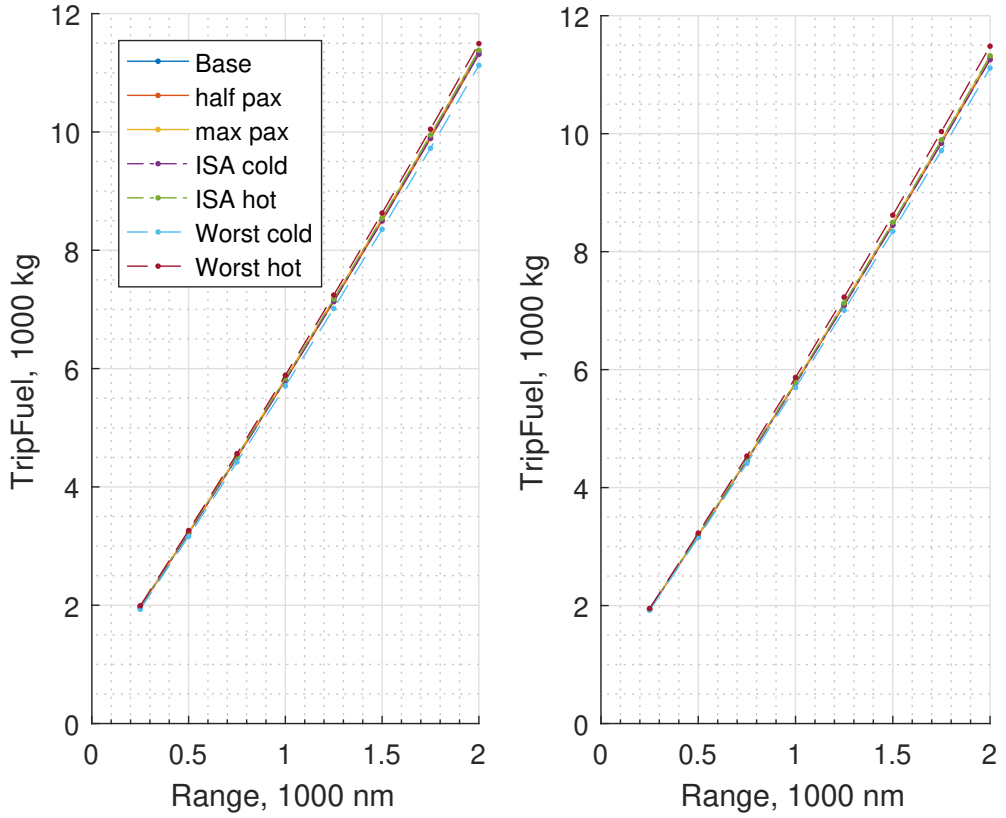

Figure A.1: Comparison of absolute trip fuel for missions with 8000 kg payload for CECS on the left and EECS on the right for all cases.

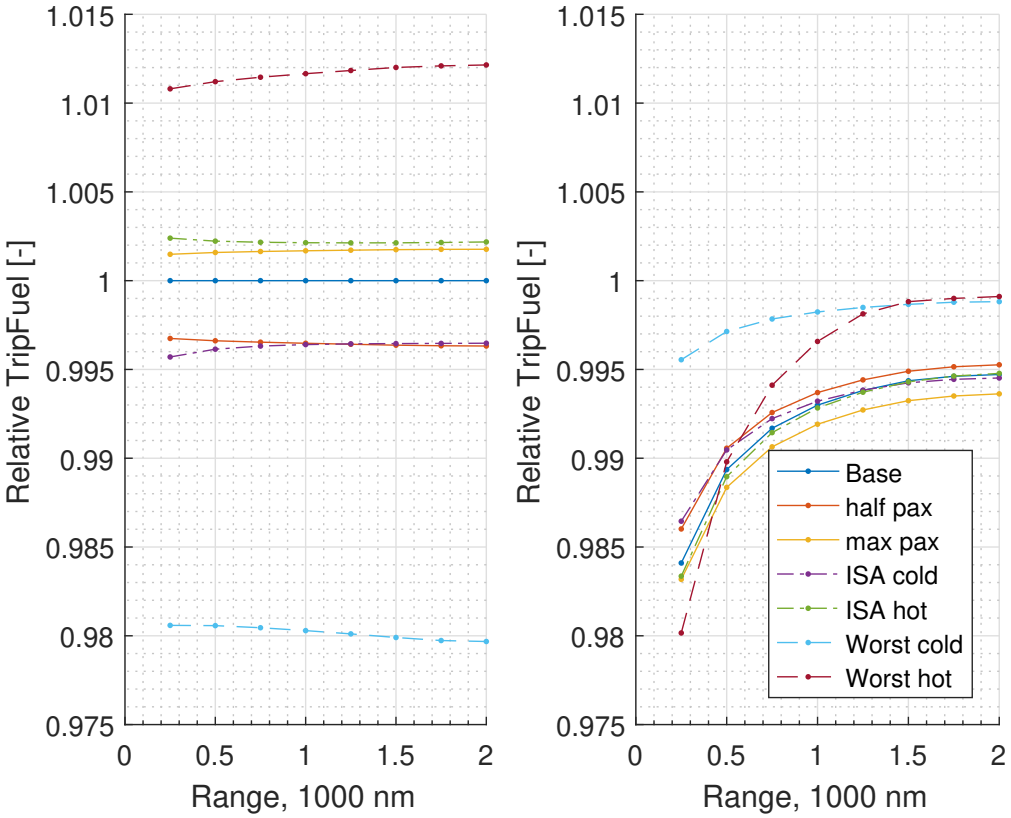

Figure A.2: Relative comparison of trip fuel for missions with 8000 kg payload for CECS on the left with respect to baseline and EECS on the right with respect to the same case CECS fuel burn for all cases.

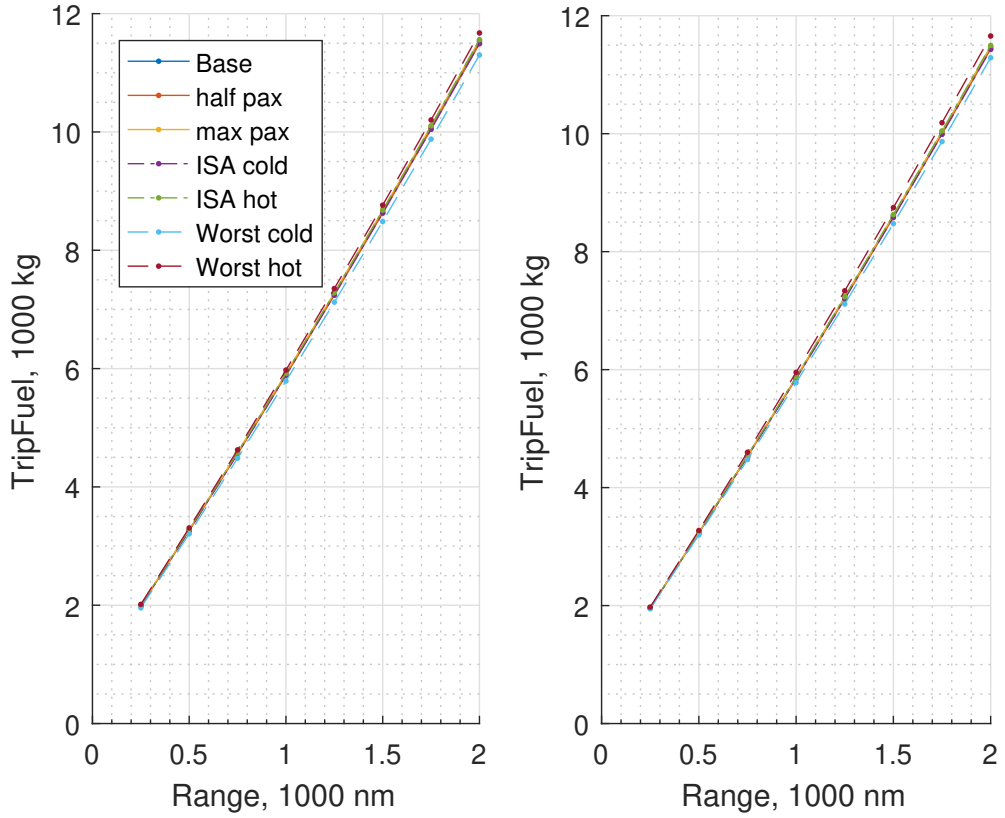

Figure A.3: Comparison of absolute trip fuel for missions with 9000 kg payload for CECS on the left and EECS on the right for all cases.

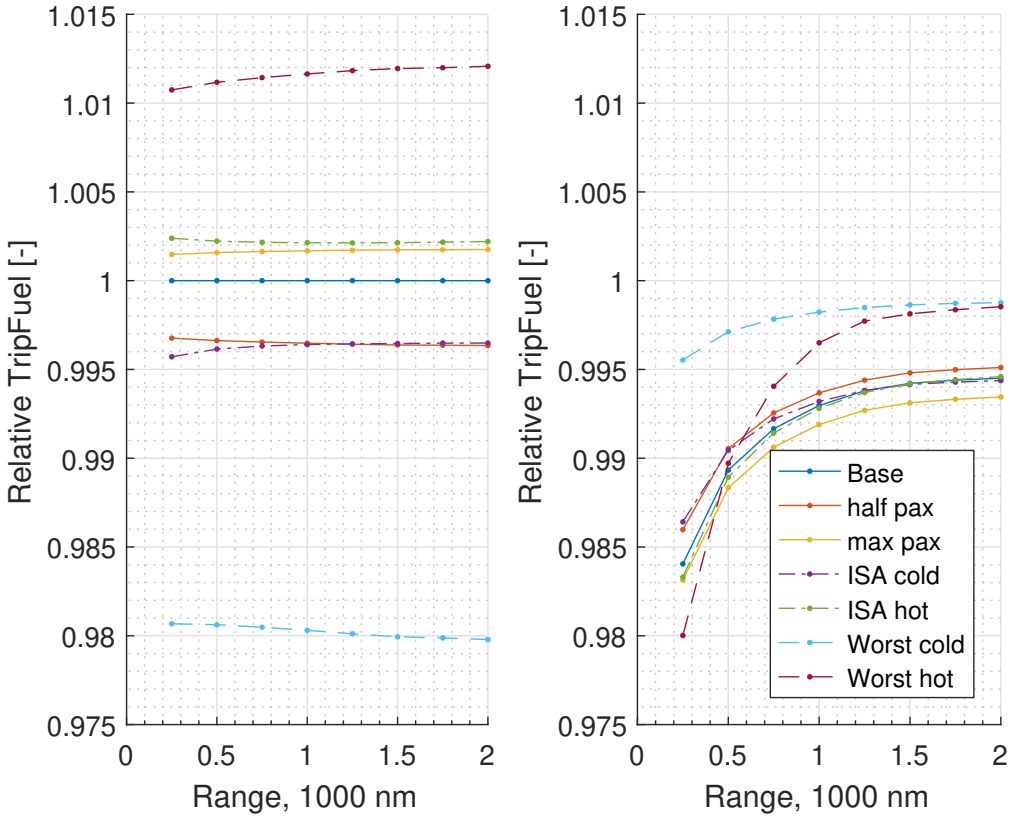

Figure A.4: Relative comparison of trip fuel for missions with 9000 kg payload for CECS on the left with respect to baseline and EECS on the right with respect to the same case CECS fuel burn for all cases.

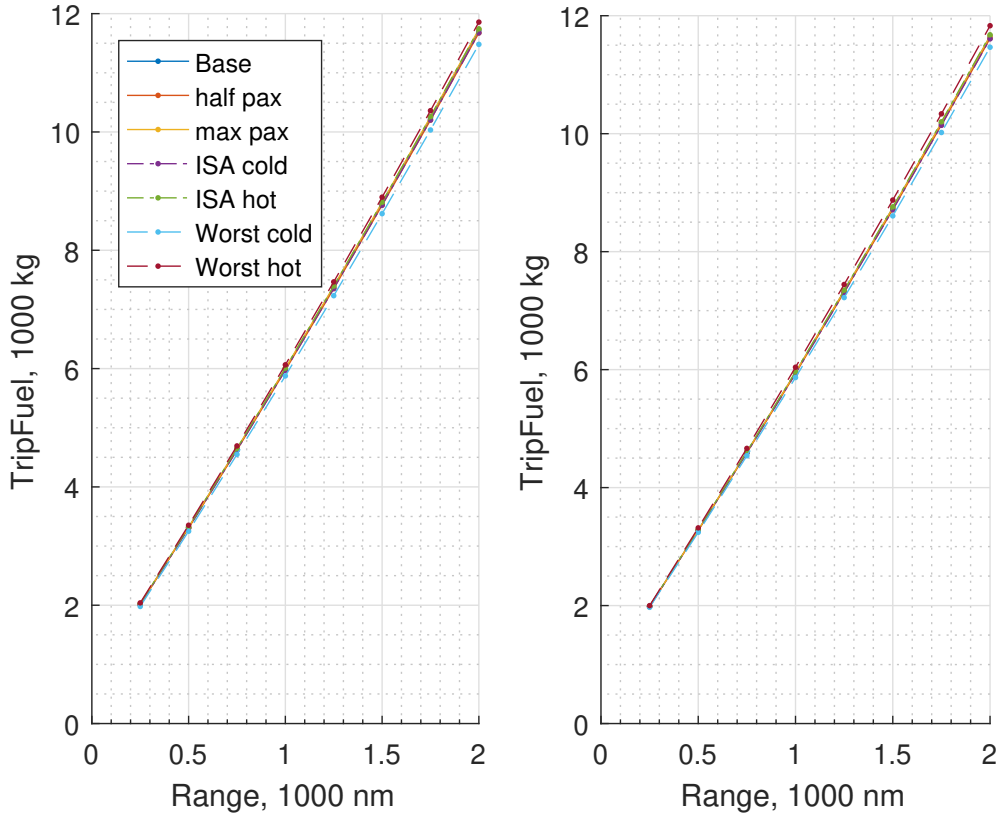

Figure A.5: Comparison of absolute trip fuel for missions with 10000 kg payload for CECS on the left and EECS on the right for all cases.

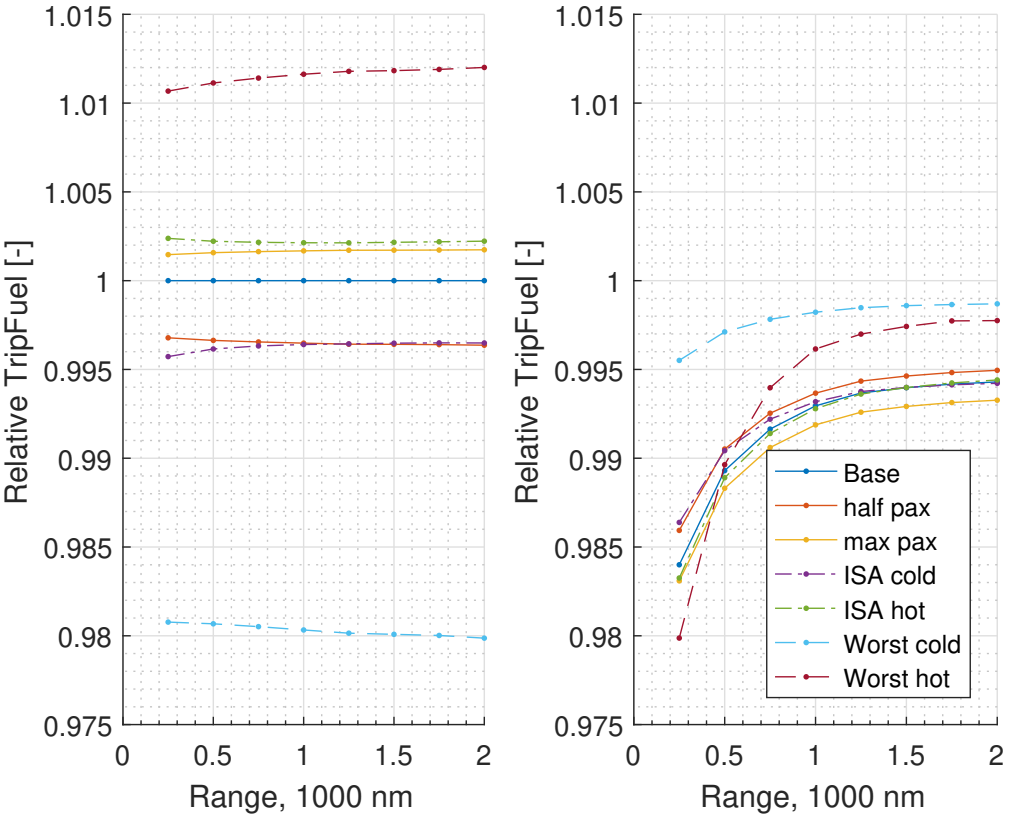

Figure A.6: Relative comparison of trip fuel for missions with 10000 kg payload for CECS on the left with respect to baseline and EECS on the right with respect to the same case CECS fuel burn for all cases.

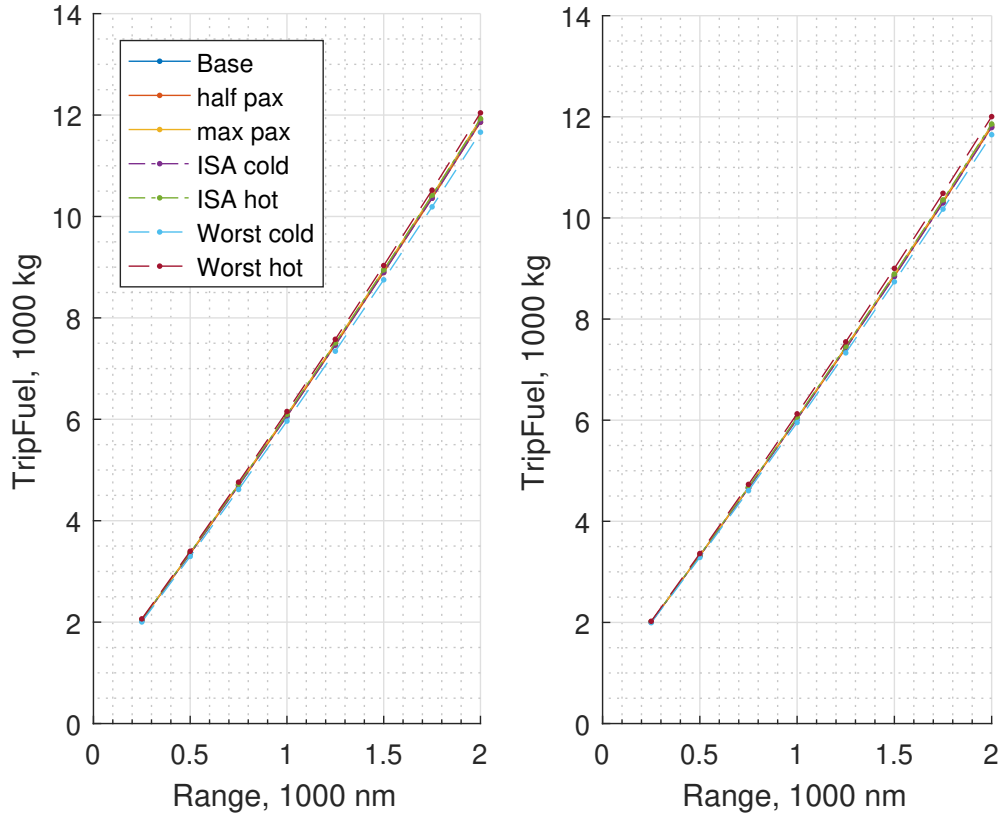

Figure A.7: Comparison of absolute trip fuel for missions with 11000 kg payload for CECS on the left and EECS on the right for all cases.

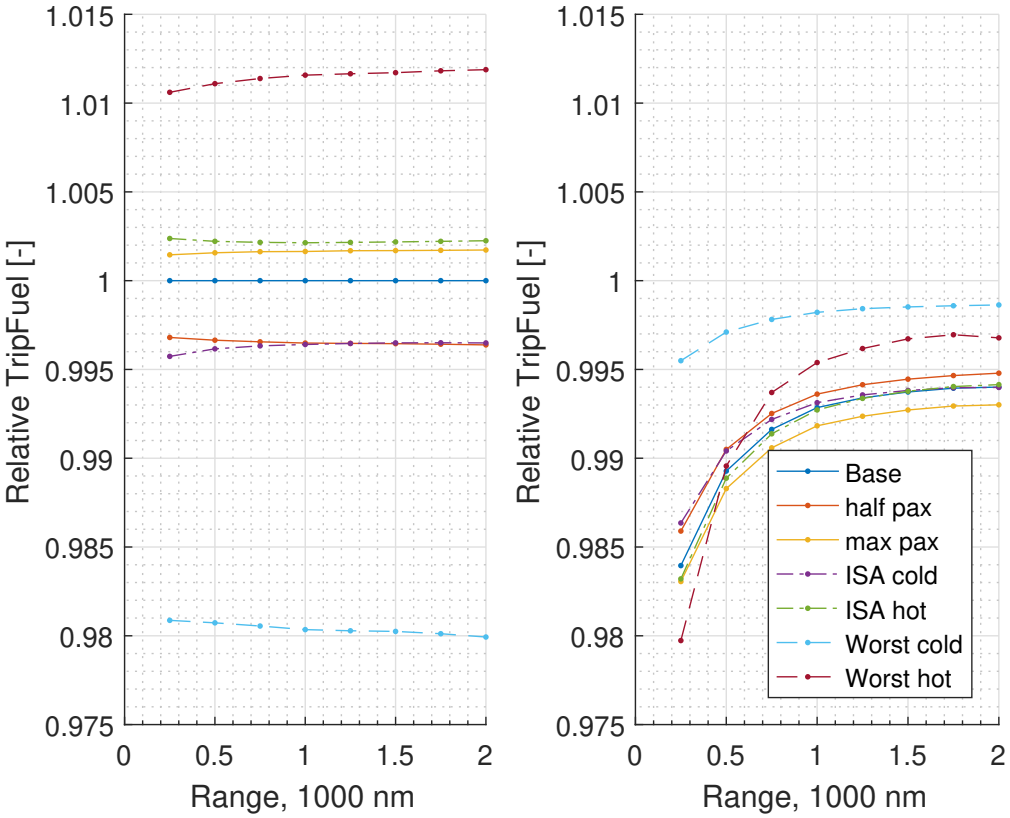

Figure A.8: Relative comparison of trip fuel for missions with 11000 kg payload for CECS on the left with respect to baseline and EECS on the right with respect to the same case CECS fuel burn for all cases.

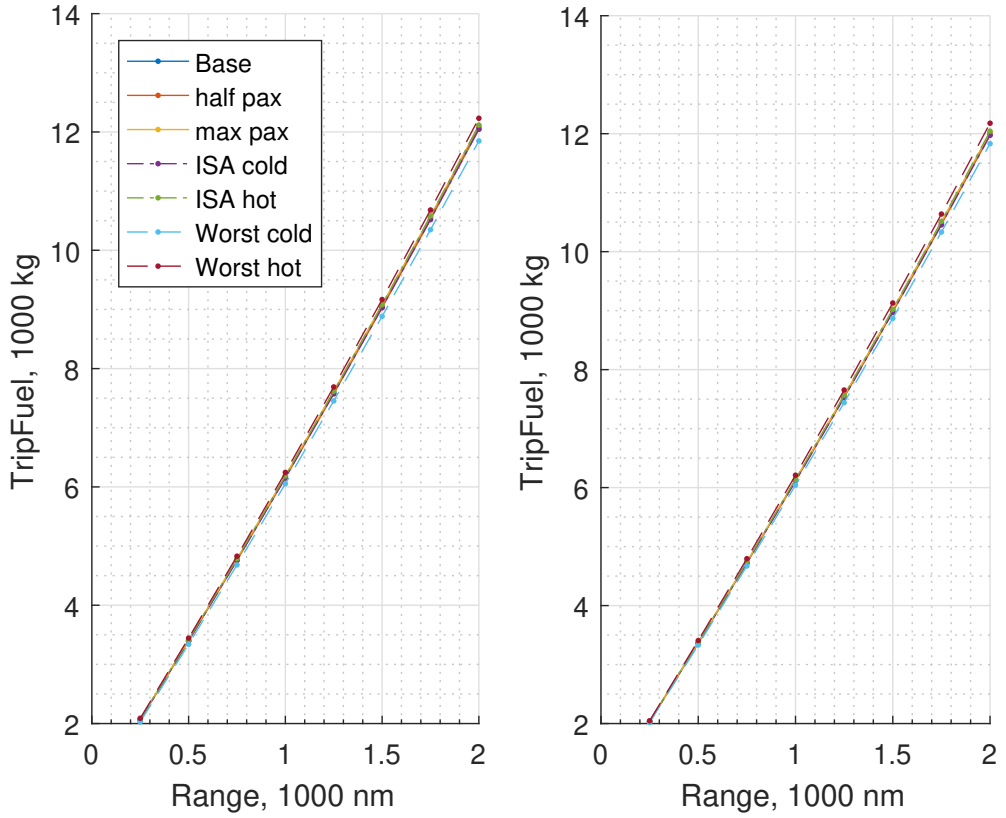

Figure A.9: Comparison of absolute trip fuel for missions with 12000 kg payload for CECS on the left and EECS on the right for all cases.

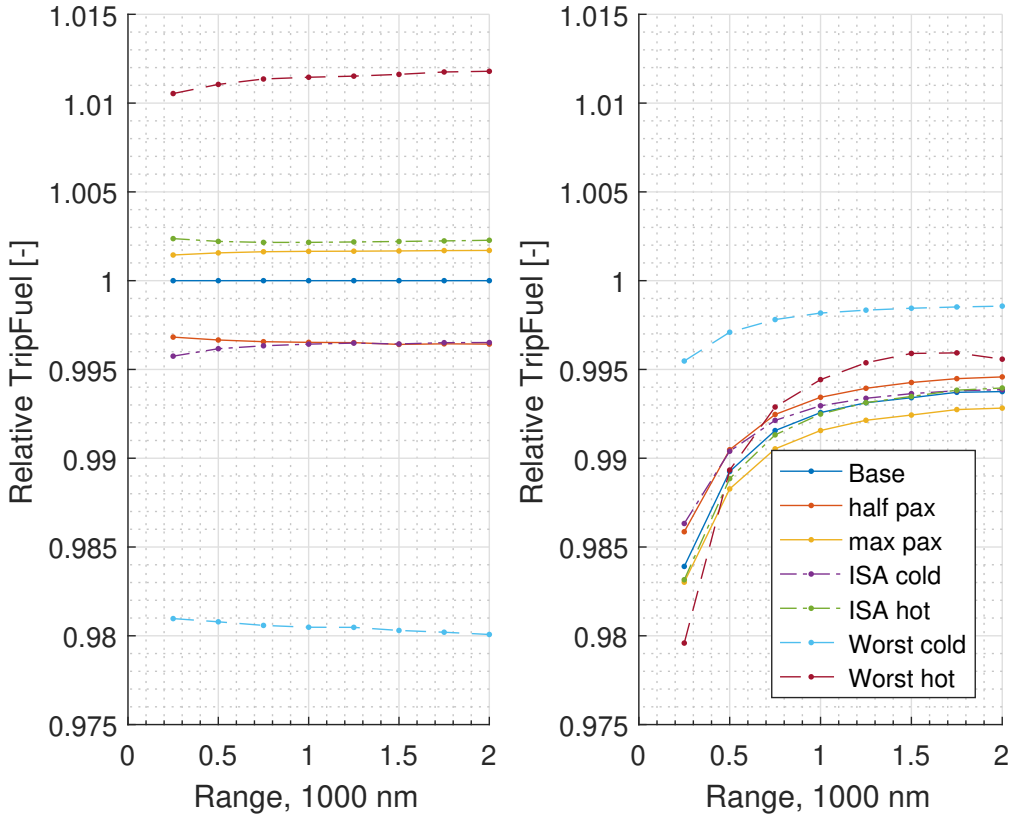

Figure A.10: Relative comparison of trip fuel for missions with 12000 kg payload for CECS on the left with respect to baseline and EECS on the right with respect to the same case CECS fuel burn for all cases.

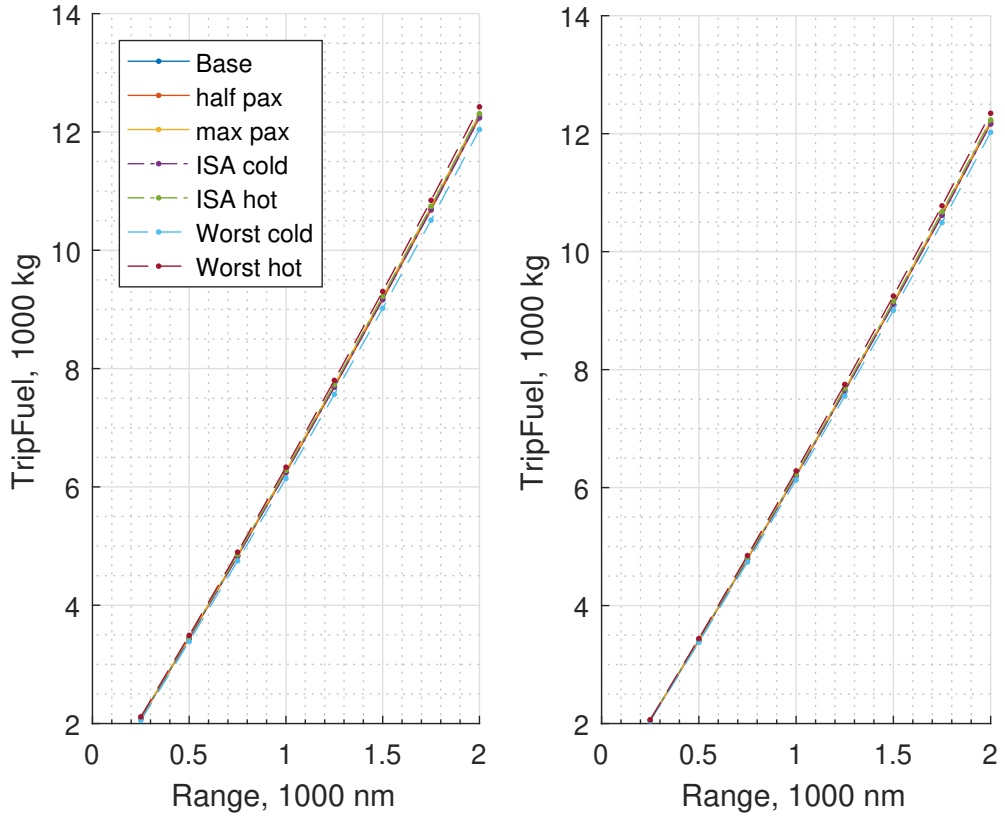

Figure A.11: Comparison of absolute trip fuel for missions with 13000 kg payload for CECS on the left and EECS on the right for all cases.

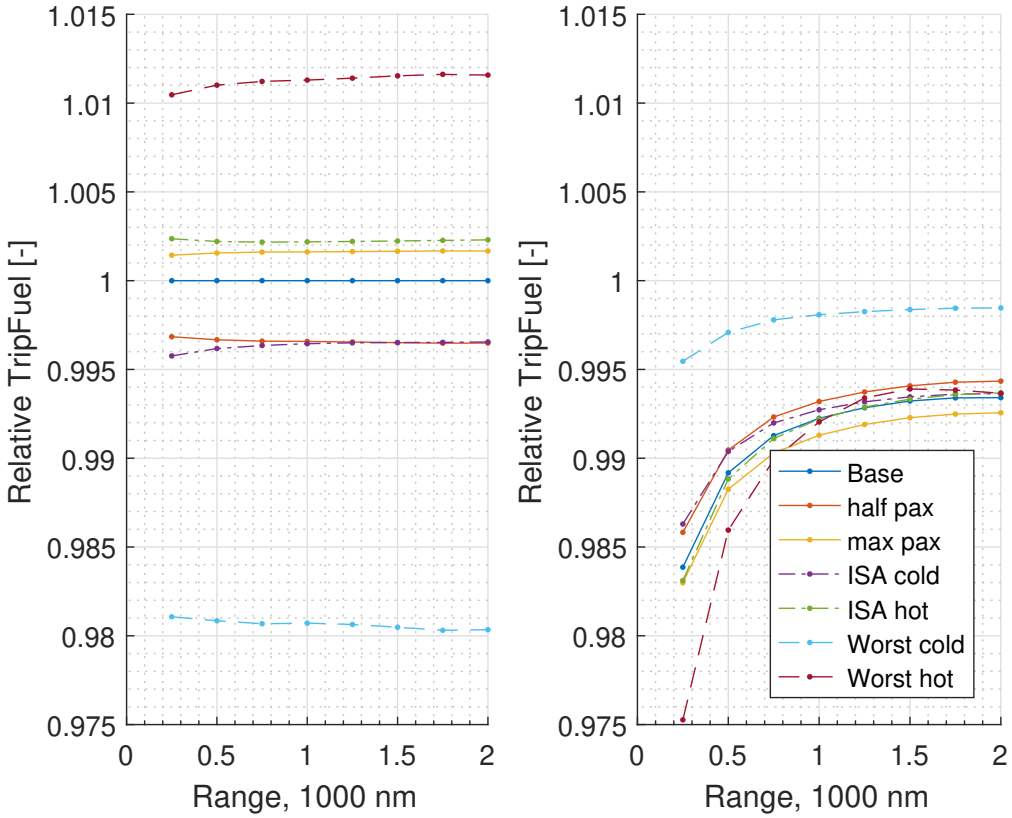

Figure A.12: Relative comparison of trip fuel for missions with 13000 kg payload for CECS on the left with respect to baseline and EECS on the right with respect to the same case CECS fuel burn for all cases.

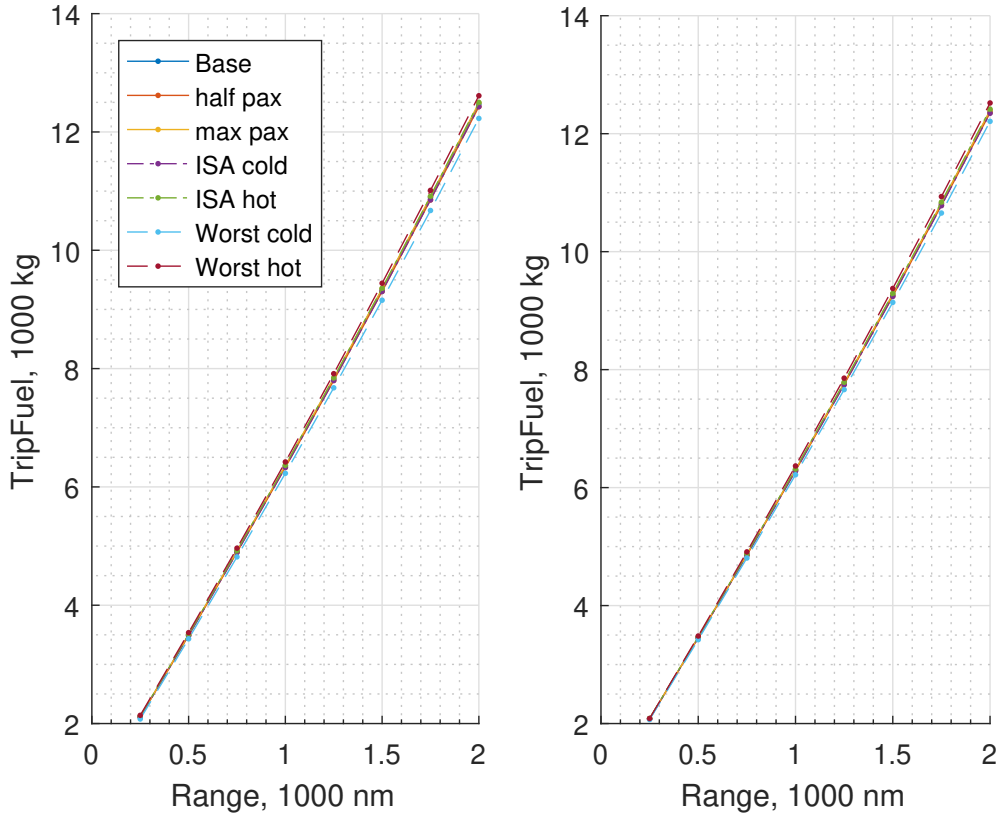

Figure A.13: Comparison of absolute trip fuel for missions with 14000 kg payload for CECS on the left and EECS on the right for all cases.

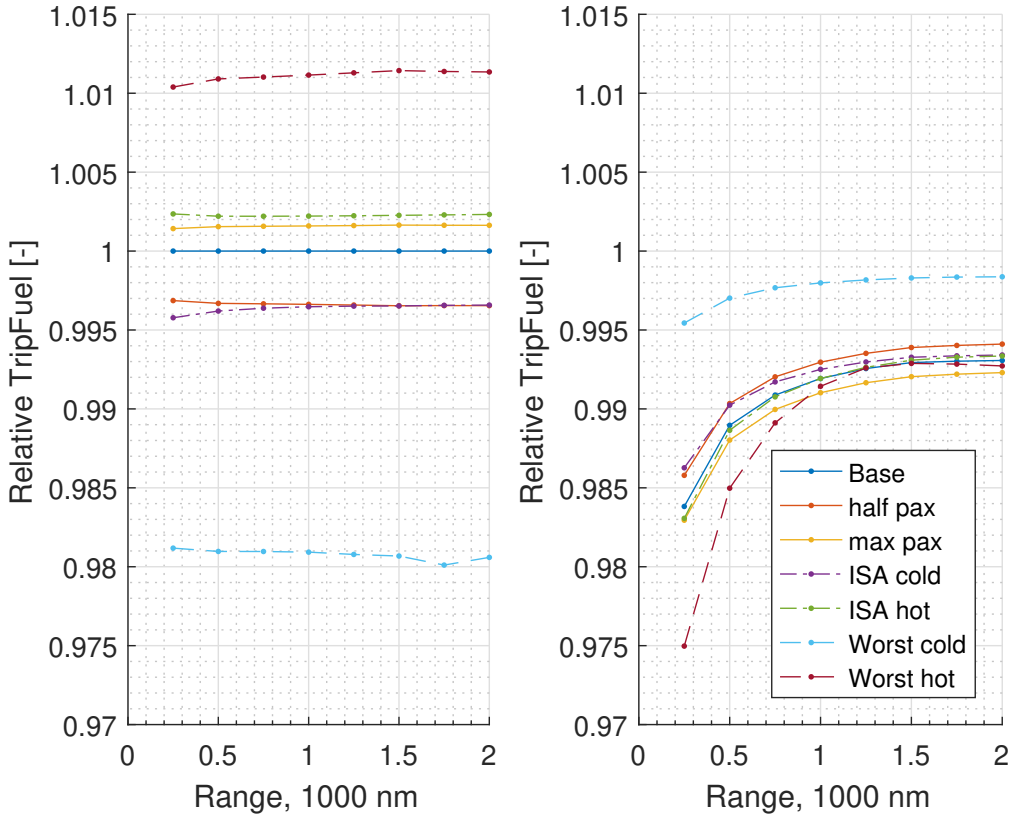

Figure A.14: Relative comparison of trip fuel for missions with 14000 kg payload for CECS on the left with respect to baseline and EECS on the right with respect to the same case CECS fuel burn for all cases.

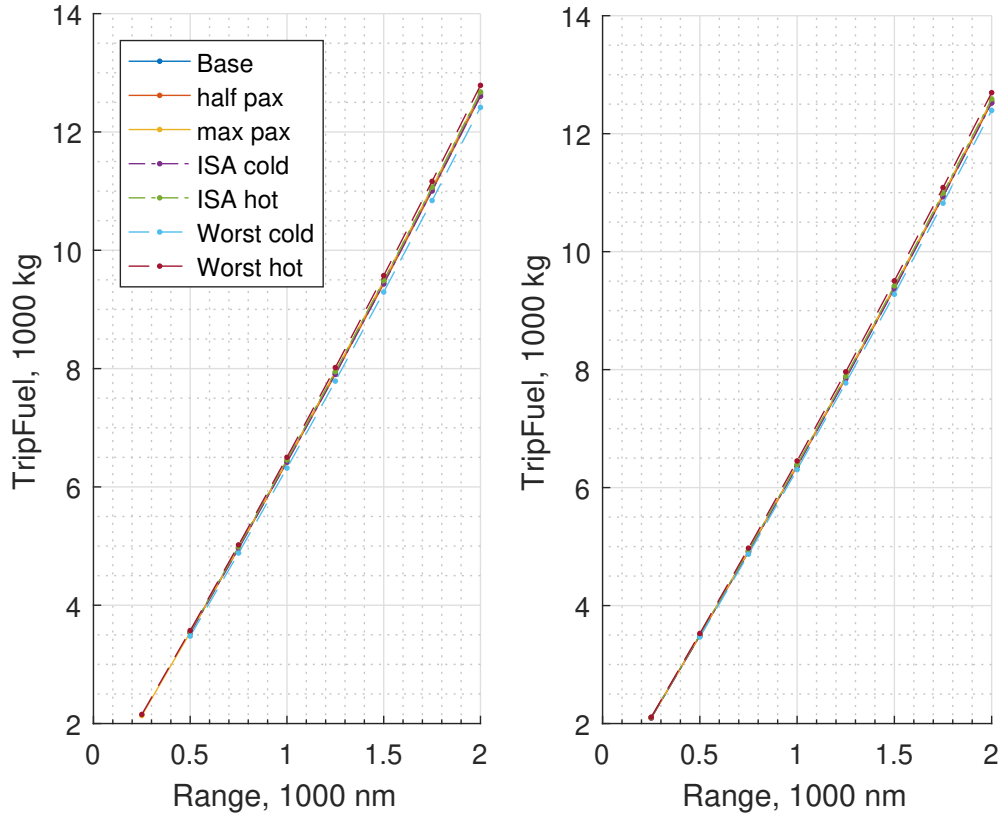

Figure A.15: Comparison of absolute trip fuel for missions with 15000 kg payload for CECS on the left and EECS on the right for all cases.

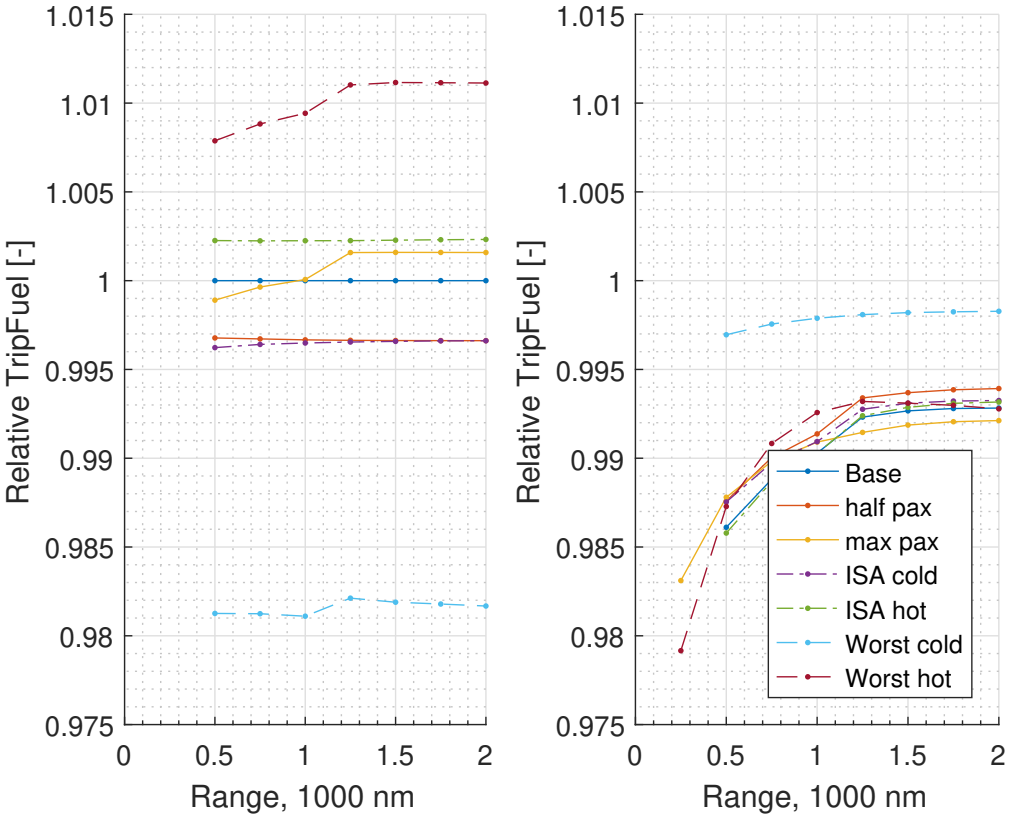

Figure A.16: Relative comparison of trip fuel for missions with 15000 kg payload for CECS on the left with respect to baseline and EECS on the right with respect to the same case CECS fuel burn for all cases.

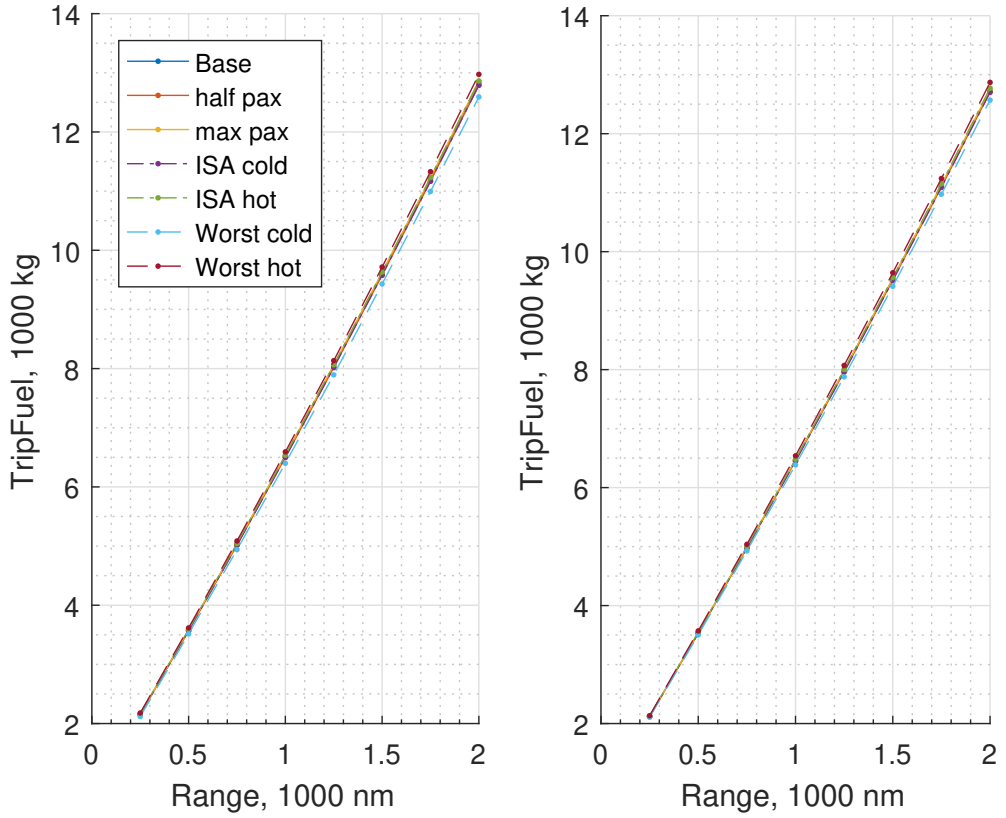

Figure A.17: Comparison of absolute trip fuel for missions with 16000 kg payload for CECS on the left and EECS on the right for all cases.

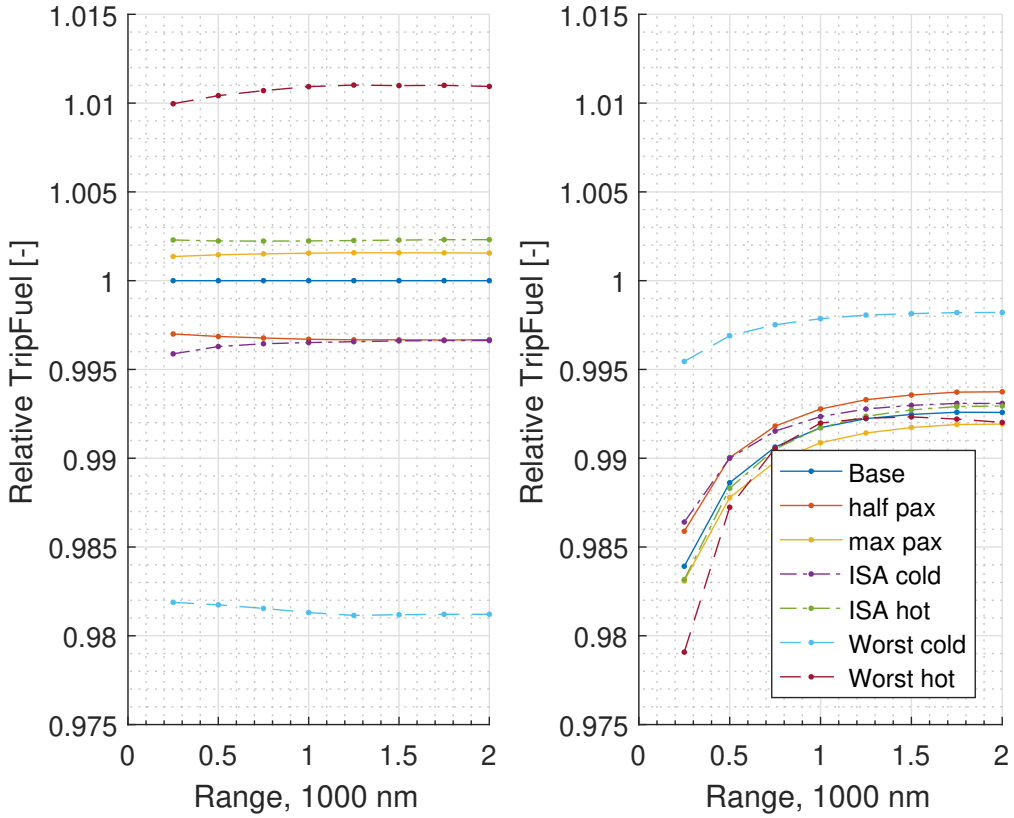

Figure A.18: Relative comparison of trip fuel for missions with 16000 kg payload for CECS on the left with respect to baseline and EECS on the right with respect to the same case CECS fuel burn for all cases.

B

Total Mission Results With 200 kg Retrofit Weight Penalty

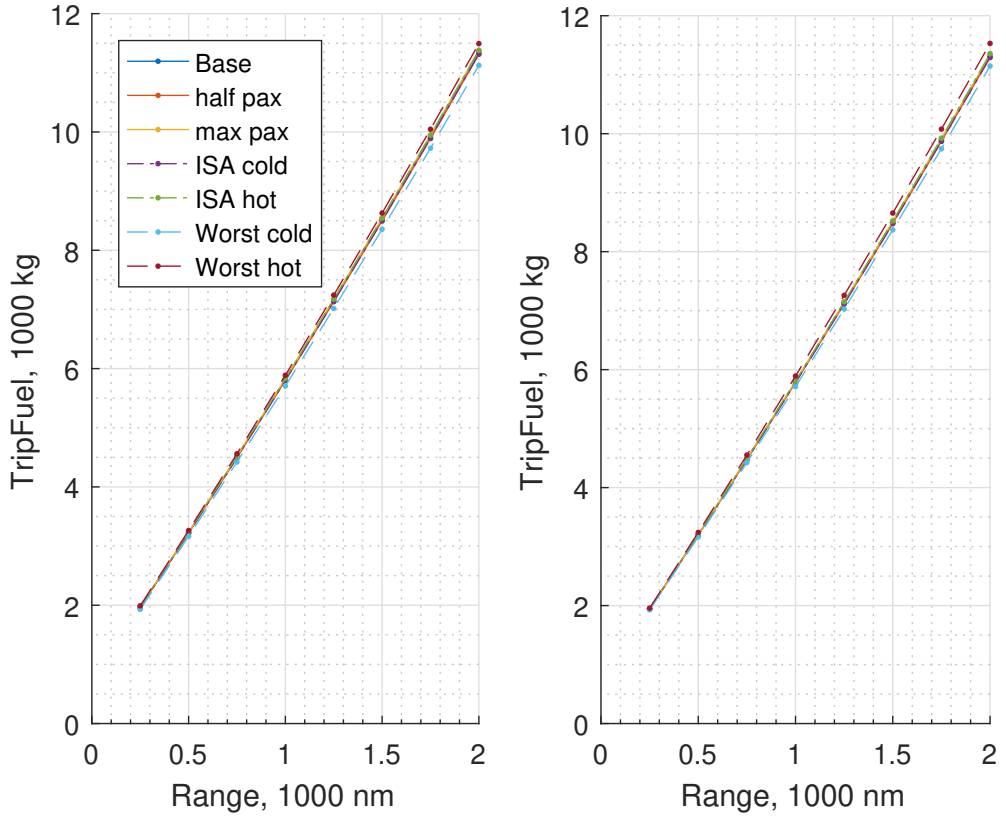

Figure B.1: Comparison of absolute trip fuel for missions with 8000 kg payload for CECS on the left and EECS on the right for all cases, including 200 kg retrofit weight penalty.

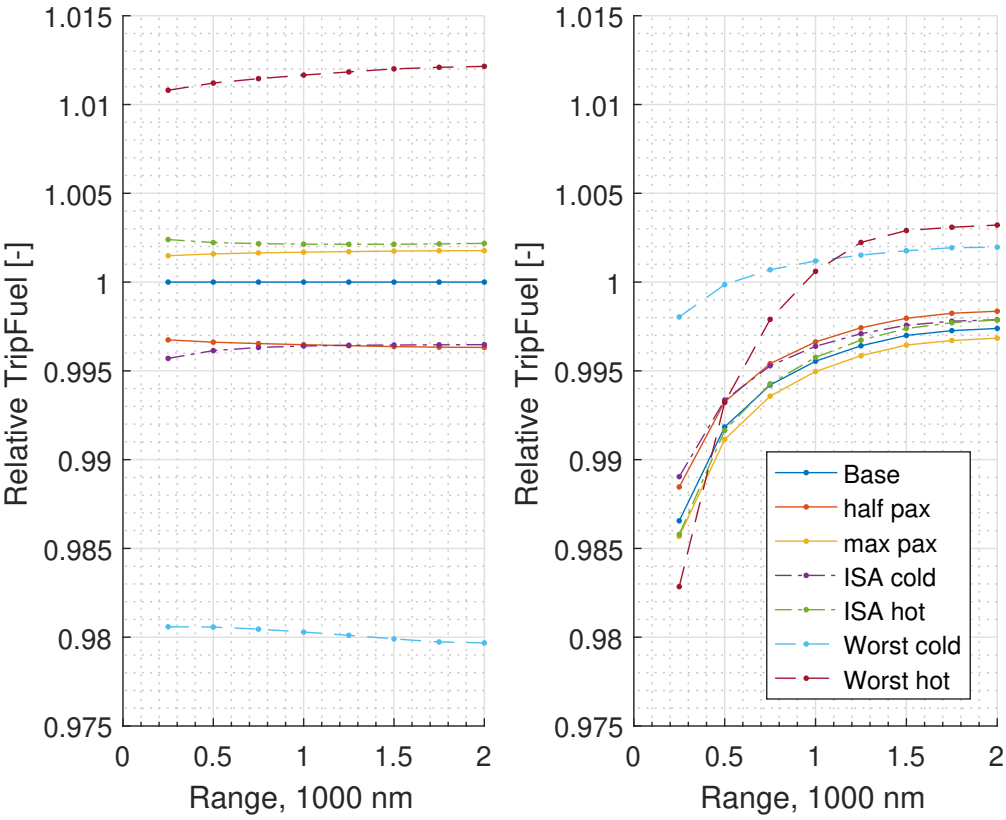

Figure B.2: Relative comparison of trip fuel for missions with 8000 kg payload for CECS on the left with respect to baseline and EECS on the right with respect to the same case CECS fuel burn for all cases, including 200 kg retrofit weight penalty.

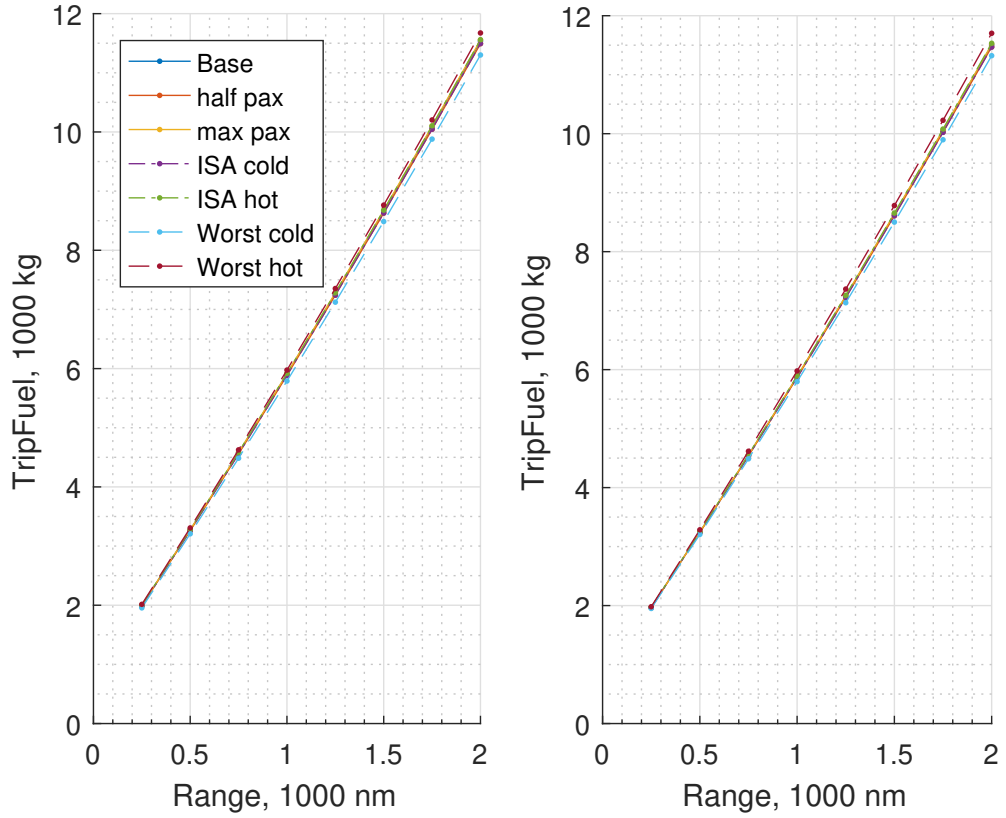

Figure B.3: Comparison of absolute trip fuel for missions with 9000 kg payload for CECS on the left and EECS on the right for all cases, including 200 kg retrofit weight penalty.

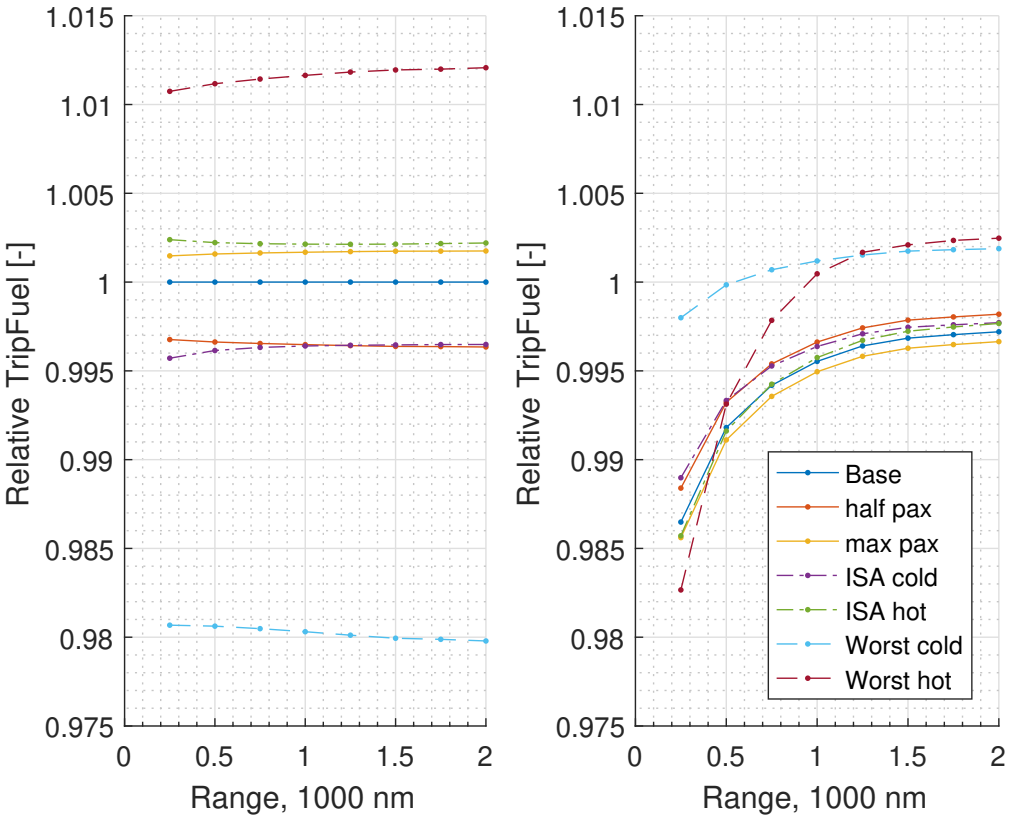

Figure B.4: Relative comparison of trip fuel for missions with 9000 kg payload for CECS on the left with respect to baseline and EECS on the right with respect to the same case CECS fuel burn for all cases, including 200 kg retrofit weight penalty.

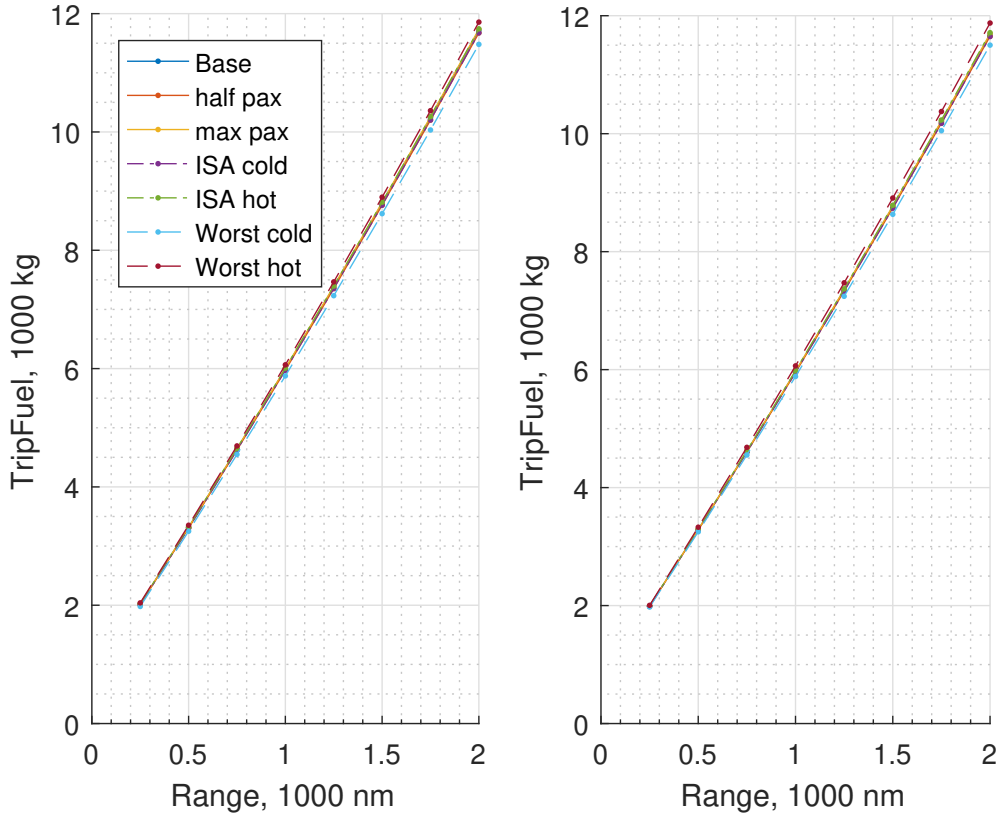

Figure B.5: Comparison of absolute trip fuel for missions with 10000 kg payload for CECS on the left and EECS on the right for all cases, including 200 kg retrofit weight penalty.

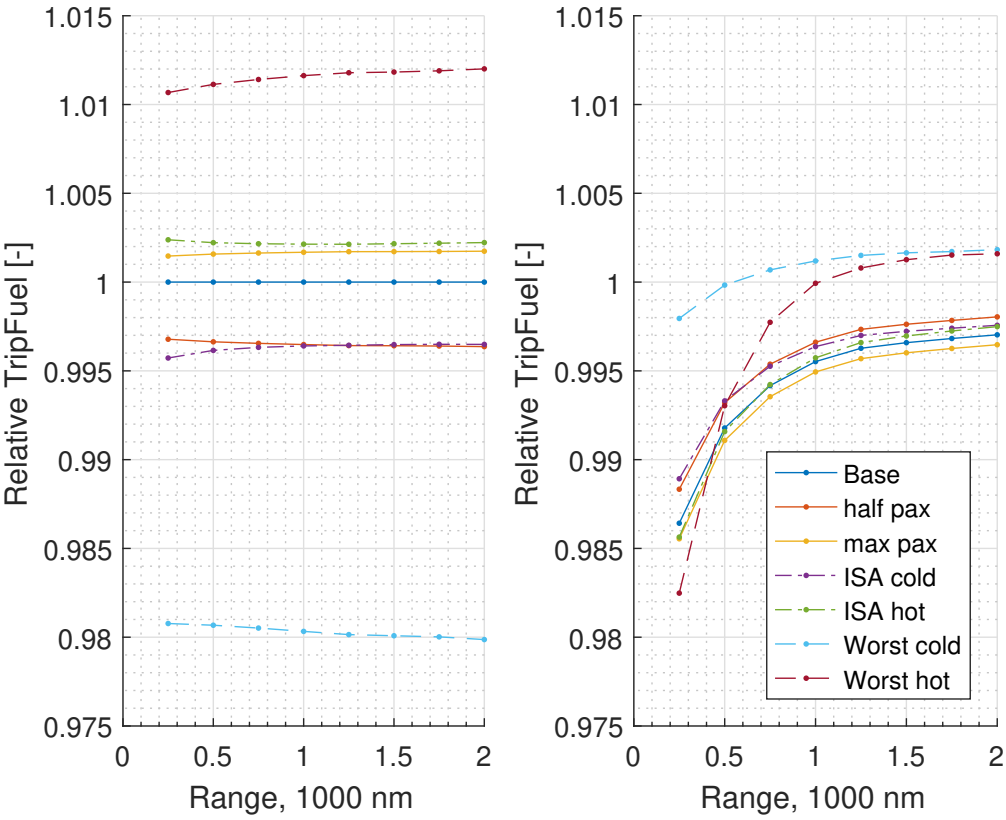

Figure B.6: Relative comparison of trip fuel for missions with 10000 kg payload for CECS on the left with respect to baseline and EECS on the right with respect to the same case CECS fuel burn for all cases, including 200 kg retrofit weight penalty.

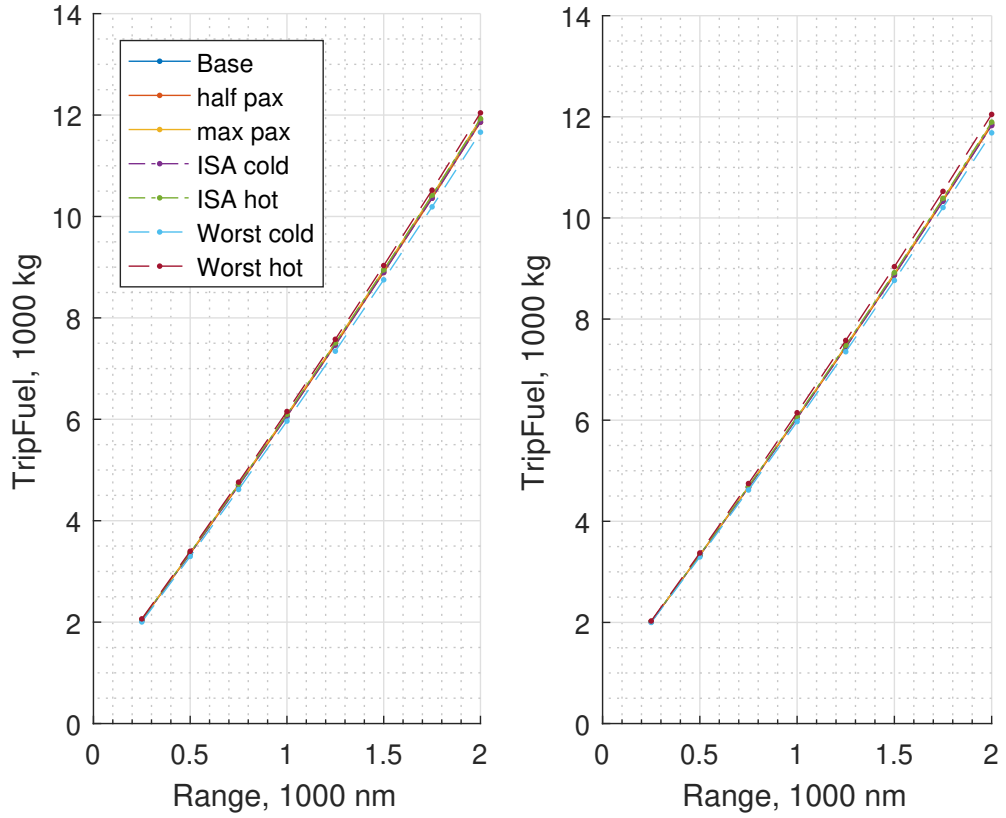

Figure B.7: Comparison of absolute trip fuel for missions with 11000 kg payload for CECS on the left and EECS on the right for all cases, including 200 kg retrofit weight penalty.

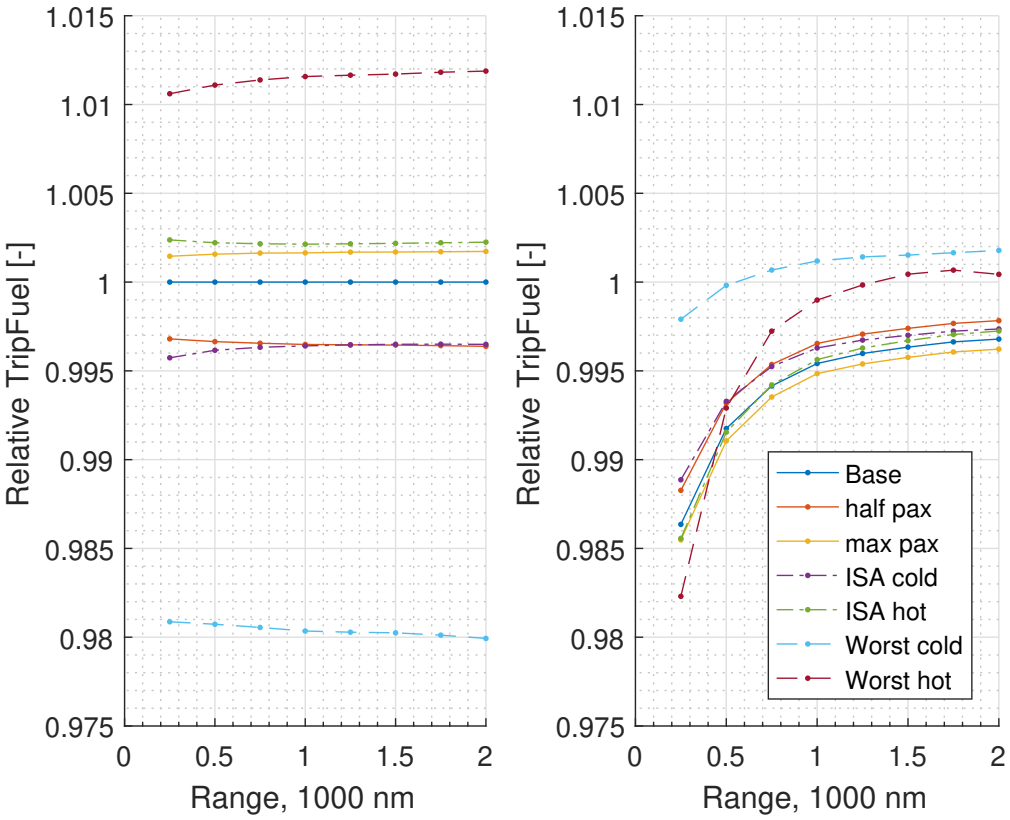

Figure B.8: Relative comparison of trip fuel for missions with 11000 kg payload for CECS on the left with respect to baseline and EECS on the right with respect to the same case CECS fuel burn for all cases, including 200 kg retrofit weight penalty.

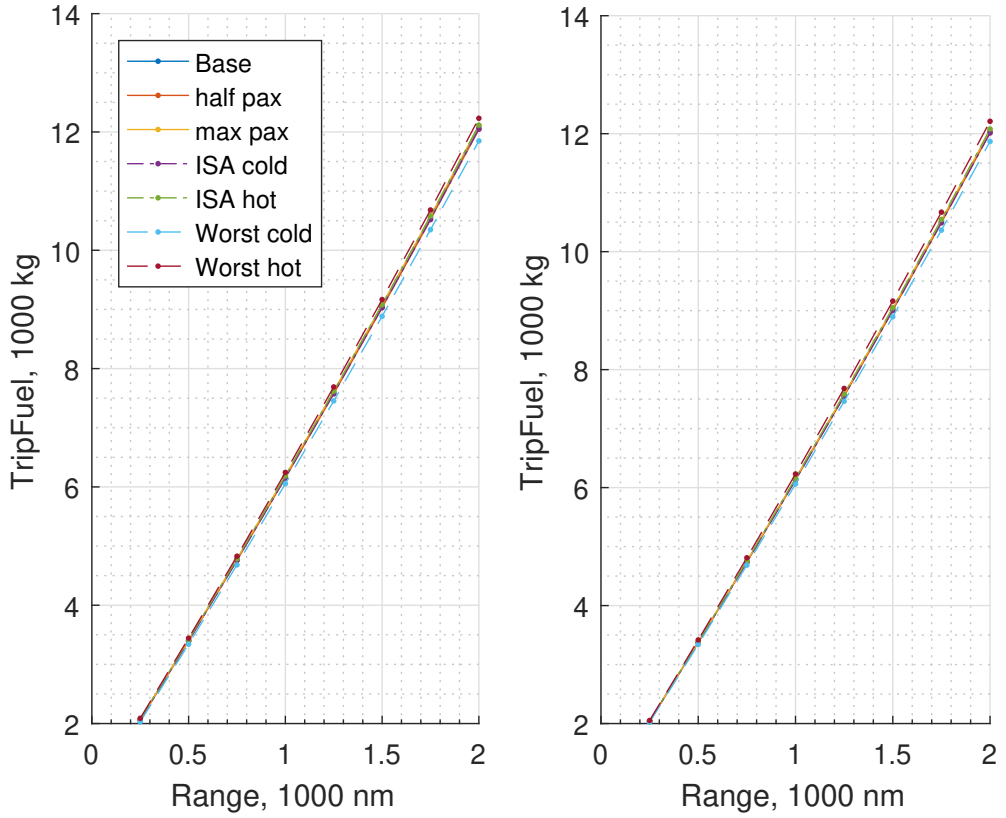

Figure B.9: Comparison of absolute trip fuel for missions with 12000 kg payload for CECS on the left and EECS on the right for all cases, including 200 kg retrofit weight penalty.

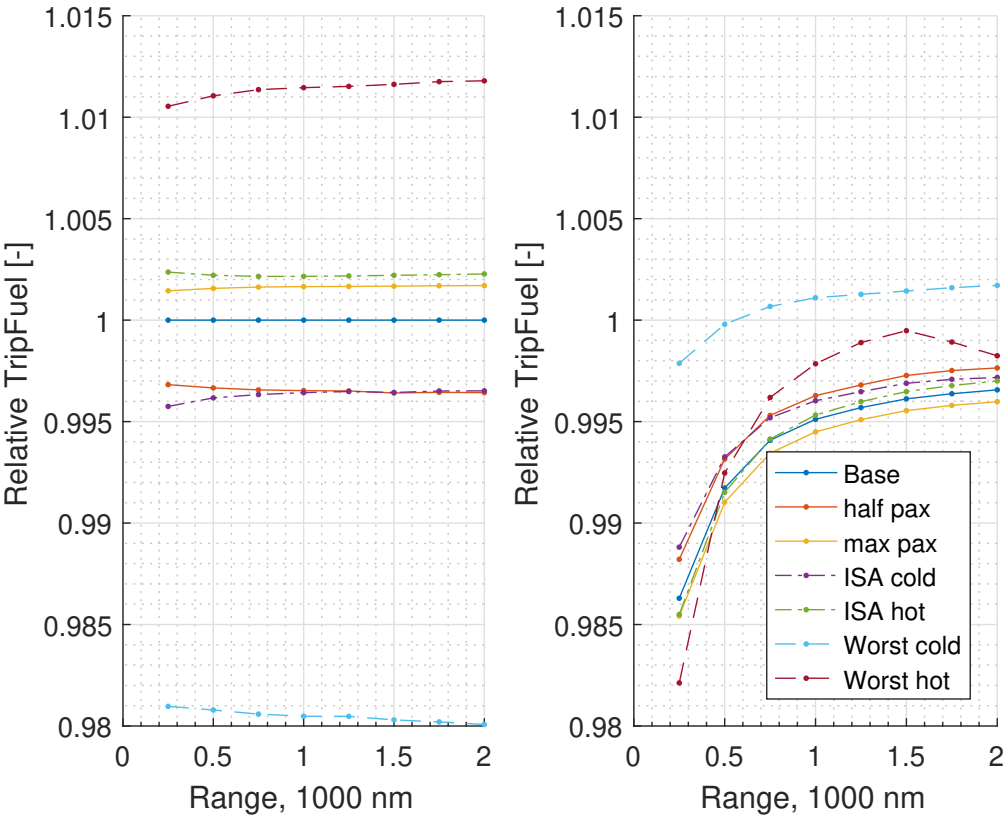

Figure B.10: Relative comparison of trip fuel for missions with 12000 kg payload for CECS on the left with respect to baseline and EECS on the right with respect to the same case CECS fuel burn for all cases, including 200 kg retrofit weight penalty.

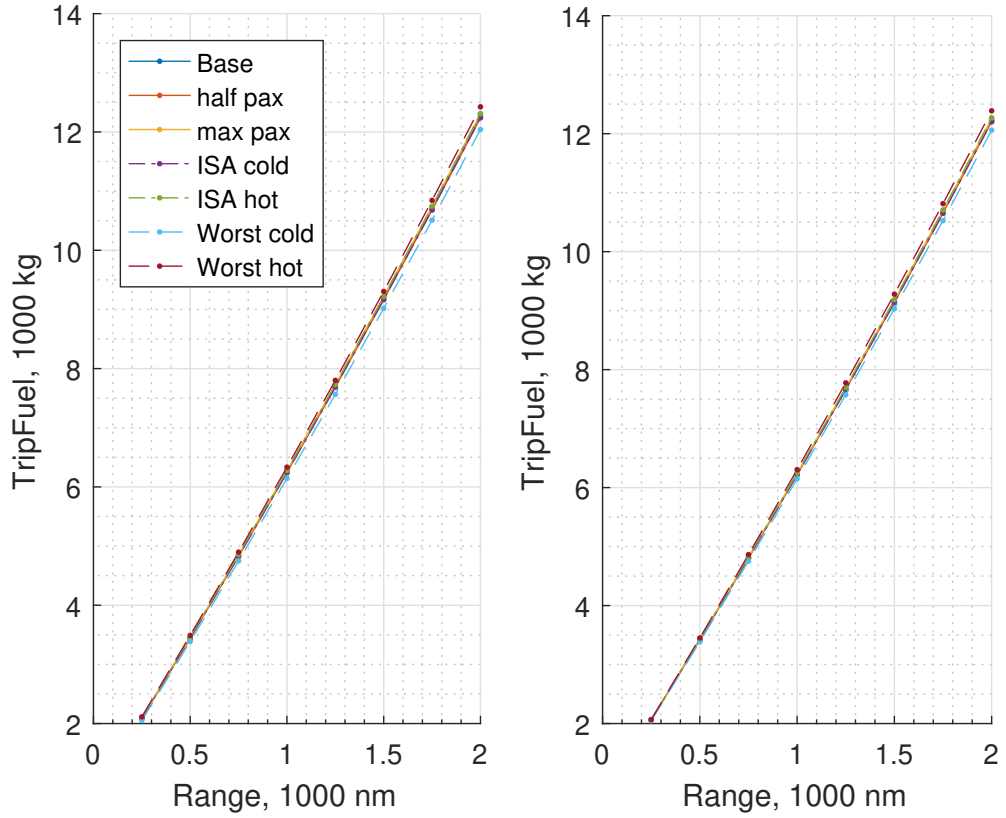

Figure B.11: Comparison of absolute trip fuel for missions with 13000 kg payload for CECS on the left and EECS on the right for all cases, including 200 kg retrofit weight penalty.

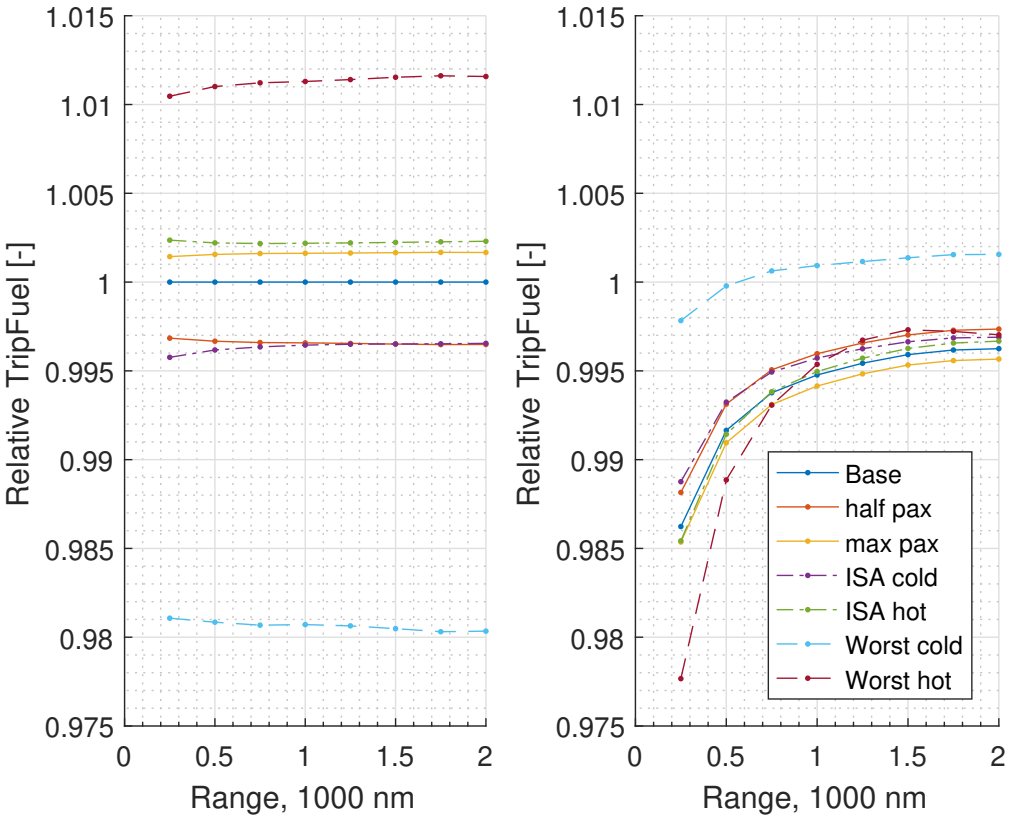

Figure B.12: Relative comparison of trip fuel for missions with 13000 kg payload for CECS on the left with respect to baseline and EECS on the right with respect to the same case CECS fuel burn for all cases, including 200 kg retrofit weight penalty.

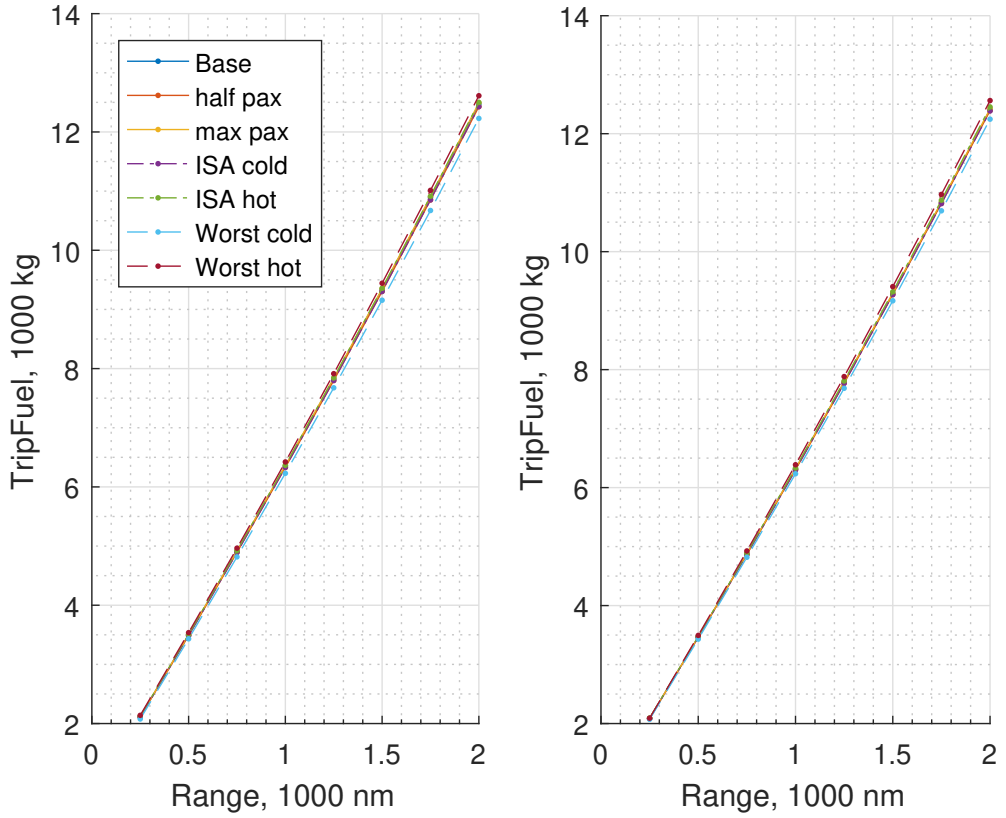

Figure B.13: Comparison of absolute trip fuel for missions with 14000 kg payload for CECS on the left and EECS on the right for all cases, including 200 kg retrofit weight penalty.

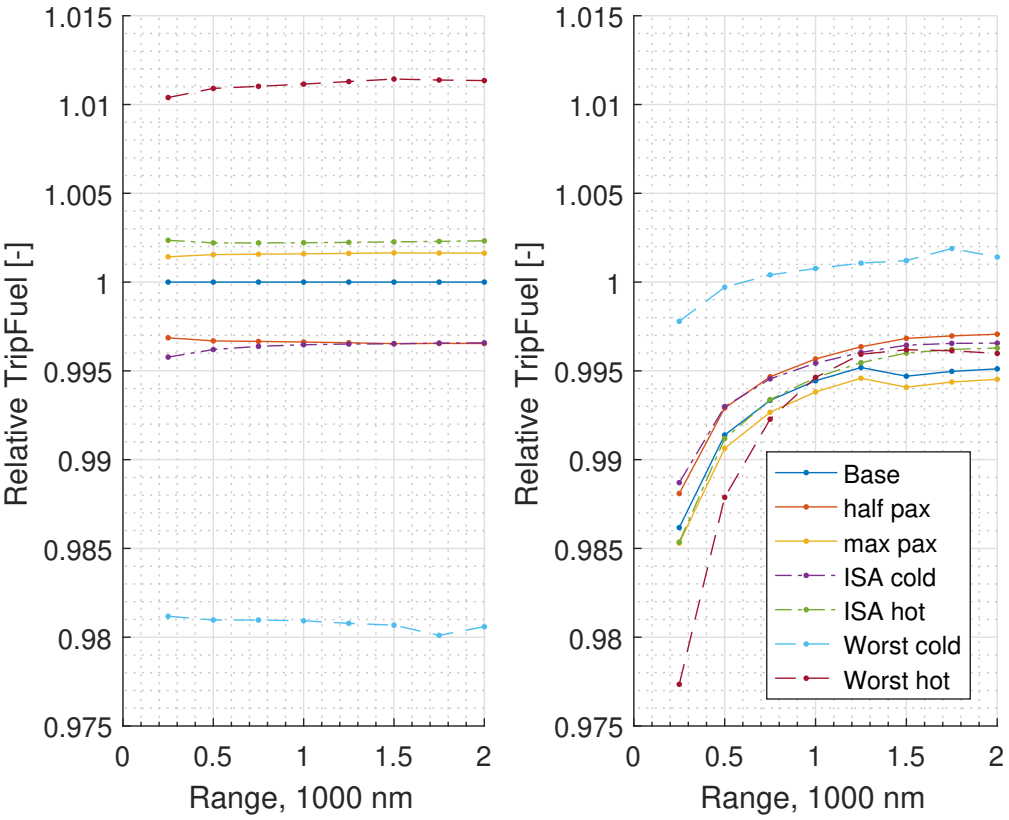

Figure B.14: Relative comparison of trip fuel for missions with 14000 kg payload for CECS on the left with respect to baseline and EECS on the right with respect to the same case CECS fuel burn for all cases, including 200 kg retrofit weight penalty.

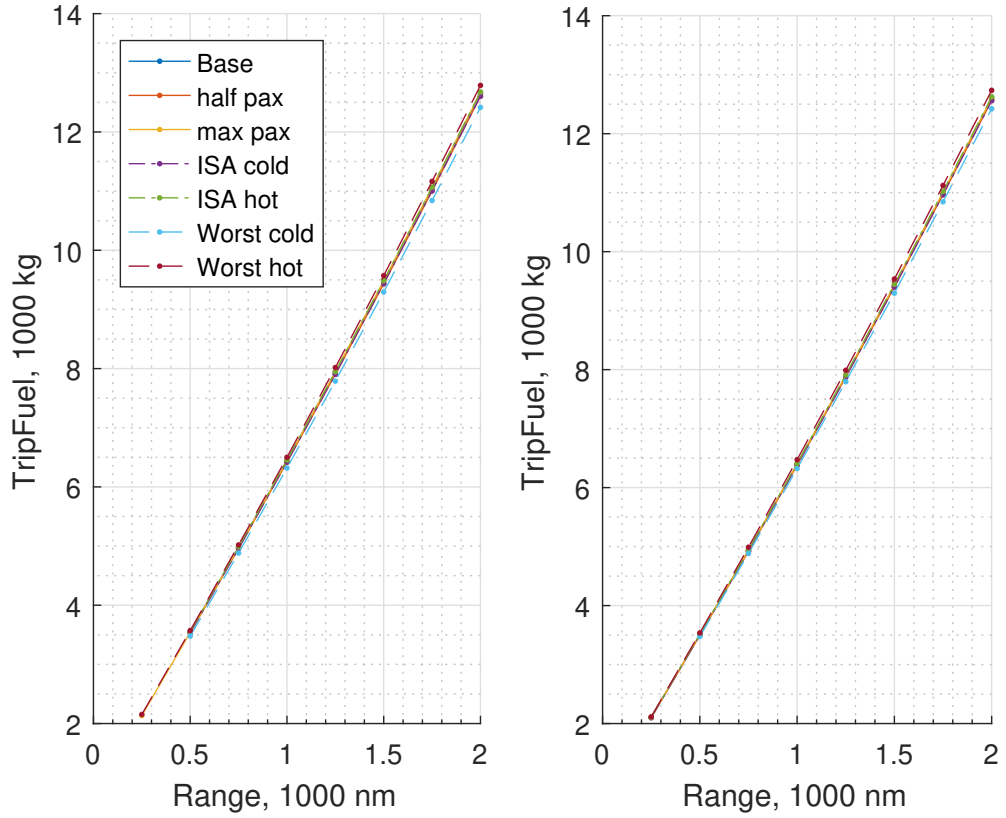

Figure B.15: Comparison of absolute trip fuel for missions with 15000 kg payload for CECS on the left and EECS on the right for all cases, including 200 kg retrofit weight penalty.

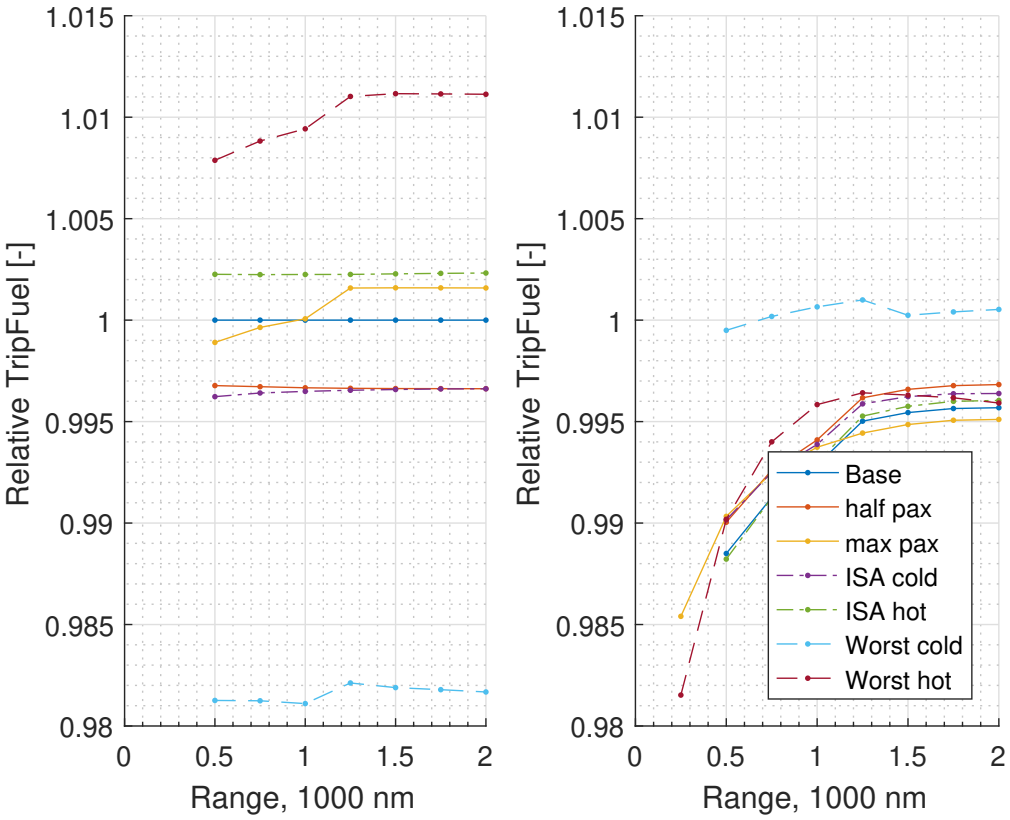

Figure B.16: Relative comparison of trip fuel for missions with 15000 kg payload for CECS on the left with respect to baseline and EECS on the right with respect to the same case CECS fuel burn for all cases, including 200 kg retrofit weight penalty.

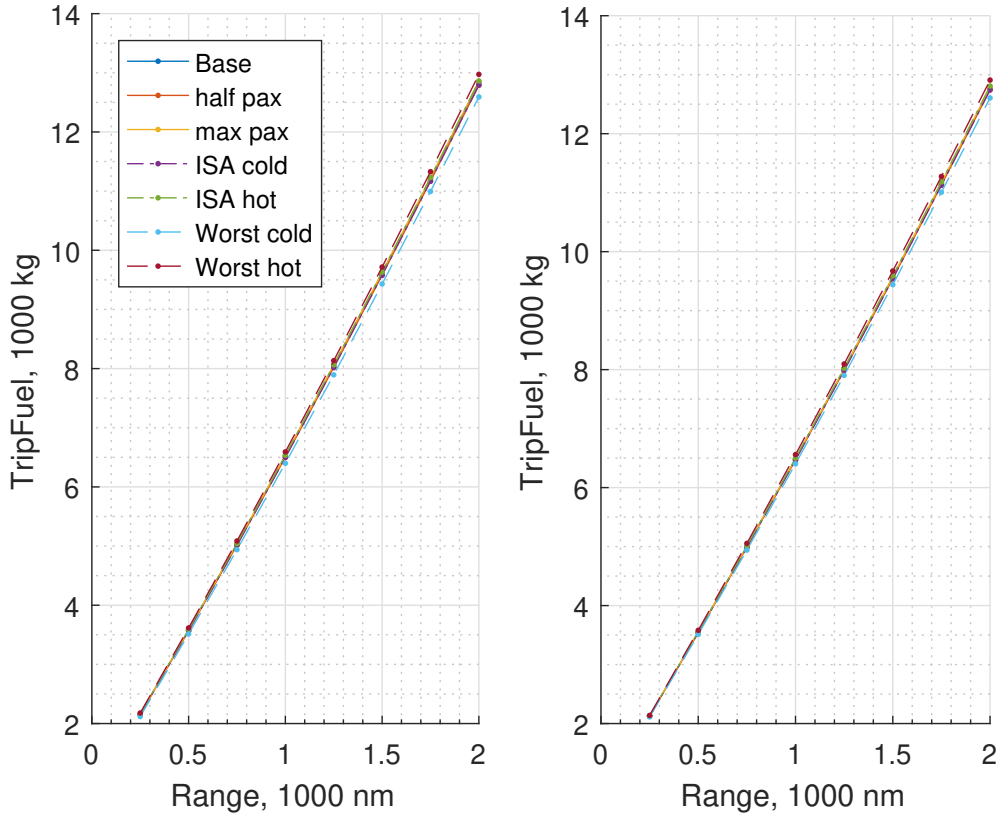

Figure B.17: Comparison of absolute trip fuel for missions with 16000 kg payload for CECS on the left and EECS on the right for all cases, including 200 kg retrofit weight penalty.

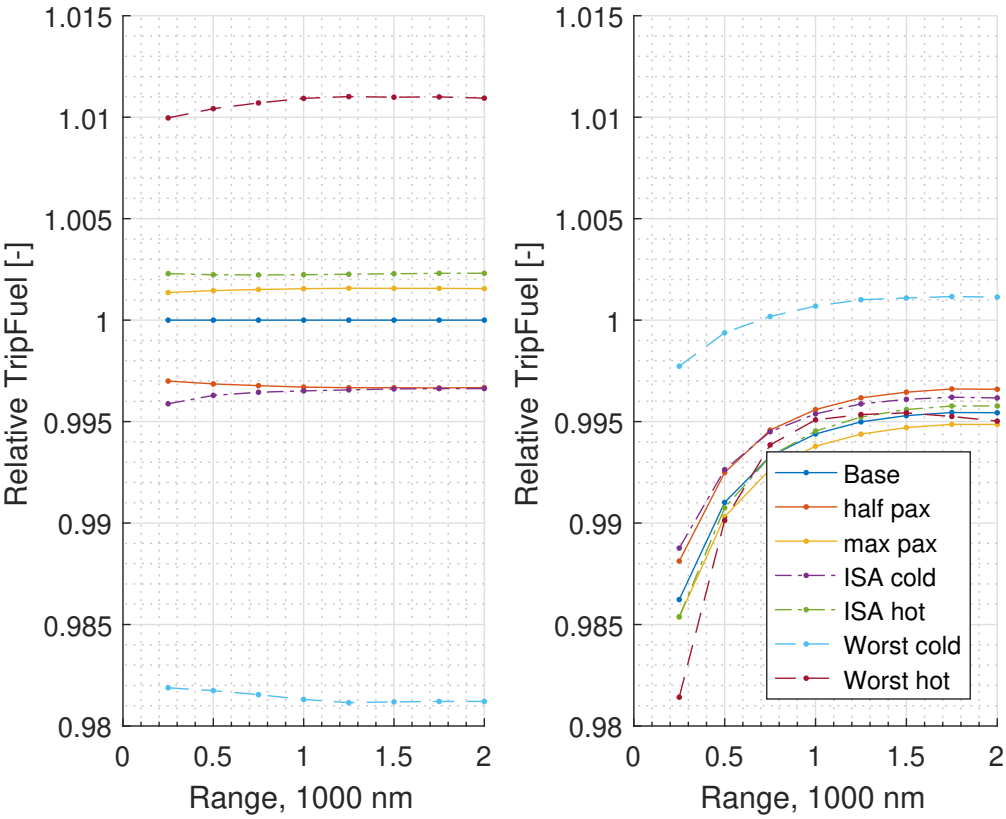

Figure B.18: Relative comparison of trip fuel for missions with 16000 kg payload for CECS on the left with respect to baseline and EECS on the right with respect to the same case CECS fuel burn for all cases, including 200 kg retrofit weight penalty.

C

Total Mission Results With 400 kg Retrofit Weight Penalty

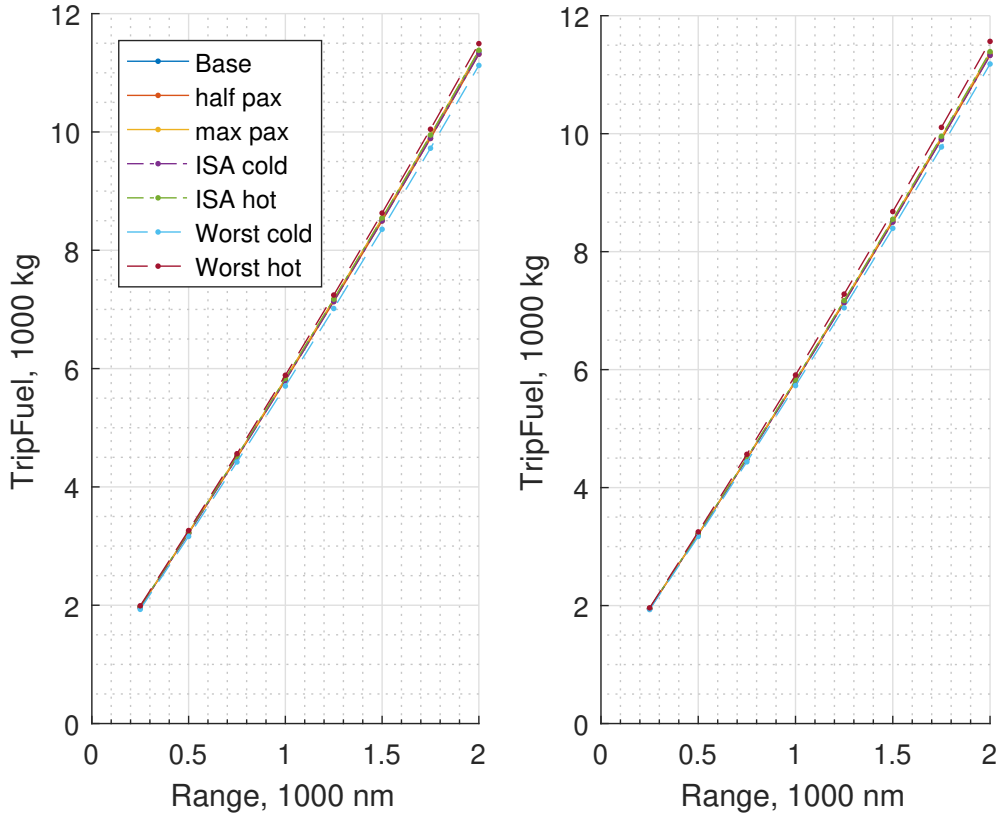

Figure C.1: Comparison of absolute trip fuel for missions with 8000 kg payload for CECS on the left and EECS on the right for all cases, including 400 kg retrofit weight penalty.

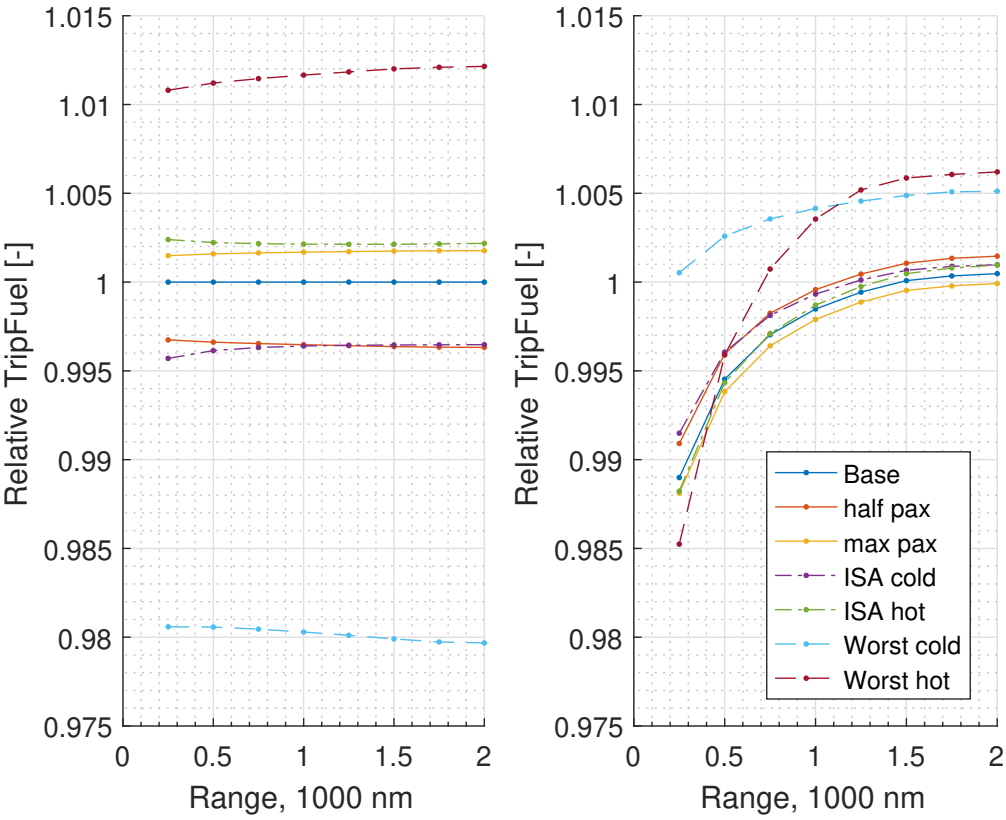

Figure C.2: Relative comparison of trip fuel for missions with 8000 kg payload for CECS on the left with respect to baseline and EECS on the right with respect to the same case CECS fuel burn for all cases, including 400 kg retrofit weight penalty.

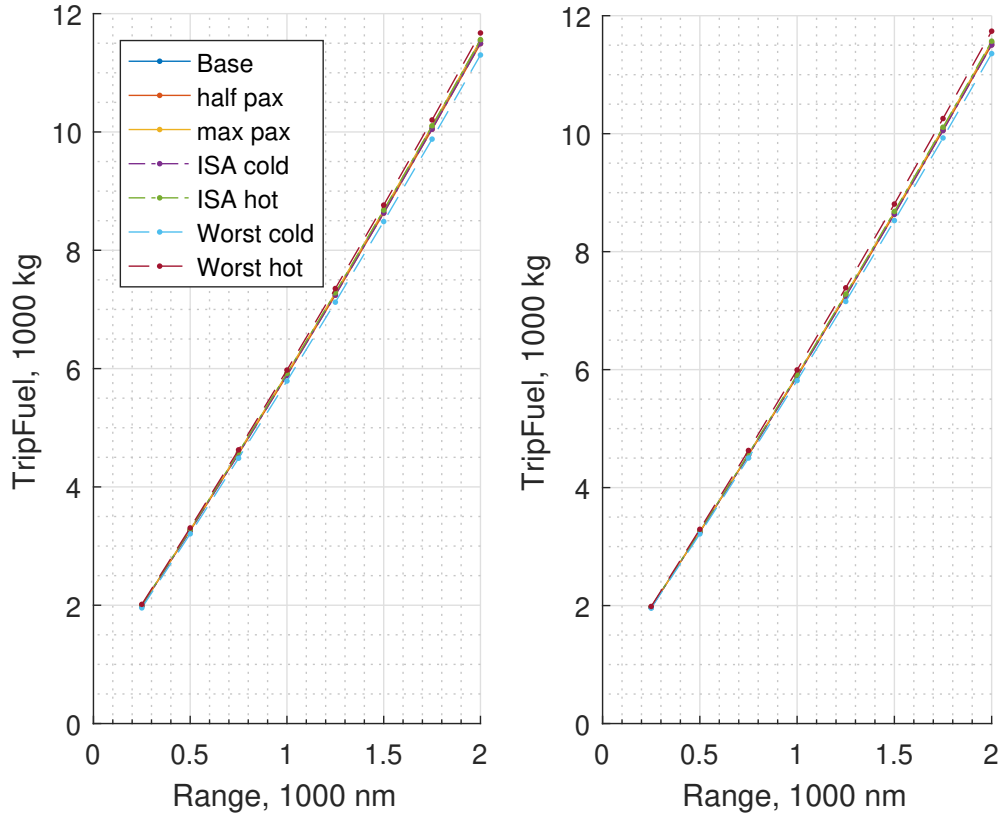

Figure C.3: Comparison of absolute trip fuel for missions with 9000 kg payload for CECS on the left and EECS on the right for all cases, including 400 kg retrofit weight penalty.

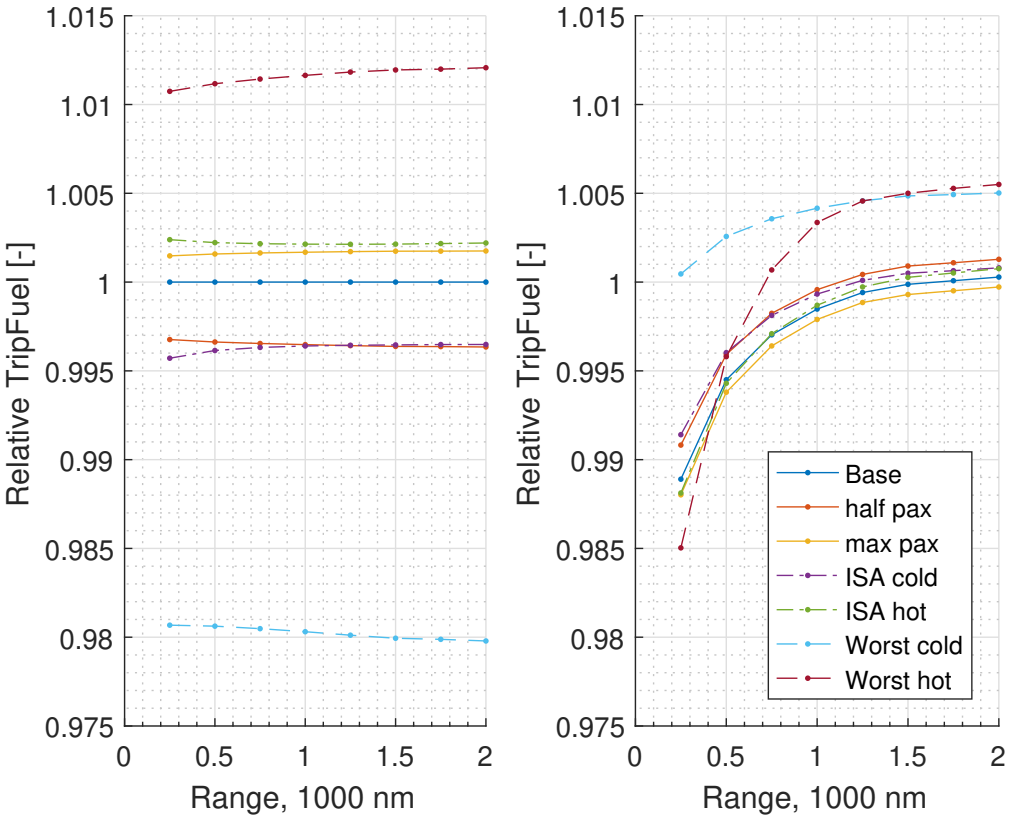

Figure C.4: Relative comparison of trip fuel for missions with 9000 kg payload for CECS on the left with respect to baseline and EECS on the right with respect to the same case CECS fuel burn for all cases, including 400 kg retrofit weight penalty.

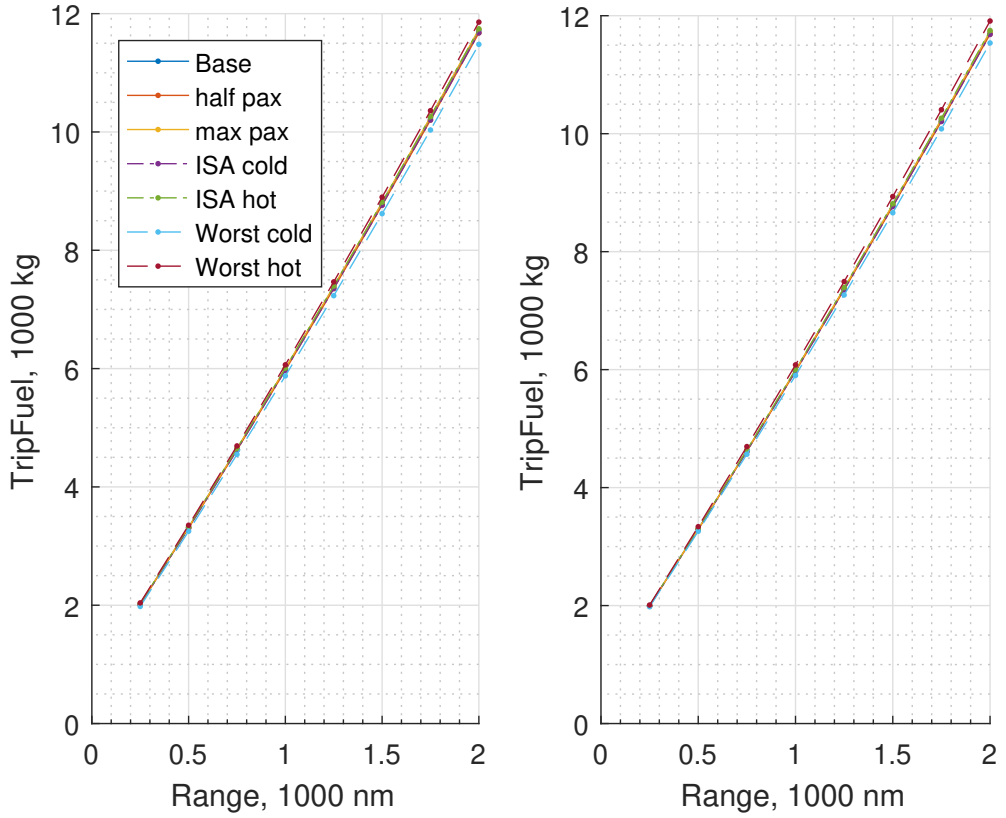

Figure C.5: Comparison of absolute trip fuel for missions with 10000 kg payload for CECS on the left and EECS on the right for all cases, including 400 kg retrofit weight penalty.

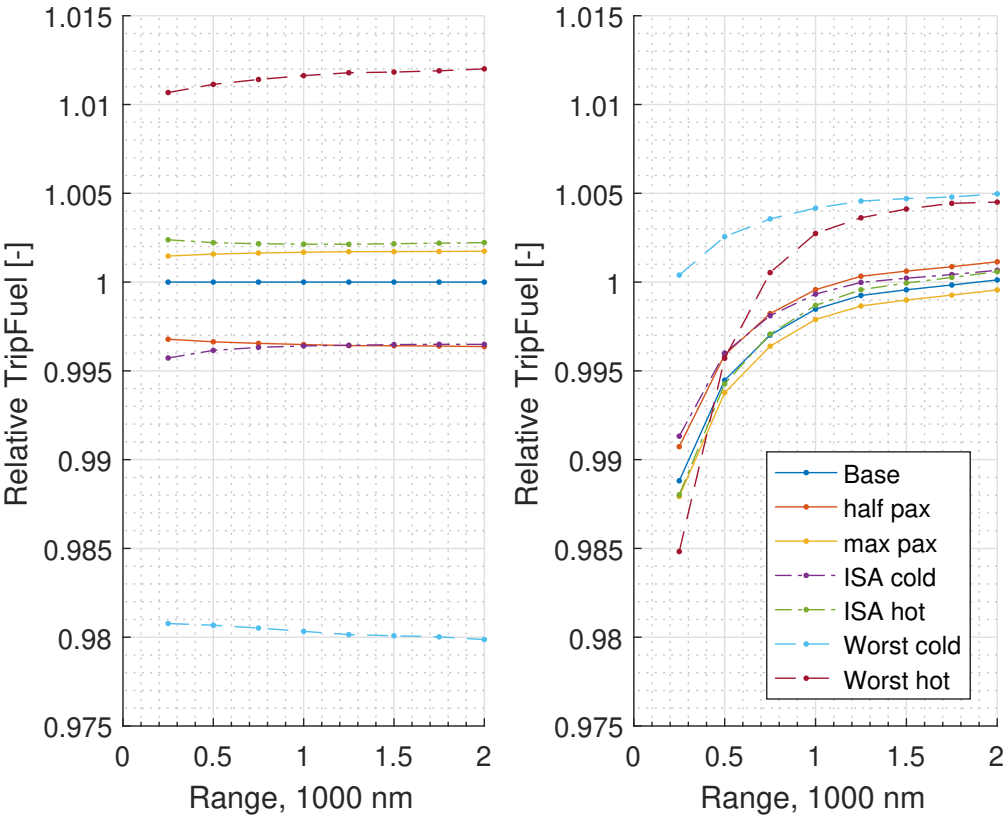

Figure C.6: Relative comparison of trip fuel for missions with 10000 kg payload for CECS on the left with respect to baseline and EECS on the right with respect to the same case CECS fuel burn for all cases, including 400 kg retrofit weight penalty.

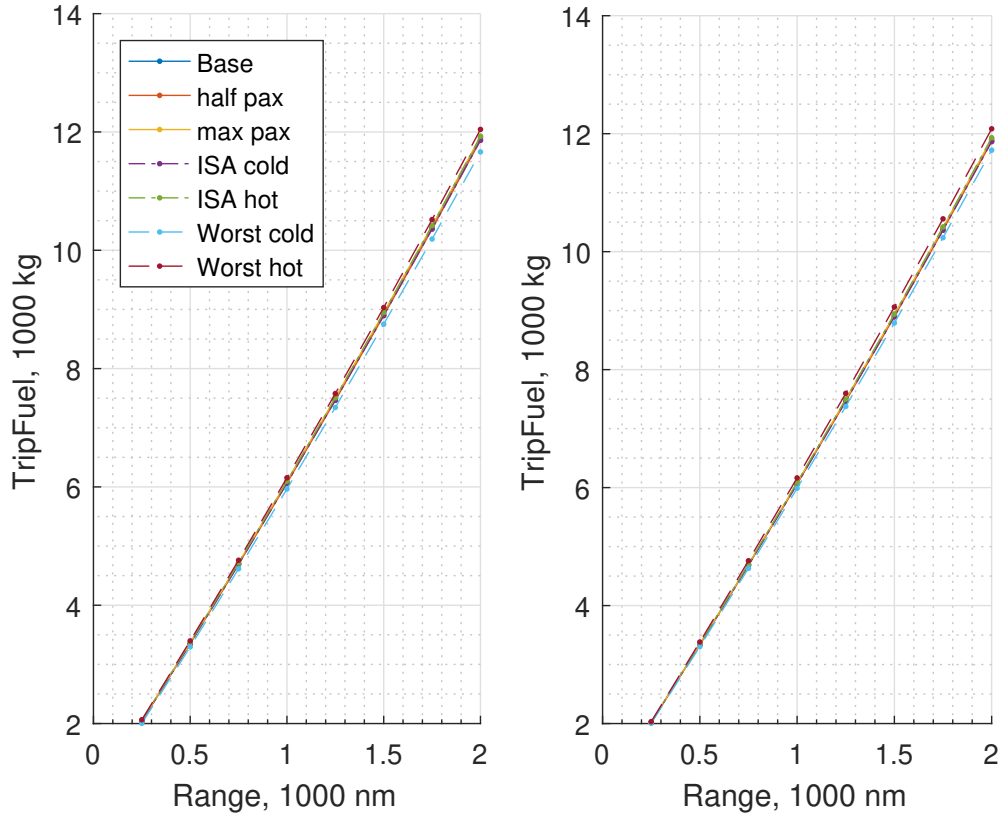

Figure C.7: Comparison of absolute trip fuel for missions with 11000 kg payload for CECS on the left and EECS on the right for all cases, including 400 kg retrofit weight penalty.

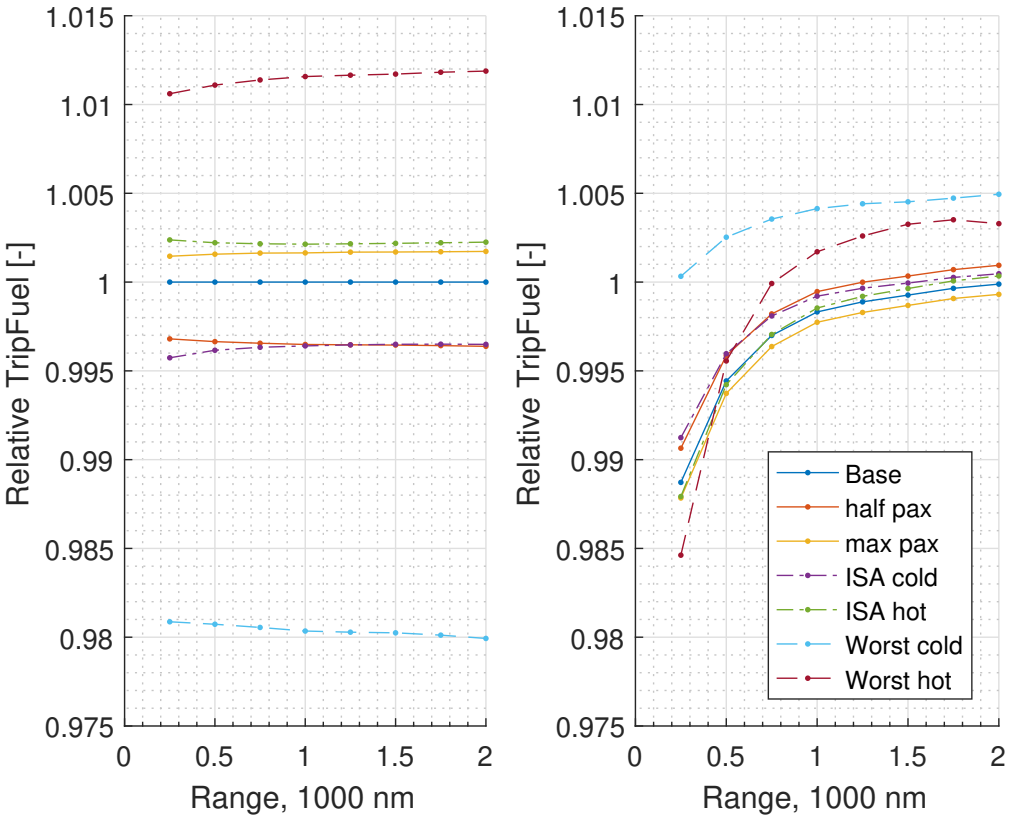

Figure C.8: Relative comparison of trip fuel for missions with 11000 kg payload for CECS on the left with respect to baseline and EECS on the right with respect to the same case CECS fuel burn for all cases, including 400 kg retrofit weight penalty.

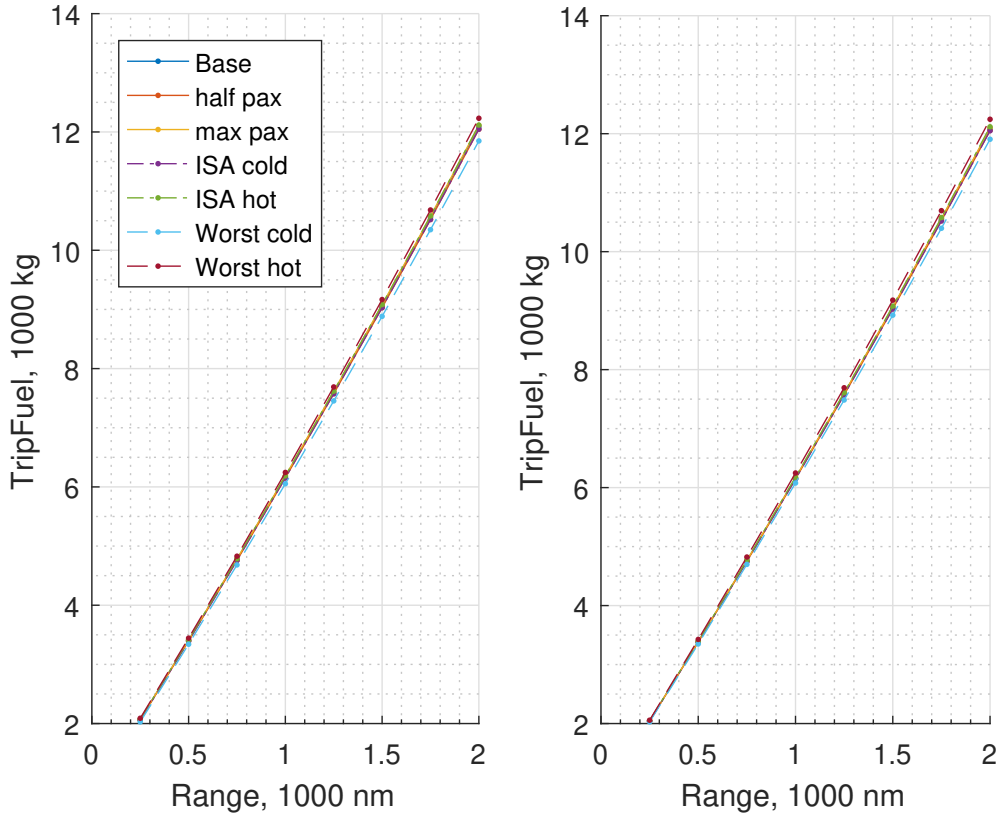

Figure C.9: Comparison of absolute trip fuel for missions with 12000 kg payload for CECS on the left and EECS on the right for all cases, including 400 kg retrofit weight penalty.

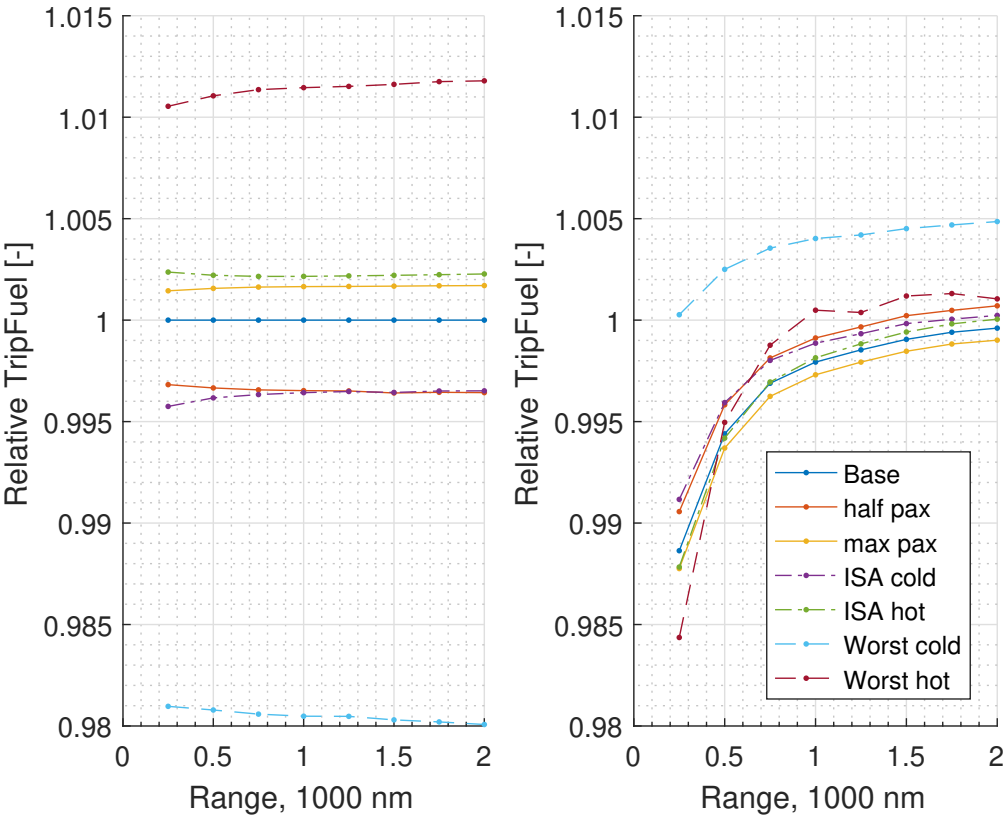

Figure C.10: Relative comparison of trip fuel for missions with 12000 kg payload for CECS on the left with respect to baseline and EECS on the right with respect to the same case CECS fuel burn for all cases, including 400 kg retrofit weight penalty.

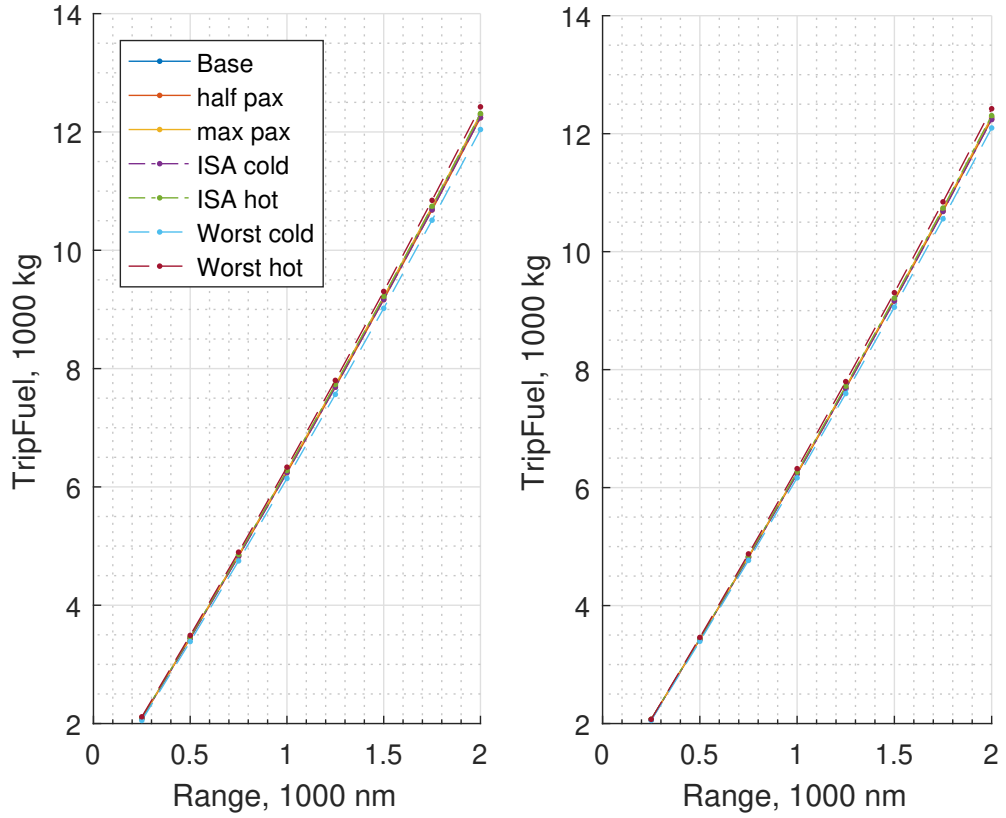

Figure C.11: Comparison of absolute trip fuel for missions with 13000 kg payload for CECS on the left and EECS on the right for all cases, including 400 kg retrofit weight penalty.

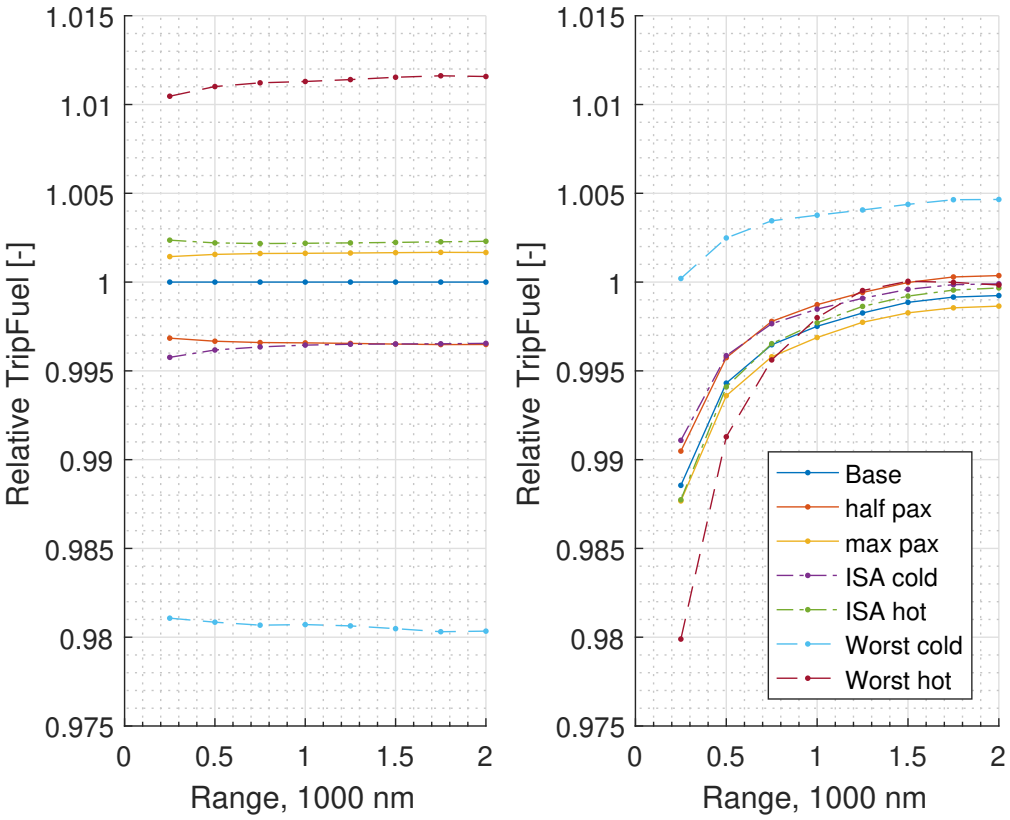

Figure C.12: Relative comparison of trip fuel for missions with 13000 kg payload for CECS on the left with respect to baseline and EECS on the right with respect to the same case CECS fuel burn for all cases, including 400 kg retrofit weight penalty.

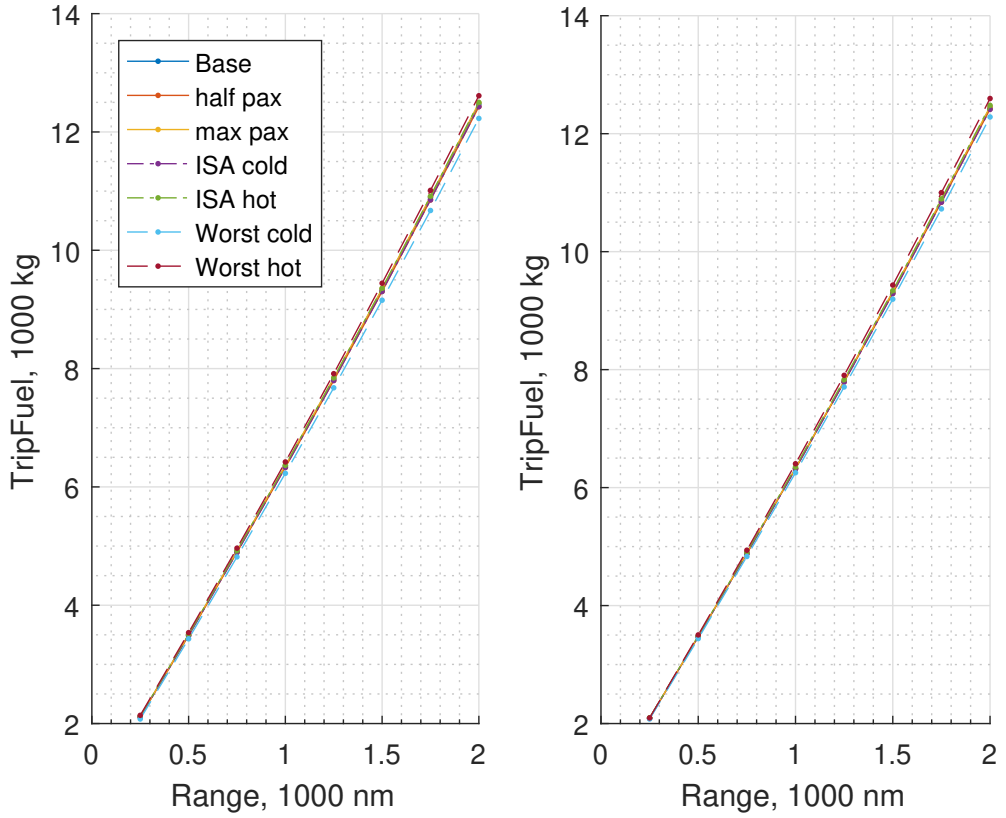

Figure C.13: Comparison of absolute trip fuel for missions with 14000 kg payload for CECS on the left and EECS on the right for all cases, including 400 kg retrofit weight penalty.

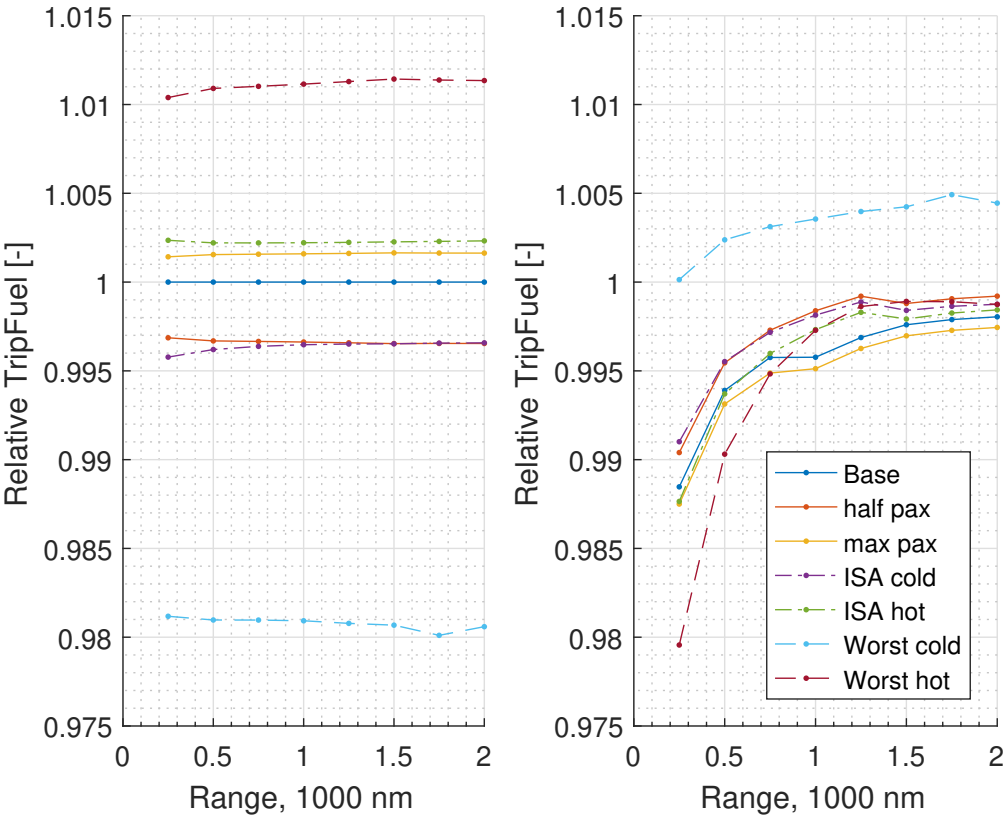

Figure C.14: Relative comparison of trip fuel for missions with 14000 kg payload for CECS on the left with respect to baseline and EECS on the right with respect to the same case CECS fuel burn for all cases, including 400 kg retrofit weight penalty.

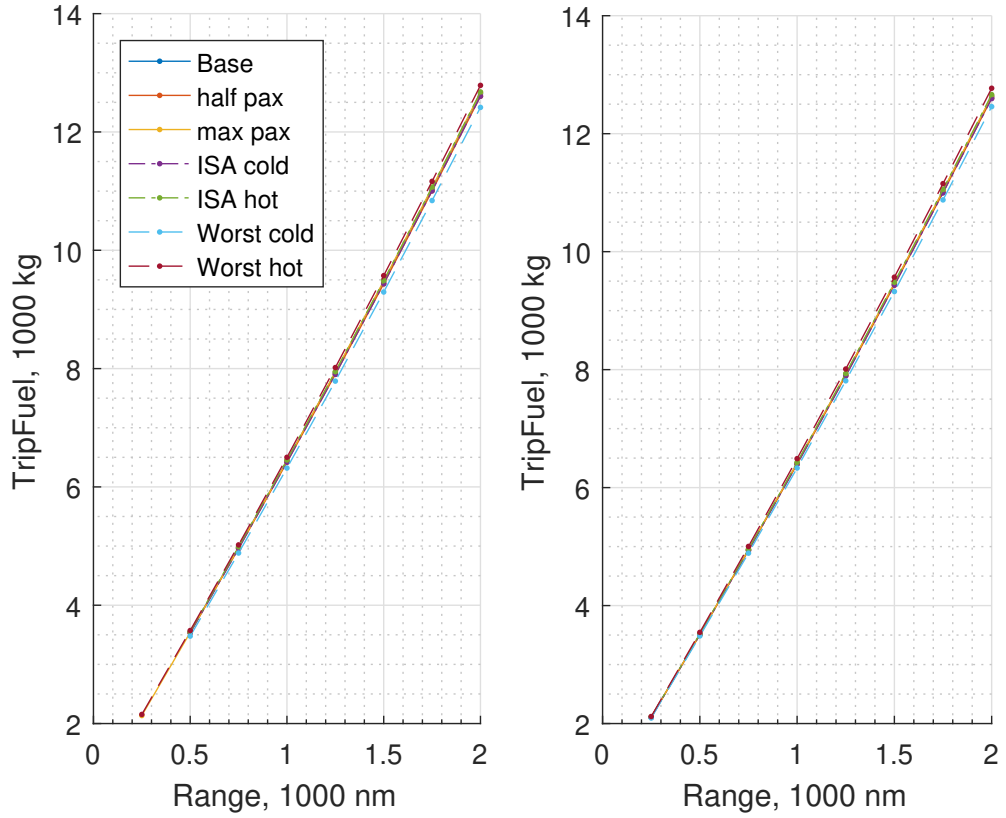

Figure C.15: Comparison of absolute trip fuel for missions with 15000 kg payload for CECS on the left and EECS on the right for all cases, including 400 kg retrofit weight penalty.

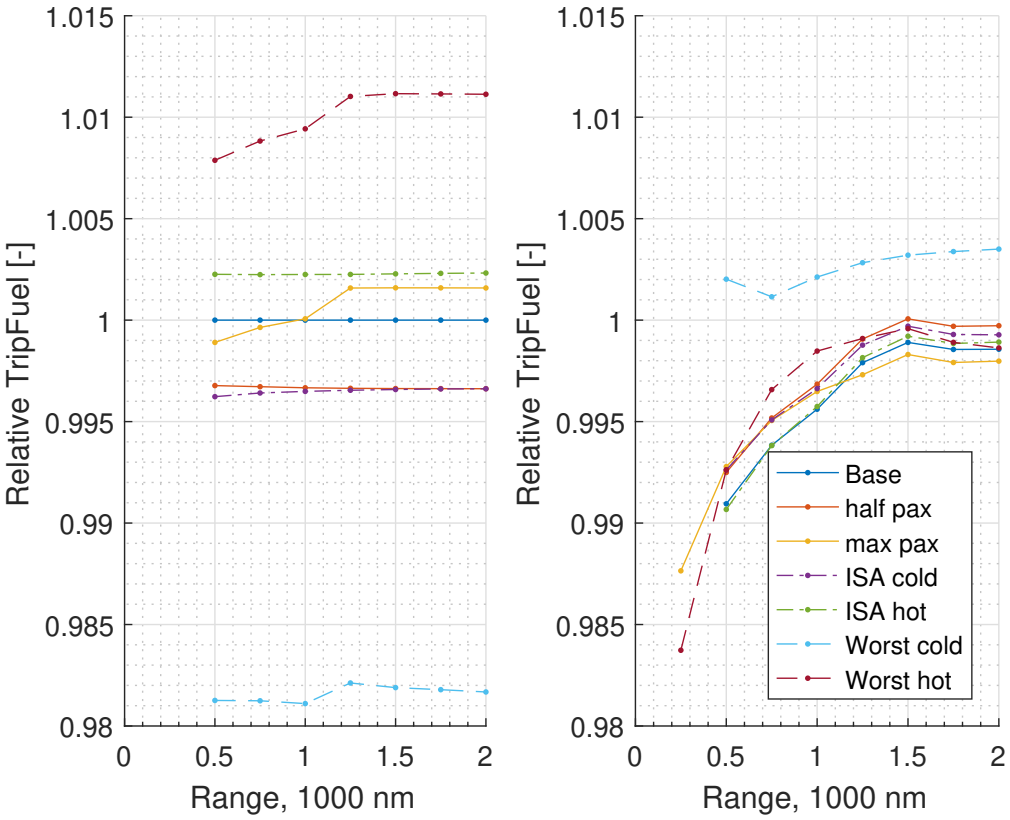

Figure C.16: Relative comparison of trip fuel for missions with 15000 kg payload for CECS on the left with respect to baseline and EECS on the right with respect to the same case CECS fuel burn for all cases, including 400 kg retrofit weight penalty.

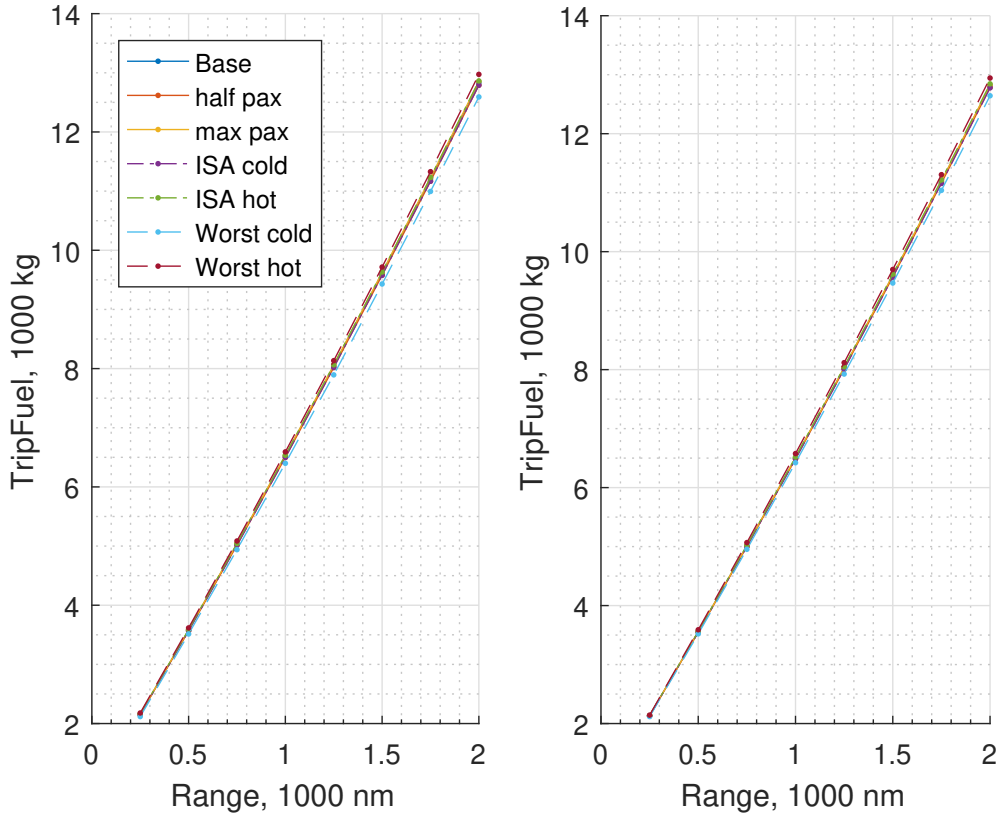

Figure C.17: Comparison of absolute trip fuel for missions with 16000 kg payload for CECS on the left and EECS on the right for all cases, including 400 kg retrofit weight penalty.

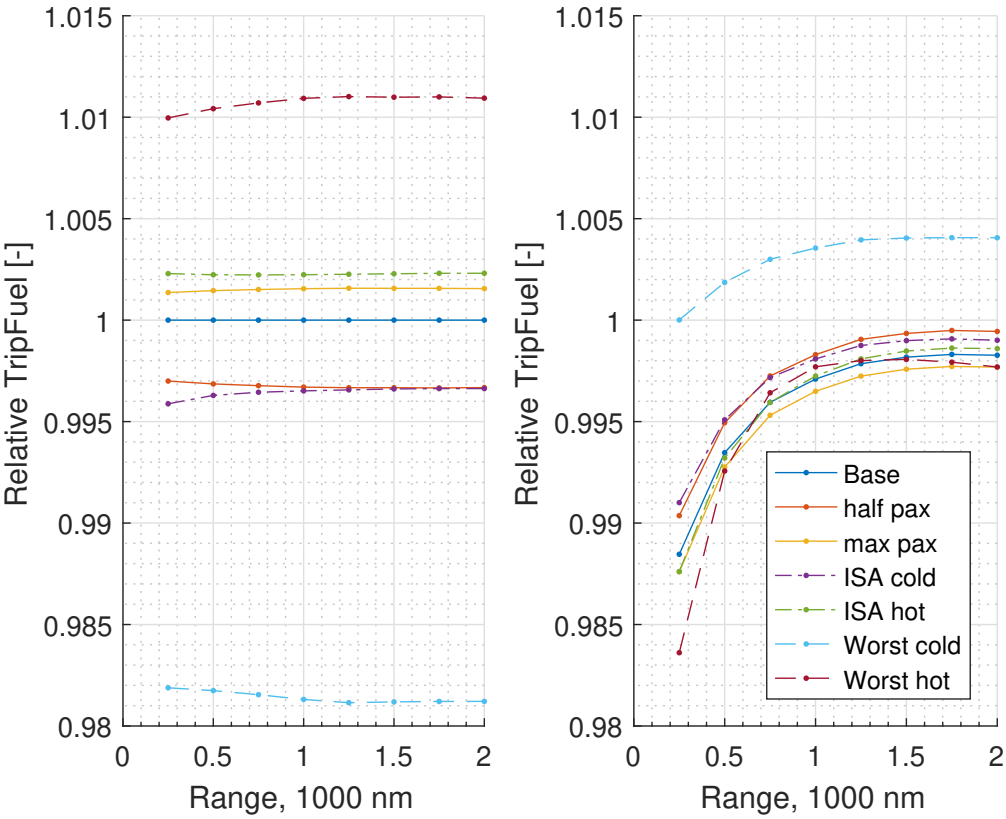

Figure C.18: Relative comparison of trip fuel for missions with 16000 kg payload for CECS on the left with respect to baseline and EECS on the right with respect to the same case CECS fuel burn for all cases, including 400 kg retrofit weight penalty.